JAERI-Research
2002-005

RELIABILITY ASSESSMENT OF HIGH ENERGY PARTICLE INDUCED RADIOACTIVITY CALCULATION CODE DCHAIN-SP 2001 BY ANALYSIS OF INTEGRAL ACTIVATION EXPERIMENTS WITH 14 MeV NEUTRONS

March 2002

Tetsuya KAI, Fujio MAEKAWA, Yoshimi KASUGAI
Kazuaki KOSAKO*, Hiroshi TAKADA and Yujiro IKEDA

日本原子力研究所
Japan Atomic Energy Research Institute

本レポートは、日本原子力研究所が不定期に公刊している研究報告書です。
入手の問合わせは、日本原子力研究所研究情報部研究情報課（〒319-1195　茨城県那珂郡東海村）あて、お申し越し下さい。なお、このほかに財団法人原子力弘済会資料センター（〒319-1195　茨城県那珂郡東海村日本原子力研究所内）で複写による実費頒布を行っております。

This report is issued irregularly.
Inquiries about availability of the reports should be addressed to Research Information Division, Department of Intellectual Resources, Japan Atomic Energy Research Institute, Tokai-mura, Naka-gun, Ibaraki-ken 〒319-1195, Japan.

編集兼発行　日本原子力研究所

JAERI－Research 2002－005

Reliability Assessment of High Energy Particle Induced Radioactivity Calculation Code DCHAIN-SP 2001 by Analysis of Integral Activation Experiments with 14 MeV Neutrons

Tetsuya KAI, Fujio MAEKAWA, Yoshimi KASUGAI, Kazuaki KOSAKO*, Hiroshi TAKADA and Yujiro IKEDA

Center for Neutron Science
Tokai Research Establishment
Japan Atomic Energy Research Institute
Tokai-mura, Naka-gun, Ibaraki-ken

(Received January 31, 2002)

Reliability assessment for the high energy particle induced radioactivity calculation code DCHAIN-SP 2001 was carried out through analysis of integral activation experiments with 14-MeV neutrons aiming at validating the cross section and decay data revised from previous version. The following three kinds of experiments conducted at the D-T neutron source facility, FNS, in JAERI were employed: (1) the decay gamma-ray measurement experiment for fusion reactor materials, (2) the decay heat measurement experiment for 32 fusion reactor materials, and (3) the integral activation experiment on mercury. It was found that the calculations with DCHAIN-SP 2001 predicted the experimental data for (1)～(3) within several tens of percent. It was concluded that the cross section data below 20 MeV and the associated decay data as well as the calculation algorithm for solving the Beteman equation that was the master equation of DCHAIN-SP were adequate.

Keywords: DCHAIN-SP 2001, High Energy Particle, Induced Radioactivity, Reliability Assessment, 14-MeV Neutron, Decay Gamma-ray, Decay Heat, Mercury

*Sumitomo Atomic Energy Industries, Ltd.

14-MeV 中性子を用いた積分放射化実験解析による 高エネルギー粒子誘導放射能計算コード DCHAIN-SP 2001 の信頼性評価

日本原子力研究所東海研究所中性子科学研究センター
甲斐 哲也・前川 藤夫・春日井 好己・小迫 和明*・高田 弘・池田 裕二郎

(2002 年 1 月 31 日 受理)

14-MeV 中性子を用いた積分放射化実験解析を通して、前バージョンの断面積データと崩壊データに対して行った改訂の妥当性を検証することを目的として、高エネルギー粒子誘導放射能計算コード DCHAIN-SP 2001 の信頼性評価を行った。解析を行った実験は、原研 FNS の D-T 中性子源を用いて行われた (1) 核融合炉材料の崩壊ガンマ線測定実験、(2) 32 種の核融合炉材料に対する崩壊熱測定実験、(3) 水銀の積分放射化実験、の 3 件である。解析の結果、DCHAIN-SP 2001 による計算は、(1)~(3) の実験値を数十パーセント以内で予測することができた。Beteman 方程式の解法アルゴリズム、及び 20 MeV 以下の放射化断面積と付属の崩壊データについて適切であるという結論が得られた。

東海研究所: 〒 319-1195 茨城県那珂郡東海村白方白根 2-4
*住友原子力工業 (株)

Contents

目次

1 Introduction

In the JAERI/KEK high-intensity proton accelerator project, a complex of accelerators (a 400 MeV linac, 3 GeV and 50 GeV synchrotoron ring) and experimental facilities are to be constructed. A great amount of radioactive nuclides are to be produced by bombardment of GeV order energy protons and associated secondary particles to surrounding materials. Appropriate estimation of radioactive nuclide inventory in such materials is essential for radiation safety design of these facilities: γ-ray dose estimation around piping for circulating liquid such as water, mercury and lead-bismuth eutectic, decay heat estimation of activated materials for loss of flow/coolant accidents, γ-ray dose estimation of activated components to make maintenance scenarios, and so on. To estimate these quantities, we have developed the high-energy particle induced radioactivity calculation code DCHAIN-SP[1, 2].

The first version of the DCHAIN-SP code[1] with a complete manual has been released in 1999. The second version of the code, DCHAIN-SP 2001[2], has been released in early 2001. The following items are enhanced in the second version compared to the first version:

1) the fission process is included in the code,

2) part of activation cross section data for neutrons below 20 MeV are revised, and

3) user-interface of the code is enhanced.

Figure 1.1 illustrates a schematic diagram of the DCHAIN-SP code system. High-energy particle transport calculation codes, e.g., NMTC/JAERI-97[3] or NMTC/JAM[4, 5, 6], calculate and make a data file of nuclide yields produced by high-energy particles such as protons, pions and neutrons above 20 MeV. On the other hand, neutron transport calculation codes such as MCNP[7, 8] take over simulation of neutron transport below 20 MeV, and provide neutron flux spectra. The DCHAIN-SP code reads the neutron flux spectra below 20 MeV, and calculates nuclide yield by using activation cross section data involved in the code. The DCHAIN-SP code merges the nuclide yield data contributed by both high-energy particles and neutrons below 20 MeV, and calculates time-evolution of decaying nuclides by using decay data libraries. Finally, radioactivity, decay heat and decay γ-ray spectrum are obtained.

Reliability assessment of calculation codes is one of the most important aspects in any code developments. Apart from calculation accuracy for particle transport simulation, reliability of calculation results by the whole DCHAIN-SP system is dominated by accuracy of nuclide yields data calculated by NMTC/JAM etc., accuracy of the activation cross section data for neutrons below 20 MeV, and validity of the calculation algorithm for solving the Beteman equation that is the master equation of DCHAIN-SP. This report deals with reliability assessment for the latter two parts, the activation cross section

data and the calculation algorithm, by analyses of integral activation experiments with 14-MeV neutrons. Although the first part, the accuracy of nuclide yields data calculated by NMTC/JAM etc., is very important for the code system, reliability for this part will be assessed in the future.

The following three series of experiments conducted at the D-T neutron source facility FNS[9] in JAERI were employed:

1) the decay γ-ray measurement experiment for fusion reactor materials[10, 11, 12],

2) the decay heat measurement experiment for 32 fusion reactor materials[13, 14, 15], and

3) the integral activation experiment on mercury.

These experiments were selected because the source neutron energy of ~14-MeV was suitable for testing the activation cross section data below 20 MeV, experimental data for many materials were available, and experimental conditions were clear enough for reliability assessment of calculation codes. Chapters 2 through 4 describe results of the reliability assessment basing on the three series of the experiments. Chapter 5 summarizes this report.

2 Benchmarking with the Decay Gamma-Ray Measurement Experiment

2.1 Outline of the Experiment and Benchmark Calculation

The decay γ-ray measurement experiment was carried out by using a D-T fusion neutron field of FNS[9] in JAERI. The experimental conditions and results are detailed in the Ref.10. We estimated accuracies of DCHAIN-SP calculations in terms of γ-ray intensities and energy spectra emitted from induced-radioactivity through benchmark calculations of the experiments. Table 1 shows 30 kinds of materials selected for the benchmark, neutron irradiating conditions and measuring conditions. The symbols A1, A2, B2 and C1 in the column "spectra.id" represent neutron spectra and irradiation time. The irradiation time in A1, A2, B2, C1 were 30 minutes, 9 hours, 10 hours and 9.78 hours, respectively. The neutron spectra were same in A1 and A2. As shown in Fig. 2.1, 14 MeV neutrons were dominant for all cases. Contribution of low energy neutrons decreases in the order from A to C. The chemical compositions including impurities were cited from the Table 1 in the Ref.10. The compositions of Mn-Cu alloy and stainless steel are shown in Table 2. The isotopic compositions were cited from "Chronological Scientific Tables[16]". The calculations were carried out using the activation cross section library and decay-data library included in DCHAIN-SP 2001.

2.2 Results and Discussion

Figures 2.2 through 2.31 compare the DCHAIN-SP calculations (solid lines) with experiments for the decay γ-ray spectra. Discrete energy points (diamond marks) are obtained by experiments although groupwise energy spectra are given by the DCHAIN-SP calculations. In order to compare them directly, the experimental results are converted to groupwise energy spectra of VITAMINE-J[17] 42 groups (dotted lines). General agreement could be seen between calculations and experiments in the γ-ray energy spectra. However, large discrepancies are observed in some energy groups. For the purpose of radiation protection against γ-ray emitted from induced radioactivity, it is reasonable to discuss about a total amount of γ-ray energy release instead of γ-ray intensities at every energy group. As shown in Fig. 2.32, we compared experiments and calculations by amounts of γ-ray energy release for all the cases. The experiments and calculations agreed within 30% in 22 cases. In five cases of SIA11(silicon), TAA21(tantalum), SNC13(tin), INA22(indium) and WA23(tungsten), discrepancies between the calculations and experiments ranged between 30% and 50%. The calculations overestimated the integrated intensities by a factor of 2.5$\sim$3.0 for three cases of CRA22(chromium), MOA11(molybdenum) and MCA11(manganese-copper alloy). We discuss about the 8 cases in which differences more than 30% are observed.

(1) SIA11(silicon)

Figure 2.33 shows the comparison between the DCHAIN-SP calculation and measurement by the γ-ray energy release at each group. It is found that the calcu-

lated values are smaller than the experiment for the 16th (3.0∼3.5 MeV), the 18th (2.0∼2.5 MeV) and the 28th (0.510∼0.512 MeV) groups. The γ-ray energies which were observed in the experiments but not found in the DCHAIN-SP result were 2.128, 0.511, 3.303, 2.737 and 1.176 MeV (the contributions to energy release decreased in this order). These energies are identical to those of the decay γ-rays of ^{34m}Cl. The C/E value improves to be 0.99 when these γ-rays are excluded from the experimental results. Therefore, the discrepancy between the calculation and experiment are attributed to ^{34m}Cl produced probably from the ^{35}Cl(n, 2n)^{34m}Cl reaction. It was thought that the silicon sample was contaminated by chlorine.

(2) TAA21(tantalum)

As shown in Fig. 2.34, the dominant γ-rays of the energy release are in the 23rd (1.0∼1.33 MeV) and the 35th (0.075∼0.1 MeV) groups in both the experiment and the calculation. These γ-rays are emitted from ^{182g}Ta and ^{180g}Ta, respectively. The calculation overestimates the yields of both nuclides about 40%. There is no problem in the decay data and the cross section of ^{181}Ta(n,γ)^{182g}Ta and ^{181}Ta(n,2n)^{180g}Ta reaction. DCHAIN-SP calculation generally overestimates (n,γ) reaction rates due to an inadequate treatment of self-shielding effect since the cross section library is groupwised assuming the infinite dilution. One of the reasons about the overestimation for the energy release from ^{182g}Ta seems to be the self-shielding effect. However, the reason for the ^{180g}Ta overestimation has not been found.

(3) SNC13(tin)

The γ-ray energy release for the 30th group (0.40∼0.45 MeV) in the experiment is much larger than that in the DCHAIN-SP calculation as shown in Fig. 2.35. The 417 keV γ-ray observed in the experiment corresponds to the 30th group. No explanation was found for the 417 keV γ-ray, however, the C/E value is improved to be 0.92 by eliminating the 417 keV γ-ray.

(4) INA22(indium)

The γ-ray energy release from INA22 sample is compared by nuclide in Fig. 2.36. The yields of ^{24}Na, $^{114m+g}$In and ^{115m}In are underestimated in the calculation.

The ^{24}Na is considered to be produced from impurities since the reaction to produce ^{24}Na from indium dose not take place.

Although the ^{114g}In and ^{114m}In are produced through both the ^{113}In(n,γ) and ^{115}In(n,2n) reactions, the reaction rate of the ^{115}In(n,2n) reaction was estimated about 10^3 as large as that of the ^{113}In(n,γ) reaction under this experimental condition. Energy release of ^{114g} is proportional to the yield of the parent nuclide, ^{114m}In, since the cooling time of 16.4 hours are much longer than a ^{114g}In half-life of 72 seconds. The ^{115}In(n,2n)^{114m}In cross section data in the FENDL/A-2.0 adopted in the DCHAIN-SP is 0.8 b for 14-MeV neutron, however, the experimental data is $\sim$ 1.4 b [18]. Therefore, it was found that the ^{115}In(n,2n)^{114m}In reaction cross section caused the underestimation of energy release from $^{114m+g}$In.

The ^{115m}In is produced through the ^{115}In(n,n')^{115m}In reaction. The reaction rate was improved by 14% if the cross section data in JENDL Dosimetry file[19] was utilized in stead of that in FENDL/A-2.0, however, no explanation was found for the underestimation of energy release from ^{115m}In.

(5) WA23(tungsten)

In Fig. 2.37, the γ-ray energy release of the WA23 case is compared by each group. It is found that the calculation overestimates the energy release for the 26th (0.6~0.7 MeV) and the 29th (0.45~0.51 MeV) groups. The corresponding γ-ray energies are 685 and 479 keV which are emitted from ^{187}W produced through the ^{186}W(n,γ)^{187}W reaction. As mentioned in the TAA21 case, the DCHAIN-SP calculation generally overestimates (n,γ) reaction rates. In the WA23 case, about 90% of γ-ray energy is emitted from the ^{187}W. It was concluded that the overestimation was caused by the inconsideration for the self-shielding effect.

(6) CRA22(chromium)

The γ-ray energy release of the CRA22 case is compared by groups in the Fig. 2.38. The overestimations of the calculation are found in the 17th (2.5~3.0 MeV) and the 21st (1.34~1.5 MeV) groups. Both energy groups correspond to ^{24}Na which is produced from aluminum impurity in the chromium sample through the ^{27}Al(n,α)^{24}Na reaction. However, the aluminum content of 0.1wt% is not an actually analyzed value but a typical one. It was concluded that the discrepancy was caused by the uncertainty of the content of aluminum impurity. On the other hand, good agreement can be seen in the 31st group in which the dominant 320 keV γ-ray emitted from the ^{51}Cr is included.

(7) MOA11(molybdenum)

In the Fig. 2.39, the γ-ray energy release of the MOA11 case is compared by each group. The dominant discrepancy is found at 511 keV γ-ray in the 28th group. According to the calculation, 99.8% of the 511 keV γ-ray is associated with the decay of ^{91g}Mo produced through the ^{92}Mo(n,2n)$^{91m+g}$Mo reaction (the ^{91m}Mo decay to the ^{91g}Mo with half-life of 65 s). The reaction cross section and the decay data of ^{91m}Mo and ^{91g}Mo in the DCHAIN-SP libraries were compared with the existing experimental data. However, no problem has been recognized. A reason for the discrepancy can be attributed in the experiment for measurement of annihilation γ-rays. Positrons emitted following β^+-decay run away from the sample, and annihilation γ-rays are produced at positions far from the sample. This effect degrades experimental data significantly. The reason for the discrepancy was inferred that no consideration was paid for the effect mentioned above.

(8) MCA11(manganese)

In the Fig. 2.40, the γ-ray energy release of the MCA11 case is compared by each group. The overestimation for 511 keV γ-ray is the dominant reason of the discrepancy. As a result of the calculation, 99.0% of the 511 keV γ-ray is emitted

from ^{62}Cu produced through the ^{63}Cu(n,2n)^{62}Cu reaction. No problem was found in the reaction cross section and the decay data. As similar to the MOA11 case, the discrepancy seems to be caused by positrons which run away from the sample.

Note that it is only 2 cases (MOA11 and MCA11) that the annihilation γ-ray of β^+ is dominant in the 511 keV γ-ray. The ^{91g}Mo and ^{62}Cu emit the high-energy β^+-ray with maximum energy of 3.412 and 2.926 MeV, respectively. The assumption that the γ-rays were produced in the sample is incorrect for these cases since these β^+-ray emit the annihilation γ-ray far from the sample.

2.3 Summary

The DCHAIN-SP calculations and the experiments were compared by the energy spectra of γ-rays emitted from induced activities. Reasonable agreement could be seen although discrepancies were found in some cases.

The comparison was also carried out for the total amount of γ-ray energy release. In three cases, the calculations overestimated the values of γ-ray energy release compared with the experiments by a factor of 2.5 $\sim$ 3. The discrepancies could be attributed to the experiment, the uncertainty in the composition of impurities (CRA22) or the inadequate estimation of the annihilation γ-ray from positrons at the experiments (MOA11, MCA11). In five cases, the differences were between 30% and 50%. The reasons for the differences were considered as that some impurities were not included in the calculation (SIA11, INA22) and the contribution of (n,γ) reaction was dominant (WA23). In other 22 cases, agreement within 30% could be seen.

We carried out benchmark calculations for 30 kinds of materials. More than 30% of differences were found for eight cases. However, the differences for six cases out of eight were due to the experiments. Therefore, it was found that the DCHAIN-SP can predict adequately the energy spectrum and γ-ray energy release from radioactivity induced in 14-MeV neutron fields.

3 Benchmarking with the Decay Heat Measurement Experiment

3.1 Outline of the Experiment and Benchmark Calculation

In this experiment, thirty-two kinds of fusion reactor relevant materials were irradiated in a 14-MeV neutron field of FNS/JAERI, and decay heat produced in the samples were measured. Details of the experiment are described in Refs. 13, 14 and 15. Two combinations of irradiation and cooling time were employed to cover a wide variety of radioactive nuclides having short and long half-lives:

(1) irradiation time: 5 minutes, cooling time: 1 min. ~60 min.

(2) irradiation time: about 7 hours, cooling time: 0.6 days ~ 400 days.

Since this experiment measures total decay heat by all radioactive nuclides produced in a sample, comparisons of decay heat for individual species of radioactive nuclides are impossible. However, since experimental data are obtained at many data points in the wide range of cooling time from 1 minute to 400 days and also for many kinds of samples, reliability of the DCHAIN-SP calculations for production of many radioactive nuclides can be verified through this benchmark.

According to the experimental conditions[13], decay heat values for 28 sample materials were calculated with DCHAIN-SP, and the calculated results were compared with the experimental data. The activation cross section library used in the previous version of the DCHAIN-SP code[1] refers the FENDL/A-2.0 library[20] as it is, while many activation cross section data in FENDL/A-2.0 are revised in the DCHAIN-SP 2001[2]. Some data in the decay data library used in the previous version of DCHAIN-SP are also revised in DCHAIN-SP 2001. To confirm the effects of the revisions, calculations were performed with the original and revised data libraries. Comparisons were also made with another series of calculation[13] using the ACT4 code and the original FENDL/A-2.0. The ACT4 code is the main calculation module of the THIDA code system[21]. Table 3 summarizes combinations of code and data libraries adopted in this benchmark.

3.2 Results and Discussion

Results for the 28 sample materials are shown in Figs. 3.1 through 3.28. Each figure consists of six sub-figures. Three sub-figures in the left-hand side are for the 5 minutes irradiation and those in the right-hand side are for 7 hours irradiation. Two sub-figures at the top compare the results calculated by DCHAIN-SP with the experimental data in absolute values. Two sub-figures at the middle show the ratios of calculated to experimental values (C/E) for DCHAIN-SP and ACT4. Two sub-figures at the bottom show the contributions to the total decay heat by individual radioactive nuclides based on the ACT4 calculation. In the sub-figures for the C/E values, calculated results of DCHAIN-SP with the nuclear data finally adopted, that is the DCHAIN-SP 2001, are

shown with solid circles; the case (a) in Table 3 when some data needed for calculation for a sample have been revised while the case (b) when no data have been revised. Since experimental errors for the bismuth sample for the 7 hours irradiation are large, results for supplemental experiment in which a bismuth sample is irradiated for 10 hours are shown instead.

In the sub-figures for the C/E values, when we compare the DCHAIN-SP 2001 calculations with the experimental data indicated by solid circles, most of C/E values are within the range of experimental error bands plus 20%. The good agreement indicates that decay heat can be calculated adequately with the DCHAIN-SP 2001 code for 28 kinds of sample materials irradiated in the 14-MeV neutron field for the wide cooling time range from 1 minute to 400 days. For the S, Ti, Mn, Ni, Cu, $SrCO_3$, Mo, SnO, W, Ta, Pb and Bi samples, the results of DCHAIN-SP 2001 are improved remarkably from those of the previous version due to the revision of activation cross section data. In some cases, however, the calculated results with DCHAIN-SP 2001 still disagree with the experimental data. As explained below, the disagreement is not attributed to the DCHAIN-SP 2001 code.

(1) Radioactive nuclides produced mainly by the (n,γ) reactions

In the experiment, neutron flux spectra at the irradiation fields are defined in detail around the 14-MeV neutron peak, but not for low energy region below 10 MeV. Since most of threshold reactions are induced by 14-MeV neutrons, uncertainties associated with the neutron spectra at the irradiation fields are considered to be small for threshold reactions. On the other hand, uncertainties ranging from several tens of percentages to a factor of 2 are expected for the (n,γ) reactions induced by low-energy neutrons.

Hence, the calculations could give rather large uncertainties to the decay heat values of the radioactive nuclides produced dominantly via the (n,γ) reactions dominantly by the low energy neutrons at the irradiation fields. Comparison of the calculated decay heat values with the experimental data is meaningless in these cases. This is the reason for the disagreement between the DCHAIN-SP calculations and the experimental data in some cooling time regions for the Na_2CO_3, Mn, Ta, W and Bi samples since they are predominantly produced by the $^{23}Na(n,\gamma)^{24}Na$, $^{55}Mn(n,\gamma)^{56}Mn$, $^{181}Ta(n,\gamma)^{182}Ta$, $^{186}W(n,\gamma)^{187}W$, $^{209}Bi(n,\gamma)^{210}Bi$, respectively.

(2) ^{58m}Co in the cobalt sample

In the cobalt sample irradiated for 7 hours, the ^{58m}Co nuclei (half-life: 9.15 hours) are produced from the $^{59}Co(n,2n)^{58m}Co$ reaction. According to Fig. 3.12, the decay heat produced by ^{58m}Co is about 30% of the total value at the cooling time of 0.6 days. However, decay heat from the ^{58m}Co is scarcely observed in the experiment because the ^{58m}Co emits only very low energy radiations such as X-rays of 7 keV and conversion electrons of 17 and 24 keV, and most of these radiations do not come

out from the cobalt sample. This effect makes the experimental data smaller and the corresponding C/E value larger. Although the ^{58m}Co is produced also in the nickel and stainless steel samples, the effect does not influence the experimental data meaningfully because the contribution of ^{58m}Co to the total decay heat is small.

(3) Yttrium oxide
Samples of yttrium oxide powder spread on adhesive plastic tape are used in the experiment. During the 14-MeV neutron irradiation, protons included in the plastic tape are recoiled into the yttrium oxide layer, and induce the proton-incident ^{89}Y(p,n)^{89m}Zr reaction, so-called the sequential charged particle reaction (SCPR). In the case of the yttrium oxide sample irradiated for 5 minutes shown in Fig. 3.16, decay heat values calculated with DCHAIN-SP neglecting the SCPR are much smaller than the experimental data in the period of cooling time from several minutes to several tens of minutes due to the omission of ^{89m}Zr produced by the SCPR. Assuming the effective SCPR cross section for the ^{89}Y(p,n)^{89m}Zr reaction as 1 mb and considering the decay heat from ^{89m}Zr (half-life: 4.18 min.), the calculation agrees well with the experimental data (see Fig. 3.16). Indeed the SCPR occurs in samples other than yttrium oxide, the effect appears meaningfully only in the yttrium oxide case. The reason is that the decay energy of neutron-induced activities is insignificant for the yttrium oxide sample irradiated for 5 minutes.

The calculations by the first version of DCHAIN-SP (case (b) in Table 3) and the ACT4 (case (c)) utilize the same activation cross section library, the original FENDL/A-2.0. Hence, as a whole, both calculations agree well with each other. This agreement is one of the proofs to demonstrate validity of the two calculation codes developed independently. In some cases, however, discrepancies are found between the two calculations. These can be explained as follows.

(1) Differences in the decay data library
Differences in the decay data libraries for the DCHAIN-SP and ACT4 calculations are very small for relatively light radioactive nuclides having the mass numbers roughly less than 100. Most parts of decay energies are conveyed by β- and γ-rays for these nuclides. When a mass number of a radioactive nuclide reaches to $\sim$ 200, conversion electrons and X-rays sometimes convey a significant fraction of decay energy. The decay data library used in the ACT4 calculations do not treat the decay energies associated with the conversion electrons and X-rays properly as described in Ref.13, and this could be one of the reasons to degrade calculated results with the ACT4 code.

(2) Differences in the energy group structure
The VITAMIN-J[17] 175-energy group structure is used in the DCHAIN-SP calculation while the 125-energy group structure is used in the ACT4 calculation. Energy bin widths for the 125-group structure is finer than those for the 175-group structure

as far as 14-MeV neutron peak region is concerned. Both energy group structures are fine enough to describe the 14-MeV neutron peak. Nevertheless, the difference in the energy group structure could cause the differences in the calculated results by the DCHAIN-SP and ACT4 codes although they are estimated to be several percentages at most.

3.3 Summary

Both the algorithm of the DCHAIN-SP code and the associated nuclear data library have been validated through the decay heat benchmark. Accuracy in the calculated results are improved significantly by the revision of the activation cross section and decay data libraries for the DCHAIN-SP 2001 code. It is concluded that the DCHAIN-SP 2001 can predict decay heat values with an accuracy of approximately 20% for the 28 materials irradiated by 14-MeV neutrons in a period of cooling time from 1 minute to 400 days.

4 Benchmarking with the Integral Activation Experiment on Mercury

4.1 Outline of the Experiment

Mercury is one of the most important materials as a spallation neutron production target. However, neither a decay γ-ray measurement experiment nor a decay heat experiment has been carried out because mercury has not been interested for fission or fusion applications. To provide experimental data for mercury, an integral activation experiment was performed by using the D-T neutron source FNS.

As shown in Fig. 4.1, three stainless steel boxes of $100 \times 100 \times 70$ mm^3 in inner dimensions, which were filled with mercury, were arranged in series to make an experimental assembly. The total thickness of mercury was 210 mm. The assembly was placed at 100 mm from the D-T neutron source. Three positions (#1 through #3) indicated in Fig. 4.1, i.e., the front surface of the assembly and two boundaries between every neighboring boxes, were served as irradiation fields. An integral experiment for neutron and secondary γ-ray transport was conducted before the activation experiment. Neutron spectra, dosimetry reaction rates, γ-ray spectra and γ-ray heating rates were measured at the irradiation positions.

A induced radioactivity measurement and a decay heat measurement were performed using mercury oxide powder of 300 mg and 30 mg, respectively. A pair of samples for induced radioactivity and decay heat was placed at each irradiation position, and irradiated for 400 minutes by D-T neutrons. After the irradiation, induced radioactivity produced in the samples was measured by high-purity germanium detectors by detecting γ-rays emitted from the samples at cooling time of 0.1, 0.3, 1, 3, 10, 30 and 100 days. In addition, decay heat was measured by the whole energy absorption spectrometer[13, 22] at the same cooling time as the induced radioactivity measurement.

4.2 Neutron Spectra of the Irradiation Field and Benchmark Calculation

A computational analysis for the integral experiment for neutron and secondary γ-ray transport was performed with the MCNP code[7]. The cross section data[23] for mercury to be adopted in JENDL-3.3 and those needed for stainless steel in JENDL Fusion File[24] were used in the analysis. Calculated results were compared with the experimental data, and the following conclusions were derived for the MeV energy neutron fluxes [25] which corresponded to a source term for the successive analysis of the activation experiment.

(1) The calculated 14-MeV neutron fluxes agreed within $\pm 10\%$ with the experimental data at all the three irradiation positions.

(2) Although the calculated neutron fluxes in the energy range from 1 to 10 MeV tended to be smaller than the experimental results as the penetration thickness increased, the agreement between the experiment and the calculation was good in general.

The calculated reaction rate of the ^{115}In(n,n')^{115m}In reaction, which has a large sensitivity to neutrons in the specific energy range from 0.5 to 10 MeV, was 20% smaller than the experimental data at the 140 mm position.

It was shown that neutron fluxes in the MeV energy region by which threshold activation reactions were induced were calculated without a significant problem with the combination of MCNP and JENDL. Accordingly, the calculated neutron flux spectra shown in Fig. 4.2 were used for the activation analysis with DCHAIN-SP. Although fractions of 14-MeV neutrons to the total decrease as we move from the position #1 to #3, most of threshold reactions at all the three positions are induced by 14-MeV neutrons due to their high threshold energies; about 8 MeV for the (n,2n) reactions and higher than 10 MeV for the (n,p) and (n,α) reactions. Therefore, it can be stated that the uncertainty associated with the neutron flux spectra used in the activation analysis is $\sim$ 10%.

Calculations of induced radioactivity and decay heat were performed with DCHAIN-SP using the neutron flux spectra at the three irradiation fields. Since activation cross section data for mercury have been revised extensively[2], both cross section data before and after the revision were used in the calculations in the decay heat benchmark.

4.3 Results and Discussion

4.3.1 Induced Radioactivity

Figures 4.3 through 4.5 show time evolutions of induced radioactive nuclides produced in the samples irradiated at the position #1 through #3, respectively. The experimental data are indicated by symbols while the calculated results with DCHAIN-SP are shown with lines. The experimental data are obtained in the period of cooling time from 0.1 to 100 days, and the radioactive nuclides having the shortest and the longest half-lives are ^{199m}Hg (half-life: $T_{1/2}$ = 42.6 min.) and ^{203}Hg ($T_{1/2}$ = 46.6 days), respectively.

When the calculated values are compared with the experimental data in Fig. 4.3$\sim$4.5, although discrepancies between them are found in some cases, the calculated time evolution curve of each radioactive nuclide agrees with the corresponding experimental data. The ^{197g}Hg nuclide ($T_{1/2}$ = 2.67 days) is produced directly by the neutron induced ^{198}Hg(n,2n)^{197g}Hg reaction during the irradiation as well as a decay product of ^{197m}Hg($T_{1/2}$ = 23.8 hours) that is produced by the ^{198}Hg(n,2n)^{197m}Hg reaction. Hence the time evolution curve for the ^{197g}Hg is not a simple exponential decay curve but has a broad peak at $\sim$ 1 day after the end of the irradiation. This trend observed in the experiment is reproduced well by the calculation. This suggests that half-lives and decay chain data used in the calculation are valid.

Total eight radioactive nuclides are observed in the experiment, and the four nuclides out of them, ^{197m}Hg, ^{197g}Hg, ^{199m}Hg and ^{203}Hg, take the major contribution to the

total. The calculated results for ^{197g}Hg and ^{203}Hg agreed with the experimental data mostly within the experimental error ranges. That for ^{197m}Hg and ^{199m}Hg, however, 20% smaller and 60% larger than the experimental data, respectively. Since the cross section data contained in the DCHAIN-SP 2001 library for the ^{198}Hg(n,2n)^{197m}Hg reaction and the Hg(n,x)^{199m}Hg reaction, i.e., sum of the ^{198}Hg(n,γ)^{199m}Hg, ^{199}Hg(n,n')^{199m}Hg and ^{200}Hg(n,2n)^{199m}Hg reactions, are revised based on the measured cross section data[2, 26], the discrepancies between the calculated and the experimental data in the integral activation experiment can not be attributed to the improper cross section data in the DCHAIN-SP library. Although a reasonable reason for the discrepancies has not been identified, there are some possible reasons: (1) inadequate decay data such as the γ-ray intensity per disintegration used in the DCHAIN-SP calculation and also in the processing of experimental data to derive radioactivity from observed γ-ray peak intensities, and (2) experimental uncertainties associated with the measurement of low-energy γ-rays and X-rays around 100 keV for which large correction of attenuation in the sample is indispensable.

Although experimental errors for the rest of nuclides, ^{195g}Hg, ^{199}Au, ^{198g}Au and ^{197m}Au, are large, no significant problem is found for those nuclides since the calculated radioactivity agrees roughly within several tens of percentages with the experimental data.

4.3.2 Decay Heat

Decay heat values measured and calculated for the three irradiation positions are compared in Figs. 4.6 through 4.8. Total decay heat contributed by all the radioactive nuclides in the sample is measured in this experiment unlike the induced radioactivity experiment. Another difference from the induced radioactivity experiment is that both photons (γ-rays and X-rays) and electrons (β-rays and conversion electrons) are measured in the decay heat experiment while only the former is measured in the induced radioactivity experiment. In Figs. 4.6$\sim$4.8, contributions from each radioactive nuclide to the total decay heat values calculated with DCHAIN-SP are also shown. Figure 4.9 shows ratios of calculated to experimental values (C/E) for the three positions. To check the effect of the revision[2, 26] of the activation cross section data, C/E values obtained with the activation cross section data before the revision, i.e., the original FENDL/A-2.0, are shown in Fig. 4.9 together with those for the DCHAIN-SP 2001.

According to Figs. 4.6$\sim$4.8, the dominant radioactive nuclides to the decay heat are ^{197m}Hg, ^{197g}Hg, ^{199m}Hg and ^{203}Hg. This aspect is similar to that of the induced radioactivity experiment. The ^{198}Hg(n,2n)^{197m}Hg and the ^{198}Hg(n,2n)^{197g}Hg reaction cross sections have been increased to be about double from their original values as indicated in Ref.2, 26. As a result, agreement between the experiment and the calculation is improved in the period from 0.3 to 10 days when the ^{197m}Hg and ^{197g}Hg nuclides contribute predominantly to the total decay heat.

By the revision for many of the activation cross section data for mercury, the calculated results reproduce adequately the experimental decay heat data as a general trend. One thing that can be remarked is that the calculated results are likely to overestimate the decay heat by 10 to 20% even the experimental errors are considered. Some inconsistencies are also found between the results derived from the decay heat benchmark and the induced radioactivity benchmark although they are not so significant. These points have not been clarified yet, but possible reasons could be in systematic errors involved in the two distinct experimental methods.

4.4 Summary

To verify induced radioactivity and decay heat calculations on mercury with DCHAIN-SP 2001, an experiment was conducted by using the 14-MeV neuron source of FNS. As a result of computational analysis of the experiment with DCHAIN-SP, the following general conclusions were derived.

(1) The revision of activation cross section data on mercury[2, 26] has improved significantly the prediction accuracy of activation calculations for neutron-induced reactions in the energy region below 20 MeV.

(2) The DCHAIN-SP 2001 code can estimate induced radioactivity and decay heat of mercury with the accuracy of ~20% for the irradiation in the neutron fields dominated by 14-MeV neutrons.

5 Concluding Remarks

The validity of the high energy particle induced radioactivity calculation code DCHAIN-SP 2001 was investigated with the three integral activation benchmark experiments conducted with the 14-MeV neutron source FNS, JAERI. The present investigation focused on the accuracy of the decay chain calculation of the DCHAIN-SP code using activation cross section data and low-energy (< 20 MeV) neutron fluxes calculated by neutron transport calculation codes such as MCNP. As a result of the present assessment, we have derived a general conclusion that induced radioactivity and decay heat for most of materials which are important for the high-intensity proton accelerator facilities, including mercury, lead, bismuth and structural materials, can be predicted within the typical uncertainty range of $\pm 20 \sim 30\%$ with the DCHAIN-SP 2001 code under the condition that the neutron flux spectra are given precisely. In principle, this conclusion is true only for 14-MeV fusion neuron environments. However, the energy of 14-MeV lies around the midpoint between 20 MeV (the maximum energy of activation cross section data library) and the threshold energies for such threshold reactions as (n,n'), (n,2n), (n,p) and (n,α). Therefore, the conclusion gives a good estimation for the calculation accuracy with the DCHAIN-SP code for any neutron fields up to 20 MeV where threshold reactions produce radioactive nuclides predominantly. It is noted that the benchmark experiments used in this study aim at the validation for radioactive nuclides produced by threshold reactions, not for those by the (n,γ) reactions induced by low-energy neutrons. Hence, the conclusion can not be adopted when the (n,γ) reactions are dominant for producing radioactive nuclides. In general, the DCHAIN-SP calculation overestimates reactions rate of (n,γ) since the cross section library was groupwised assuming the infinite dilution.

In the near future, we will investigate the calculation accuracy for another feature of the DCHAIN-SP 2001 code system, that is, the decay chain calculation with using nuclides yield data provided by the high-energy particle simulation code NMTC/JAM.

References

1) Takada H. and Kosako K.: "Development of the DCHAIN-SP Code for Analyzing Decay and Build-Up Characteristics of Spallation Products", JAERI-Data/Code 99-008 (1999).

2) Kai T., Maekawa F., Kosako K., Takada H. and Ikeda Y: "DCHAIN-SP 2001: High Energy Particle Induced Radioactivity Calculation Code", JAERI-Data/Code 2001-016 (2001) [in Japanese].

3) Takada H., Yoshizawa N., Kosako K. and Ishibashi K.: "An Upgraded Version of the Nucleon Meson Transport Code: NMTC/JAERI97", JAERI-Data/Code 98-005 (1998).

4) Takada H.: "Recent Progress of Nucleon-Meson Transport Code Development at JAERI", Proc. International Conference on Mathematics and Computation, Reactor Physics and Environmental Analysis in Nuclear Applications, September 27-30, 1999, Madrid, Spain, pp. 929 (2000).

5) Niita K., Takada H., Meigo S. and Ikeda Y.: "High Energy Particle Transport Code NMTC/JAM", Proc. 15th Meeting of the International Collaboration on Advanced Neutron Sources, ICANS-XV, November 6-9, 2000, JAERI-Conf 2001-002, Tsukuba, Japan, pp. 964-970 (2001).

6) Niita K., Meigo S., Takada H. and Ikeda Y.: "High Energy Particle Transport Code NMTC/JAM", JAERI-Data/Code 2001-007 (2001).

7) Briesmeister J. F. (Ed.): "MCNP^{TM} - A General Monte Carlo N-Particle Transport Code, Version 4C", LA-13709-M, Los Alamos National Laboratory (2000).

8) Waters L. S. (Ed.): "MCNPX ^{TM} User's Manual", TPO-E83-G-UG-X-00001, Los Alamos National Laboratory (1999).

9) Nakamura T., Maekawa H., Ikeda Y. and Oyama Y.: "A D-T Neutron Source for Fusion Neutronics Experiments at JAERI", Proc. International Ion Engineering Congress-ISIAT '83 & IPAT '83, September 12-16, Kyoto, Japan, 567 (1983).

10) Ikeda Y., Kumar A., Konno C., Kosako K., Oyama Y., Nakamura T., Maekawa H., Youssef M. Z. and Abdou M. A.: "Joint Report of JAERI/USDOE Collaborative Program on Fusion Neutronics - Induced Radioactivity Measurements in Fusion Neutron Environment -", JAERI-M 93-018 (1993).

11) Ikeda Y., Kumar A., Konno C., Kosako K., Oyama Y., Maekawa F., Maekawa H., Youssef M. Z. and Abdou M. A.: "Measurements and Analyses of Decay Radioactivity Induced in Simulated Deuterium-Tritium Neutron Environments for Fusion Reactor Structural Materials", Fusion Technol., 28, 74 (1995).

12) Kumar A., Ikeda Y., Abdou M. A., Youssef M. Z., Konno C., Kosako K., Oyama Y., Nakamura T. and Maekawa H.: "Decay Radioactivity Induced in Plasma-Facing Materials Irradiated by Deuterium-Tritium Neutrons", Fusion Technol., 28, 99 (1995).

13) Maekawa F., Wada M. and Ikeda Y.: "Decay Heat Experiment and Validation of Calculation Code Systems for Fusion Reactor", JAERI-Research 99-055 (1999).

14) Maekawa F. and Ikeda Y.: "Decay Heat Experiment on Thirty Two Fusion Reactor Relevant Materials Irradiated by 14-MeV Neutrons", Fusion Eng. Des., 47, 344 (2000).

15) Maekawa F., Wada M. and Ikeda Y.: "Experimental Validation of Decay Heat Calculation Codes and Associated Nuclear Data Libraries for Fusion Energy", J. Nucl. Sci. Technol., 38, 53 (2001).

16) National Astronomical Observatory (ed.): "Rika nenpyo (Chronological Scientific Tables)", Maruzen Co., Ltd., (1996) [in Japanese].

17) Vontobel P., Pelloni S.: "JEF/EFF Based Nuclear Data Libraries", EIR-Bericht Nr. 636, Swiss Federal Institute for Reactor Research (1987).

18) McLane V., Dunford C. L., Rose P. F.: "Neutron Cross Sections", Academic Press, Inc, San Diego (1988).

19) Nakazawa M., Kobayashi K., Iwasaki S., Iguchi T., Sakurai K., Ikeda Y., Nakagawa T.: "JENDL Dosimetry File", JAERI 1325 (1992).

20) Pashchenko A. B.: "Summary Report for IAEA Consultants' Meeting on Selection of Evaluations for the FENDL/A-2 Activation Cross Section Library" INDC(NDS)-341, International Atomic Energy Agency (1996).

21) Seki Y., Iida H., Kawasaki H. and Yamada K.: "THIDA-2: An Advanced Code System for Calculation of Transmutation, Activation, Decay Heat and Dose Rate", JAERI 1301 (1986).

22) Maekawa F., Wada M. and Ikeda Y.: "Development of Whole Energy Absorption Spectrometer for Decay Heat Measurement", Nucl. Instrum. Meth., A450, 467 (2000).

23) Shibata K., Fukahori T., Chiba S. and Yamamuro N.: "Evaluation of Neutron Nuclear Data for Mercury", J. Nucl. Sci. Technol., 34, 1171 (1997).

24) Chiba S., Fukahori T., Yu B. and Kosako K.: "Evaluation of the Double-Differential Cross Sections of Medium-Heavy Nuclei for JENDL Fusion File", JAERI-Conf 96-005, 54 (1996).

25) Maekawa F., Meigo S., Kasugai Y., Kai T., Harada M., Shibata K., Ikeda Y., Takeuchi H.: "Experimental study on cross section data of mercury with D-T and ^{252}Cf neutron source", Proc. Int. Conf. on Nuclear Data for Science and Technology (ND2001), October 7-12, 2001, Tsukuba, Japan, 6-P-29 (2002).

26) Kasugai Y., Maekawa F., Kai T., Ikeda Y., Takeuchi H.: *ibid.*, 6-P-21 (2002).

Table 1 Identification and experimental conditions for the selected experiment cases.

ID	material	spectra id.	time		
			irradiation	cooling	counting
FEA11	Iron	A1	30 m	22.4 m	10 m
FEA25	Iron	A2	9 h	2 d 22.1 h	15 h 25.9 m
NIA11	Nickel	A1	30 m	56.3 m	30.9 m
NIA23	Nickel	A2	9 h	4 d 13 h	8 h 41.9 m
NIB22	Nickel	B2	10 h	2 d 17.6 h	4 h 13.2 m
CRA22	Chromium	A2	9 h	15 h 16.8 m	1 h 0.5 m
MOA11	Molybdenum	A1	30 m	46.3 m	30.5 m
MOA24	Molybdenum	A2	9 h	4 d 3.7 h	15 h 28.6 m
SSA24	SS316	A2	9 h	3 d 21.8 h	13 h 54.6 m
SSC14	SS-ANSI316	C1	9 h 47 m	7 d 15 h	7 h 23 m
MCA11	Mn-Cu alloy	A1	30 m	12.3 m	10 m
MCA23	Mn-Cu alloy	A2	9 h	6 d 21 h	4 h 50.3 m
MCB22	Mn-Cu alloy	B2	10 h	3 d 13.4 h	6 h 44.9 m
WA23	Tungsten	A2	9 h	2 d 19.1 h	18 h 22.7 m
ZRA21	Zirconium	A2	9 h	2 h 26.5 m	43.5 m
VB22	Vanadium	B2	10 h	2 d 22.4 h	14 h 51.3 m
ALB21	Aluminum	B2	10 h	5 h 52.3 m	1h 28.5 m
COA23	Cobalt	A2	9 h	5 d 19.2 h	3 h 21.5 m
TIB21	Titanium	B2	10 h	7 h 27.5 m	1 h 43.4 m
NBB21	Niobium	B2	10 h	13 h 39 m	1 h 13.7 m
SNC13	Tin	C1	9 h 47 m	6 d 22.6 h	15 h 52 m
PBC11	Lead	C1	9 h 47 m	12 h 19.2 m	1 h 1.4 m
TAA21	Tantalum	A2	9 h	3 h 17.2 m	25.9 m
AGC12	Silver	C1	9 h 47 m	19 h 37.3 m	24.5 m
ZNC12	Zinc	C1	9 h 47 m	21 h 26.3 m	32.3 m
SIA11	Silicon	A1	30 m	37.3 m	15 m
YC13	Yttrium	C1	9 h 47 m	6 d 18.9 h	2 h 23.7 m
INA22	Indium	A2	9 h	16 h 23.7 m	45.7 m
MGA21	Magnesium	A2	9 h	3 h 51.7 m	26.3 m
AUA22	Gold	A2	9 h	4 h 31 m	2 h 46.7 m

Table 2 Chemical composition of alloy samples (weight fraction).

	Fe	Cr	Ni	Mo	Mn	Si	Co	Cu	V
Mn-Cu alloy	0.0007	-	0.0046	-	0.7980	-	-	0.1967	-
SS316	0.6622	0.1775	0.116	0.0208	0.0133	0.0042	0.0019	0.0034	0.0006
SS-ANSI316	0.686	0.165	0.113	0.0212	0.0146	-	-	-	-

Table 3 Codes and data libraries used in the decay heat benchmark.

	Calculation code	Activation cross section library	Decay data library
(a)	DCHAIN-SP [2]	FENDL/A-2.0 (Revised) [2]	Library in DCHAIN-SP (Revised) [2]
(b)	DCHAIN-SP [2]	FENDL/A-2.0 [20]	Library in DCHAIN-SP [1]
(c)	ACT4 [21]	FENDL/A-2.0 [20]	Library in ACT4 [21]

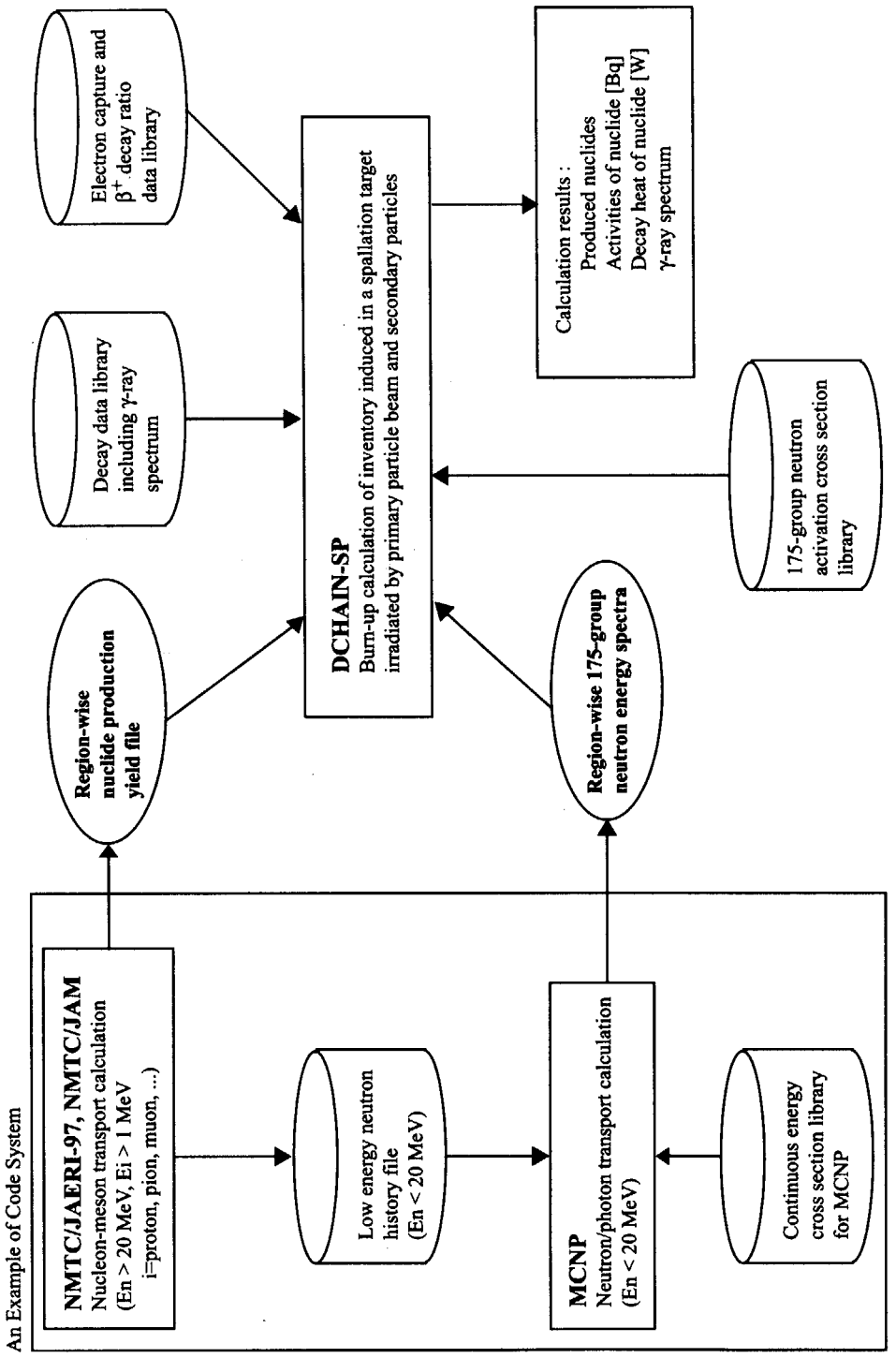

Fig. 1.1 Schematic diagram of the DCHAIN-SP code system.

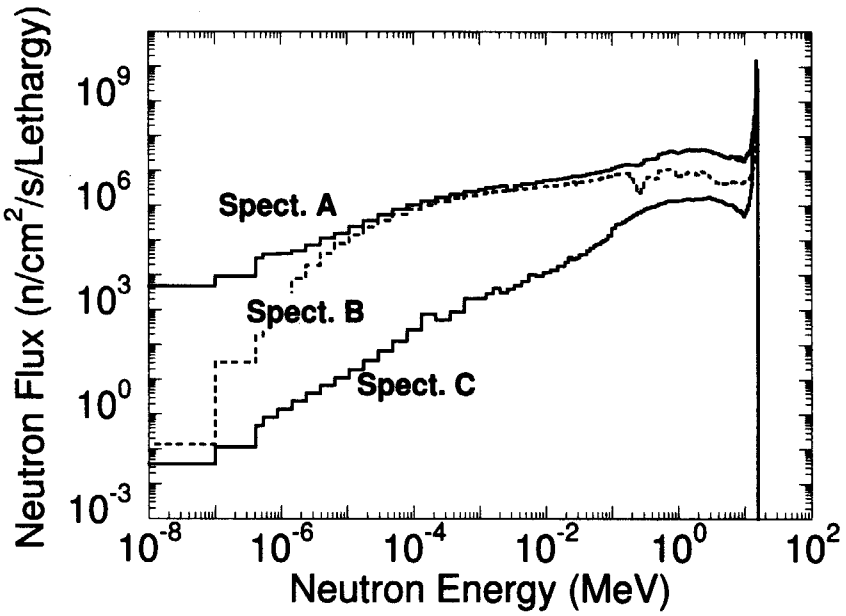

Fig. 2.1 Neutron spectra used in the benchmark calculations for decay γ-ray.

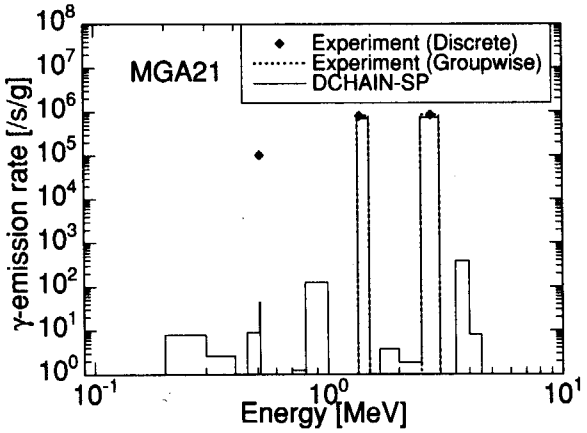

Fig. 2.2 Decay γ-ray spectrum of MGA21.

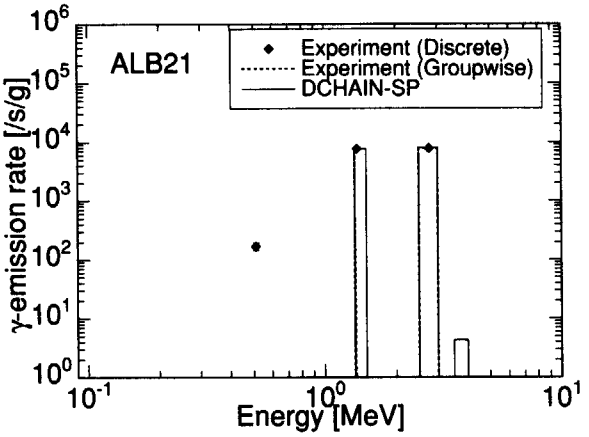

Fig. 2.3 Decay γ-ray spectrum of ALB21.

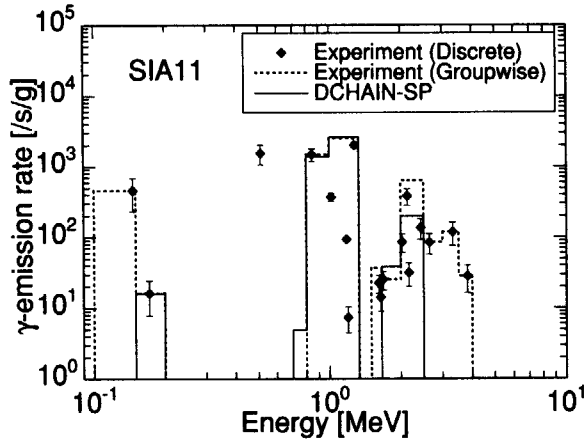

Fig. 2.4 Decay γ-ray spectrum of SIA11.

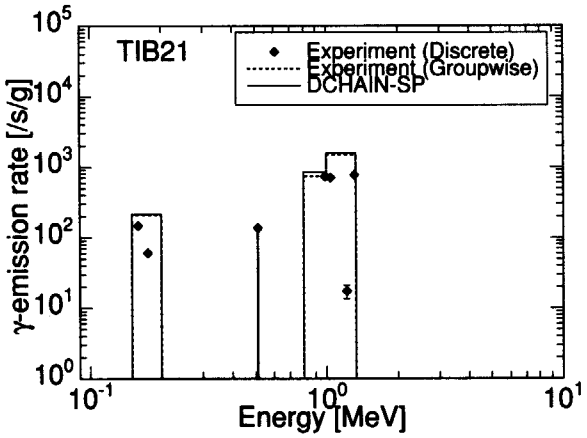

Fig. 2.5 Decay γ-ray spectrum of TIB21.

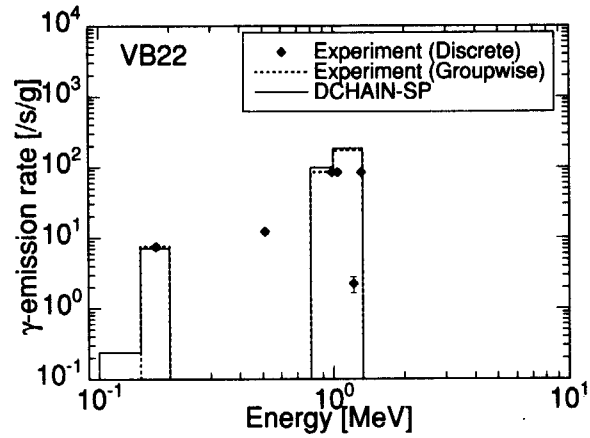

Fig. 2.6 Decay γ-ray spectrum of VB22.

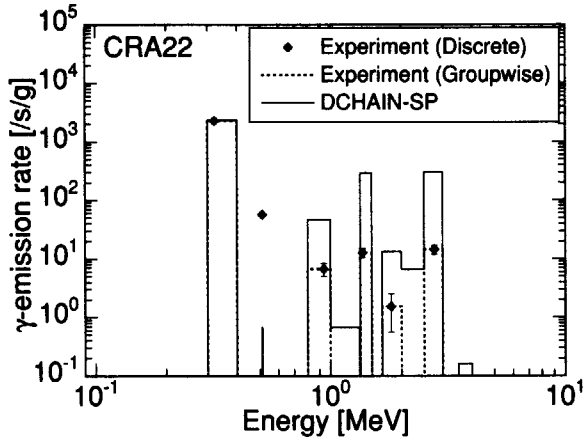

Fig. 2.7 Decay γ-ray spectrum of CRA22.

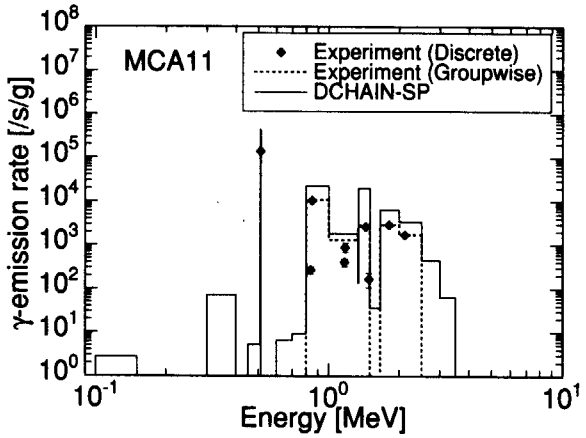

Fig. 2.8 Decay γ-ray spectrum of MCA11.

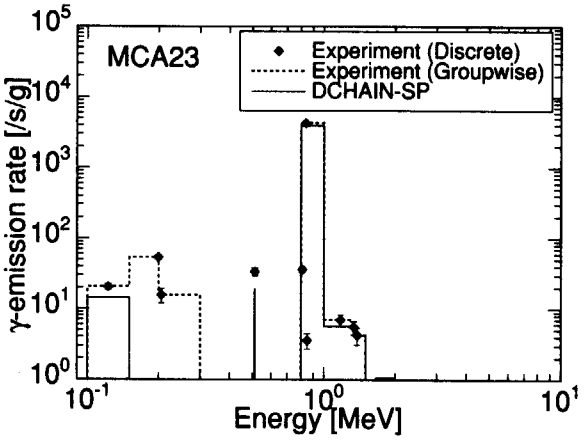

Fig. 2.9 Decay γ-ray spectrum of MCA23.

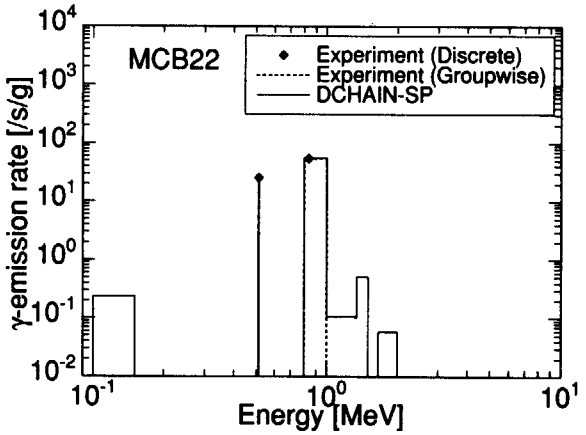

Fig. 2.10 Decay γ-ray spectrum of MCB22.

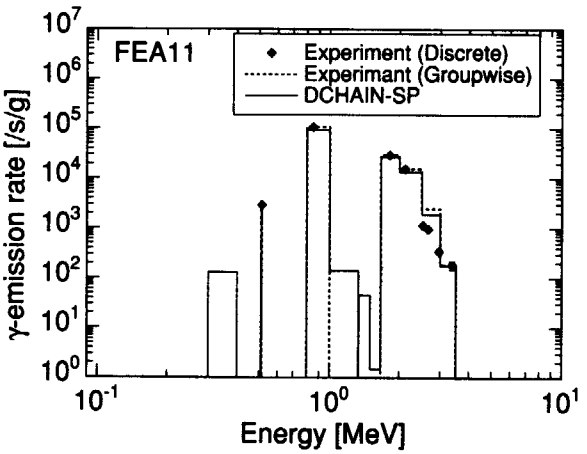

Fig. 2.11 Decay γ-ray spectrum of FEA11.

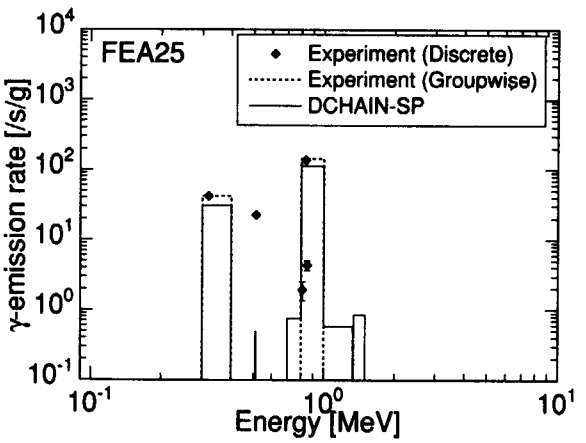

Fig. 2.12 Decay γ-ray spectrum of FEA25.

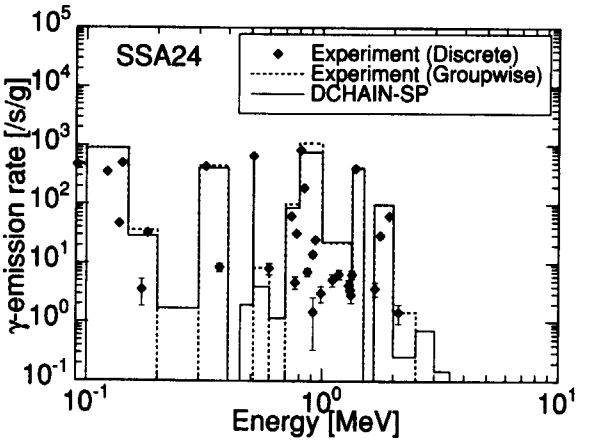

Fig. 2.13 Decay γ-ray spectrum of SSA24.

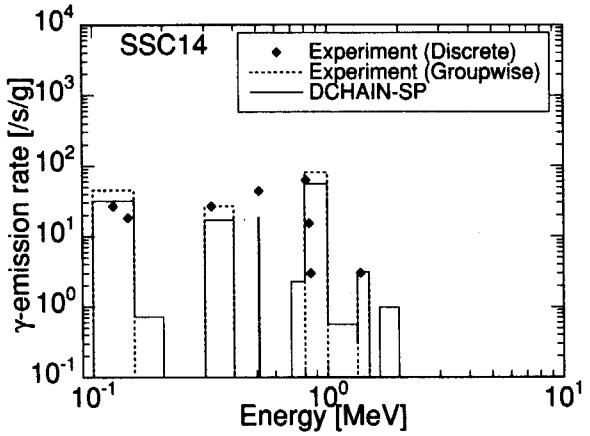

Fig. 2.14 Decay γ-ray spectrum of SSC14.

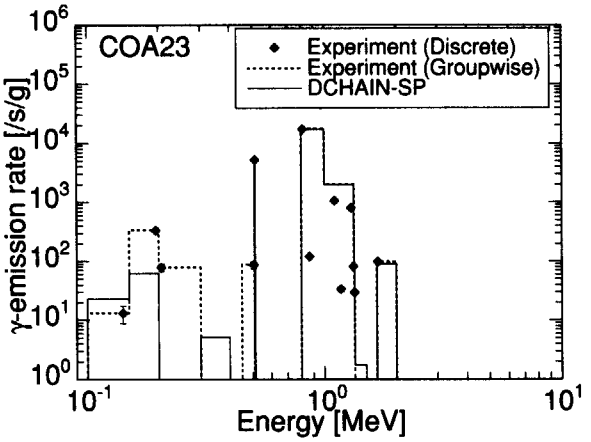

Fig. 2.15 Decay γ-ray spectrum of COA23.

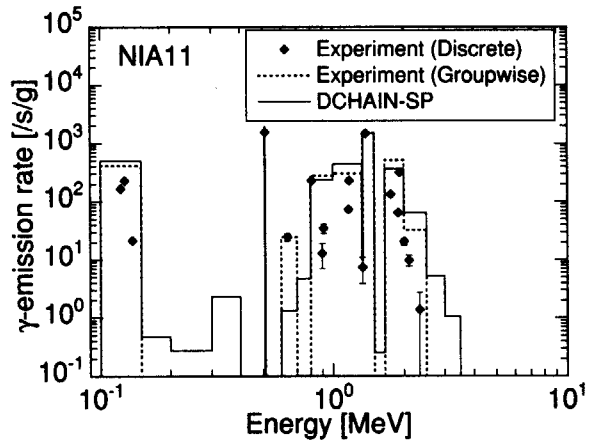

Fig. 2.16 Decay γ-ray spectrum of NIA11.

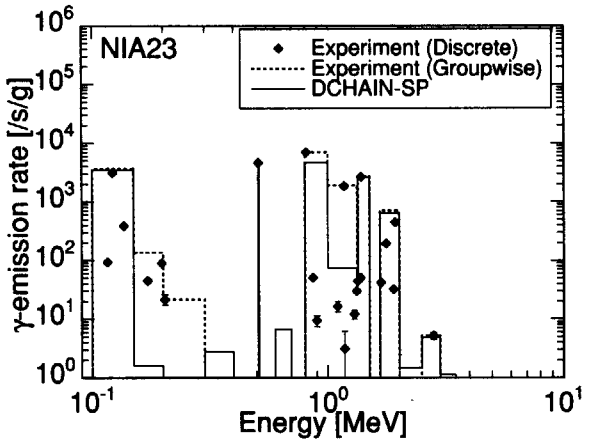

Fig. 2.17 Decay γ-ray spectrum of NIA23.

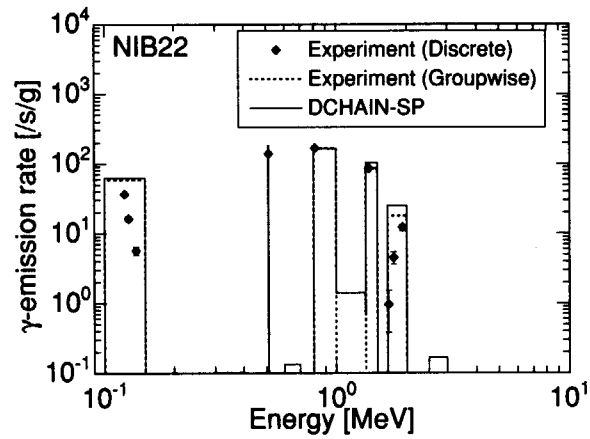

Fig. 2.18 Decay γ-ray spectrum of NIB22.

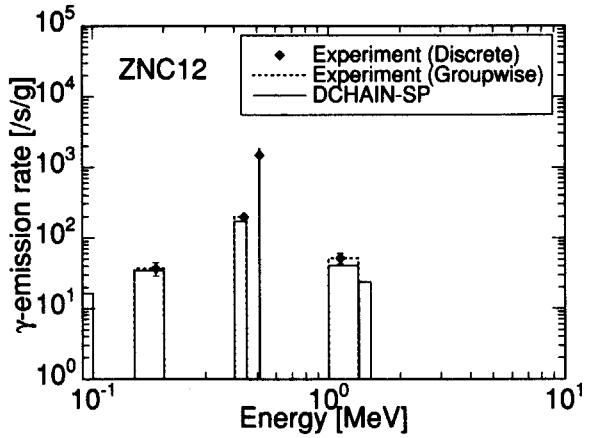

Fig. 2.19 Decay γ-ray spectrum of ZNC12.

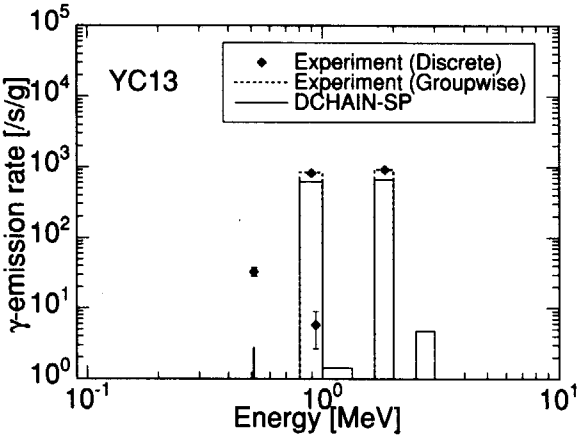

Fig. 2.20 Decay γ-ray spectrum of YC13.

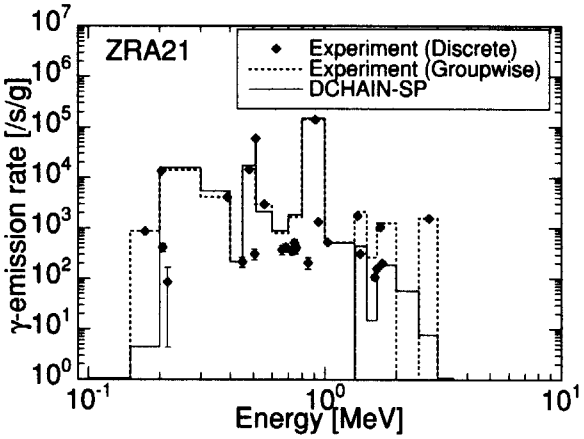

Fig. 2.21 Decay γ-ray spectrum of ZRA21.

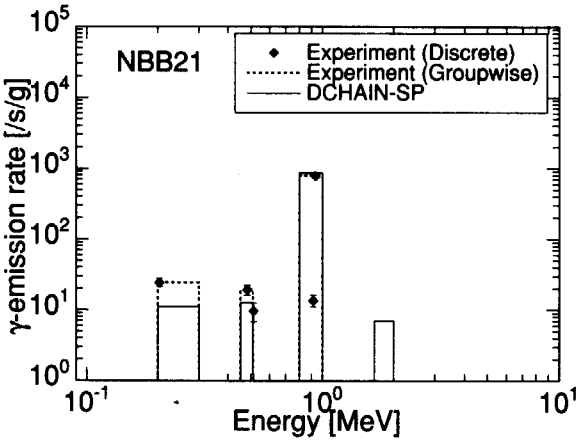

Fig. 2.22 Decay γ-ray spectrum of NBB21.

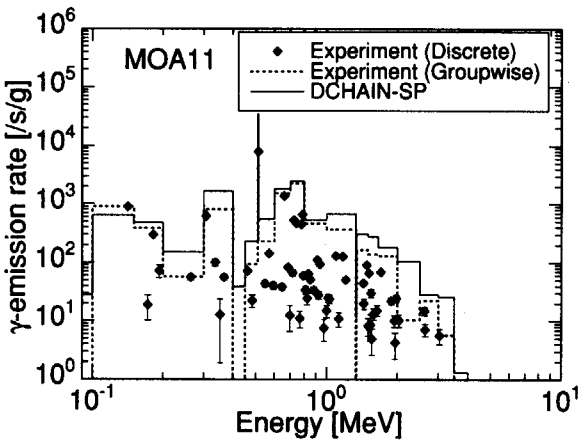

Fig. 2.23 Decay γ-ray spectrum of MOA11.

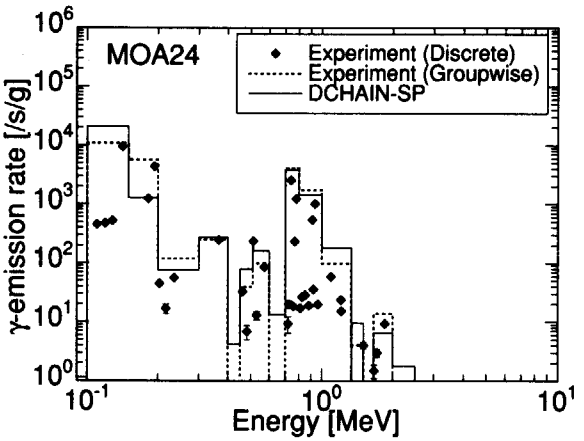

Fig. 2.24 Decay γ-ray spectrum of MOA24.

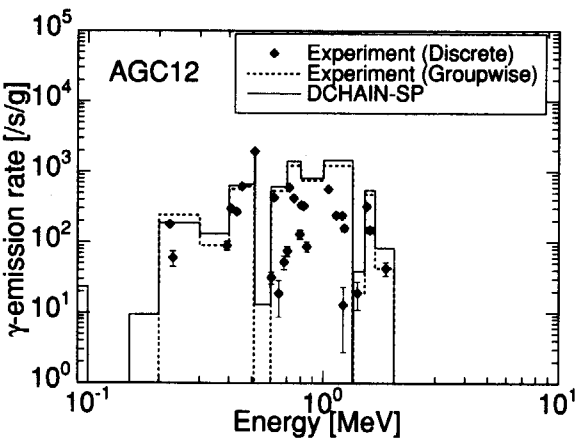

Fig. 2.25 Decay γ-ray spectrum of AGC12.

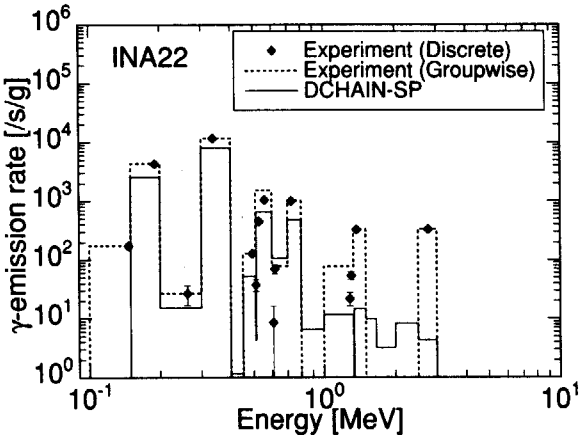

Fig. 2.26 Decay γ-ray spectrum of INA22.

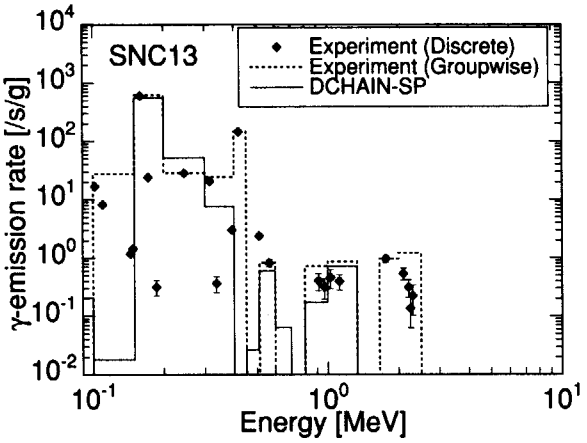

Fig. 2.27 Decay γ-ray spectrum of SNC13.

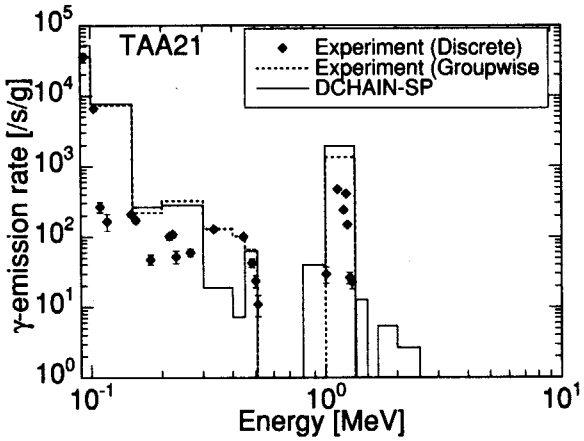

Fig. 2.28 Decay γ-ray spectrum of TAA21.

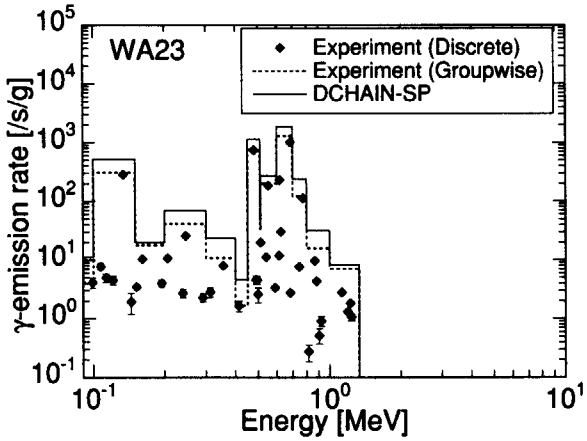

Fig. 2.29 Decay γ-ray spectrum of WA23.

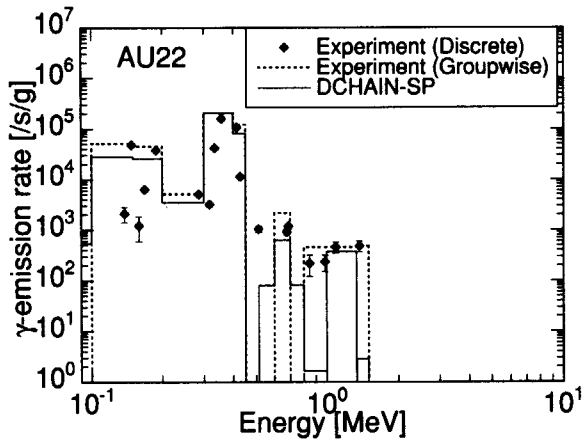

Fig. 2.30 Decay γ-ray spectrum of AU22.

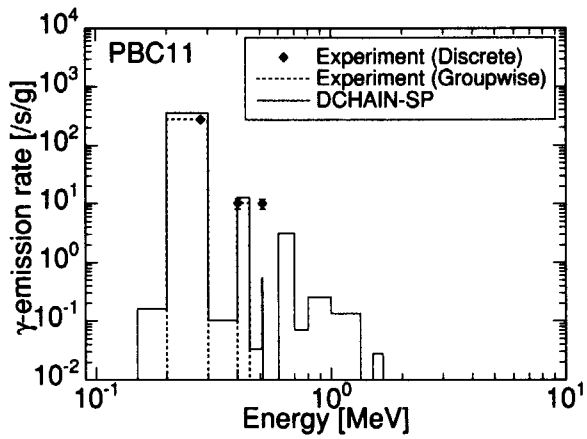

Fig. 2.31 Decay γ-ray spectrum of PBC11.

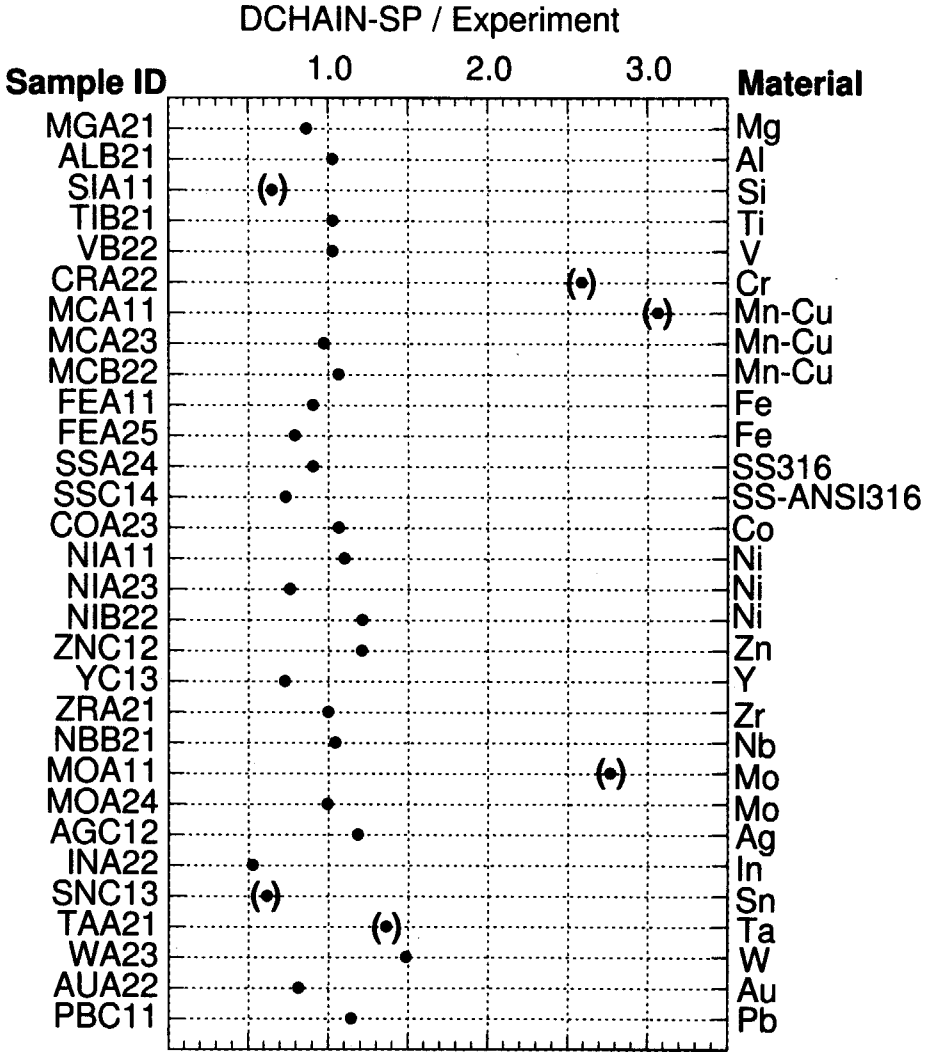

Fig. 2.32 Comparison of total amount of gamma-ray energy release between DCHAIN-SP calculations and experiments. Large discrepancies indicated in parenthesis are not due to the DHCAIN-SP calculations. See the text for details.

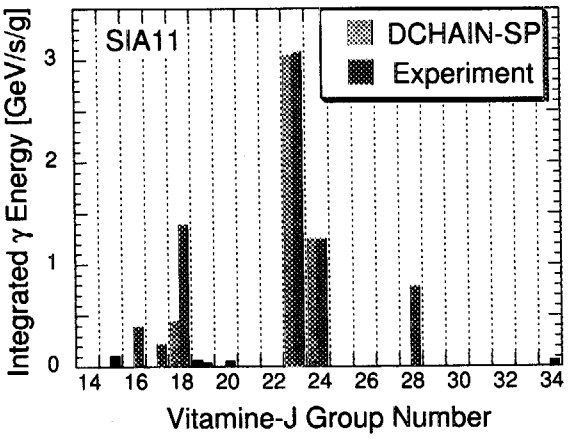

Fig. 2.33 Comparison of groupwise γ-ray energy release obtained by DCHAIN-SP calculation and experiment for case SIA11.

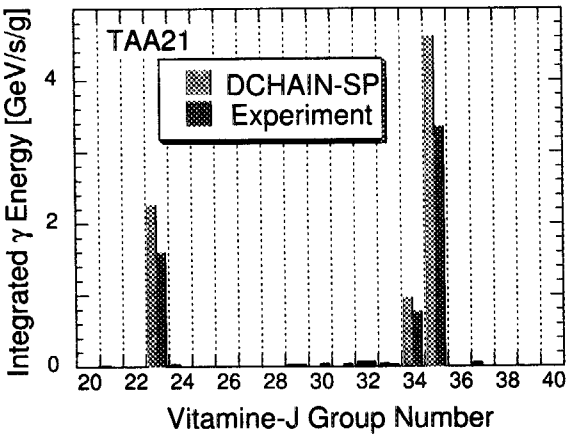

Fig. 2.34 Comparison of groupwise γ-ray energy release obtained by DCHAIN-SP calculation and experiment for case TAA21.

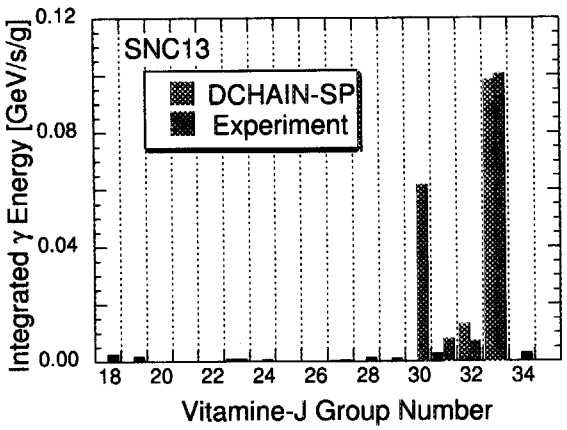

Fig. 2.35 Comparison of groupwise γ-ray energy release obtained by DCHAIN-SP calculation and experiment for case SNC13.

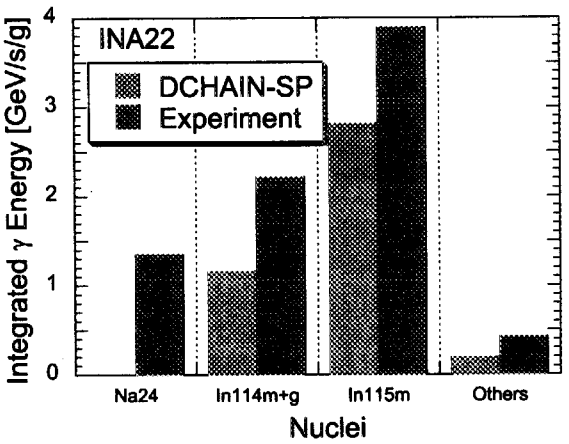

Fig. 2.36 Comparison of groupwise γ-ray energy release obtained by DCHAIN-SP calculation and experiment for case INA22.

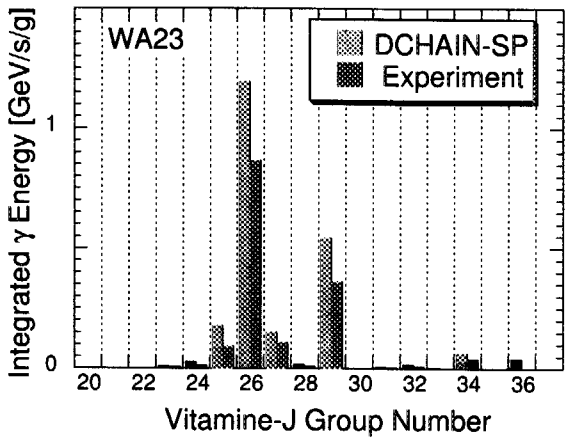

Fig. 2.37 Comparison of groupwise γ-ray energy release obtained by DCHAIN-SP calculation and experiment for case WA23.

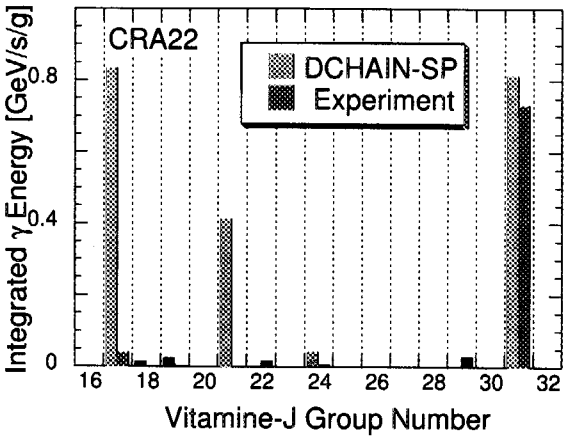

Fig. 2.38 Comparison of groupwise γ-ray energy release obtained by DCHAIN-SP calculation and experiment for case CRA22.

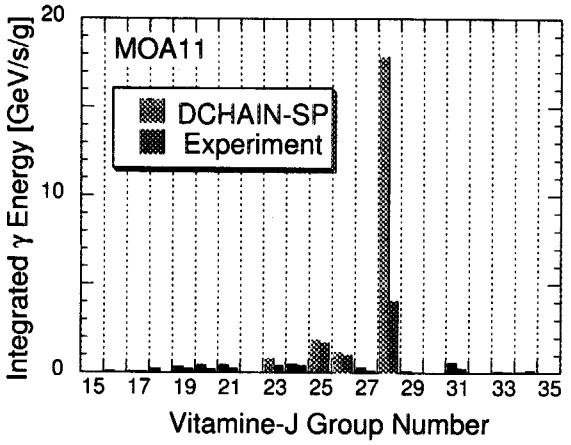

Fig. 2.39 Comparison of groupwise γ-ray energy release obtained by DCHAIN-SP calculation and experiment for case MOA11.

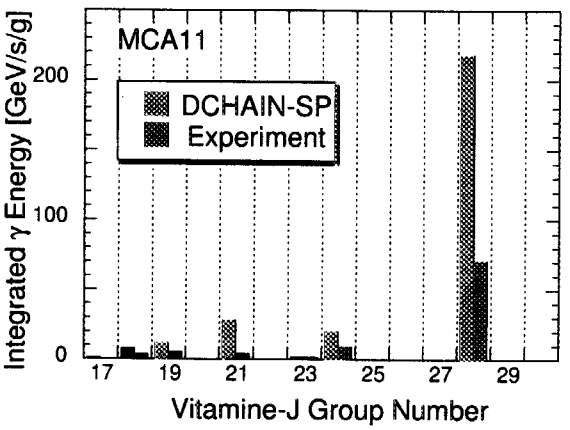

Fig. 2.40 Comparison of groupwise γ-ray energy release obtained by DCHAIN-SP calculation and experiment for case MCA11.

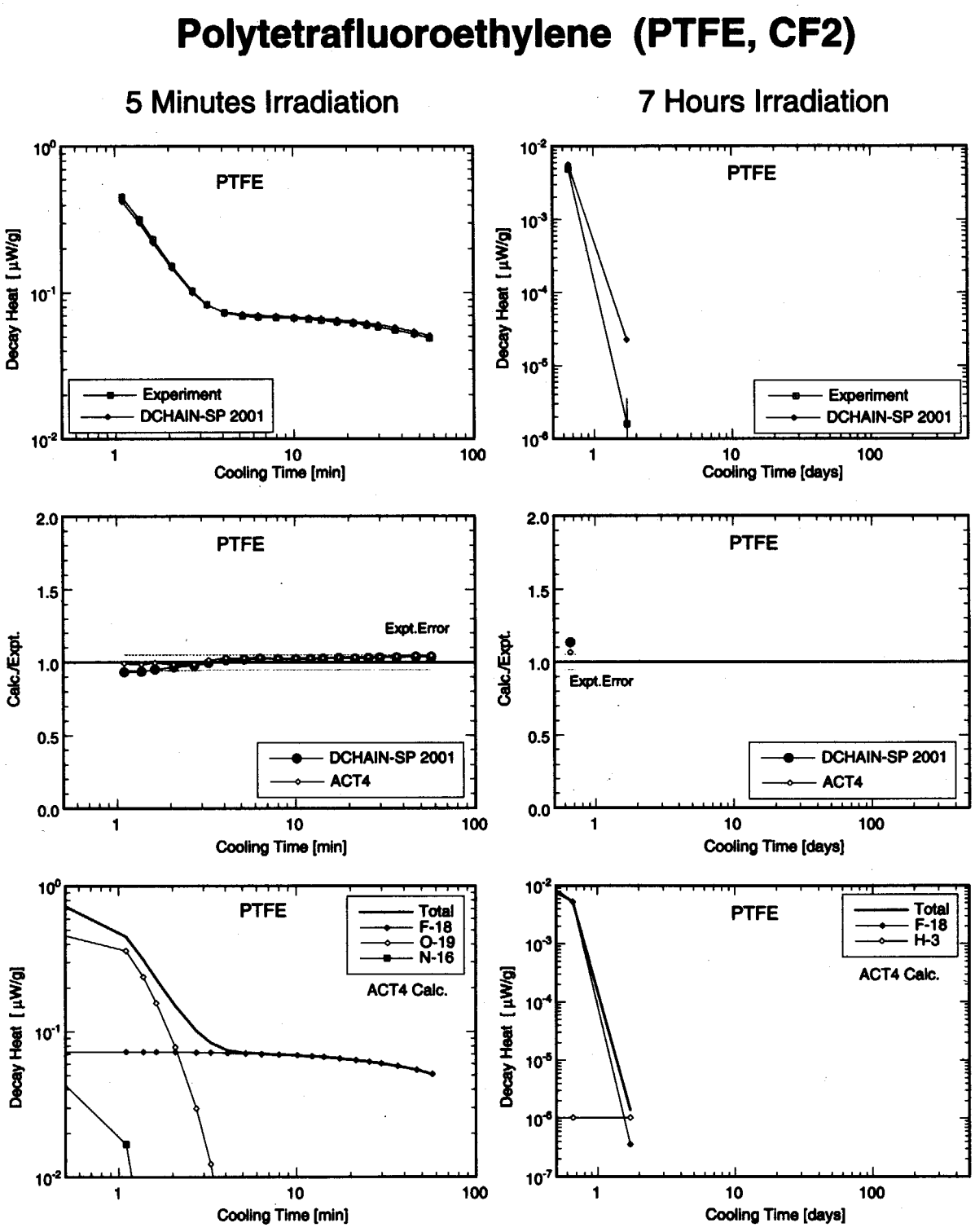

Fig. 3.1 Results for decay heat benchmark on polytetrafluoroethylene.

SODIUM CARBONATE (Na2CO3)

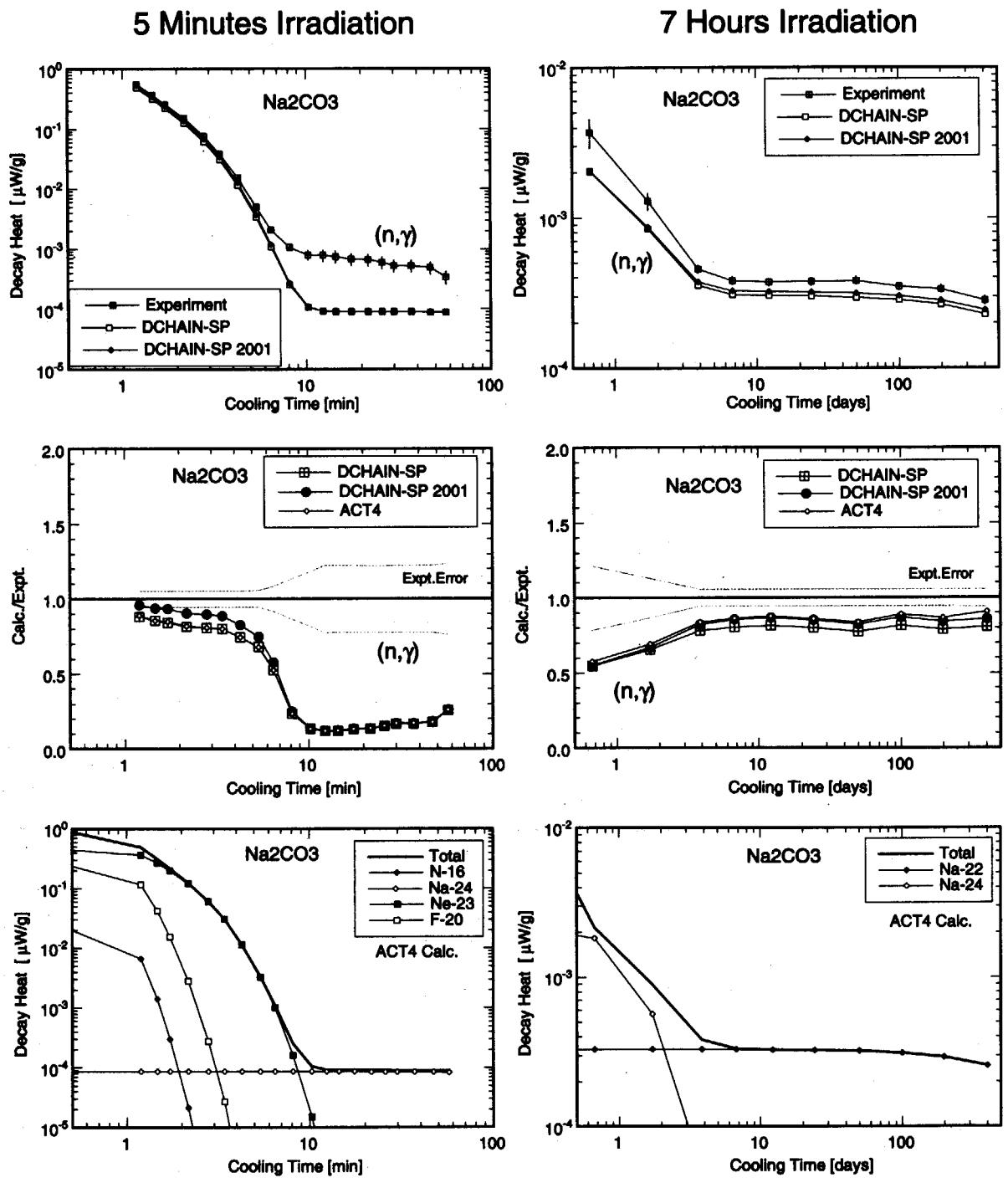

Fig. 3.2 Results for decay heat benchmark on sodium carbonate.

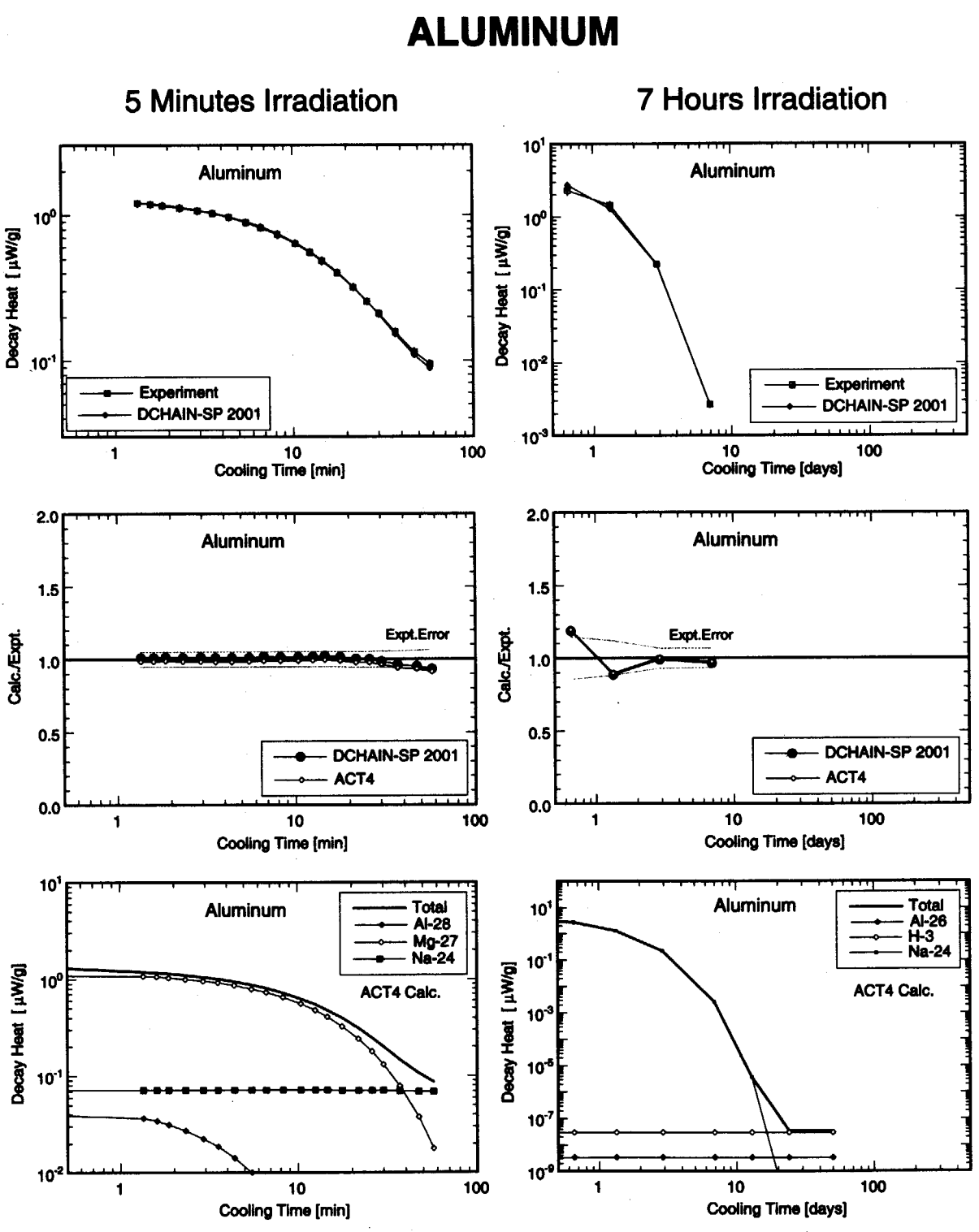

Fig. 3.3 Results for decay heat benchmark on aluminum.

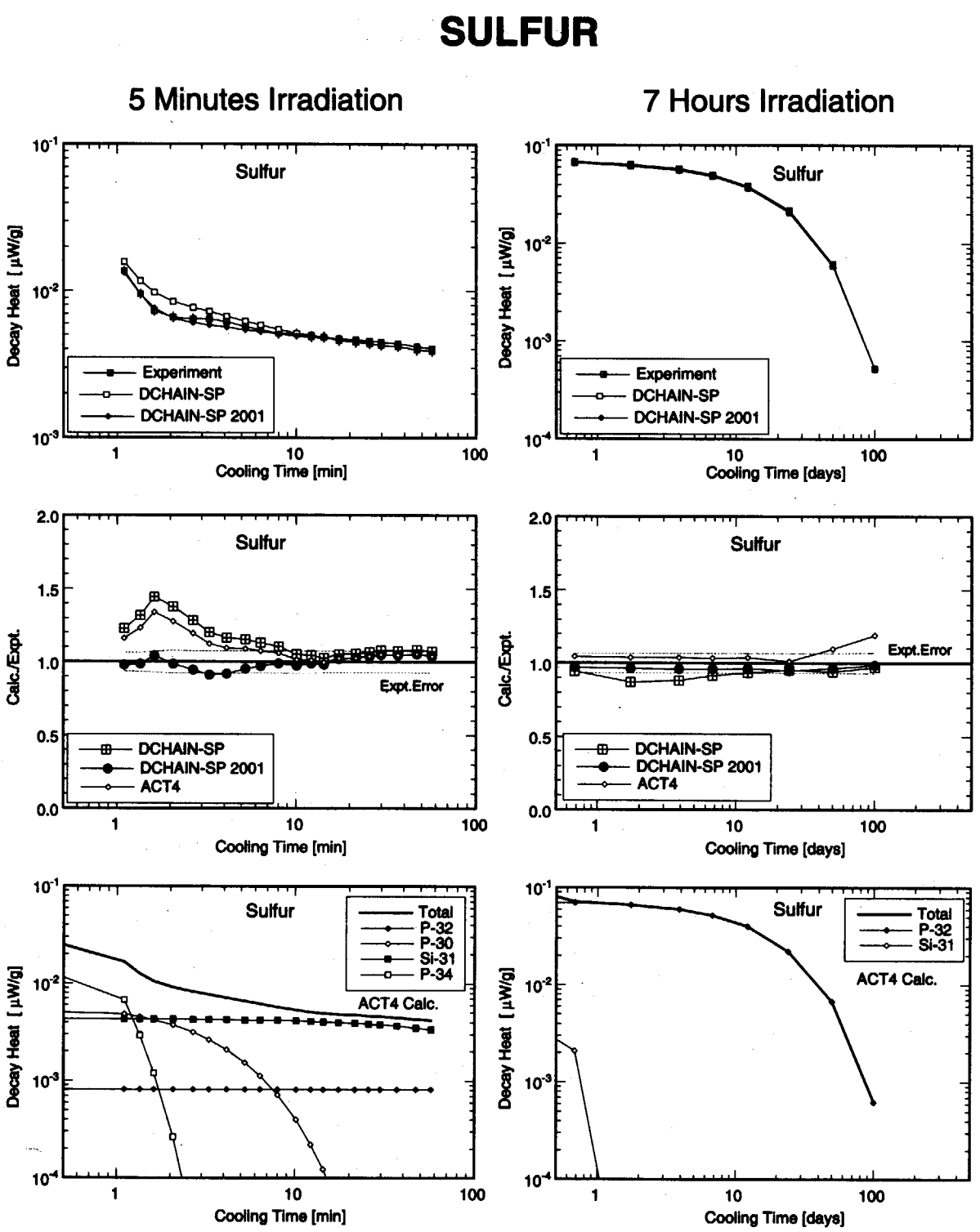

Fig. 3.4 Results for decay heat benchmark on sulfur.

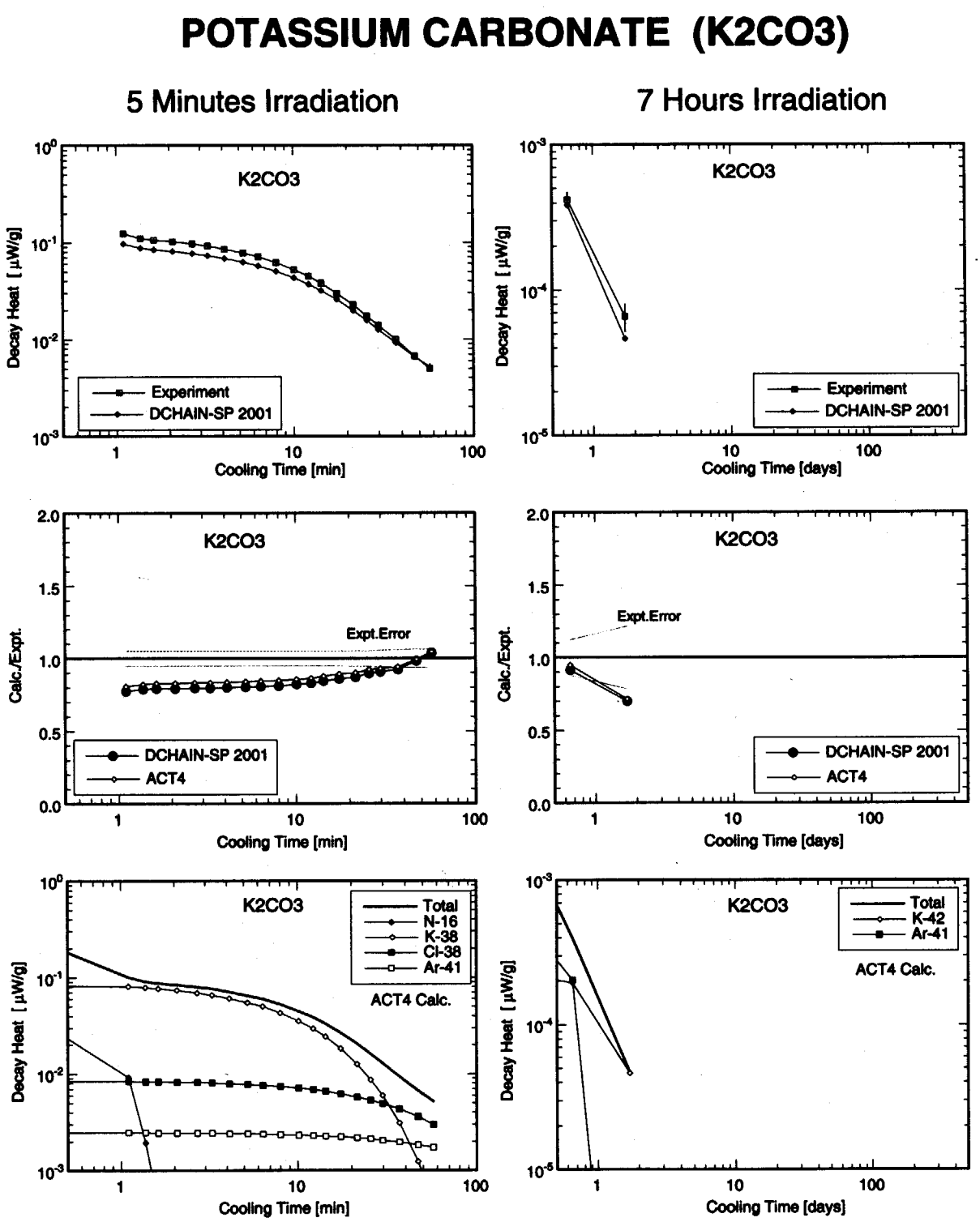

Fig. 3.5 Results for decay heat benchmark on potassium carbonate.

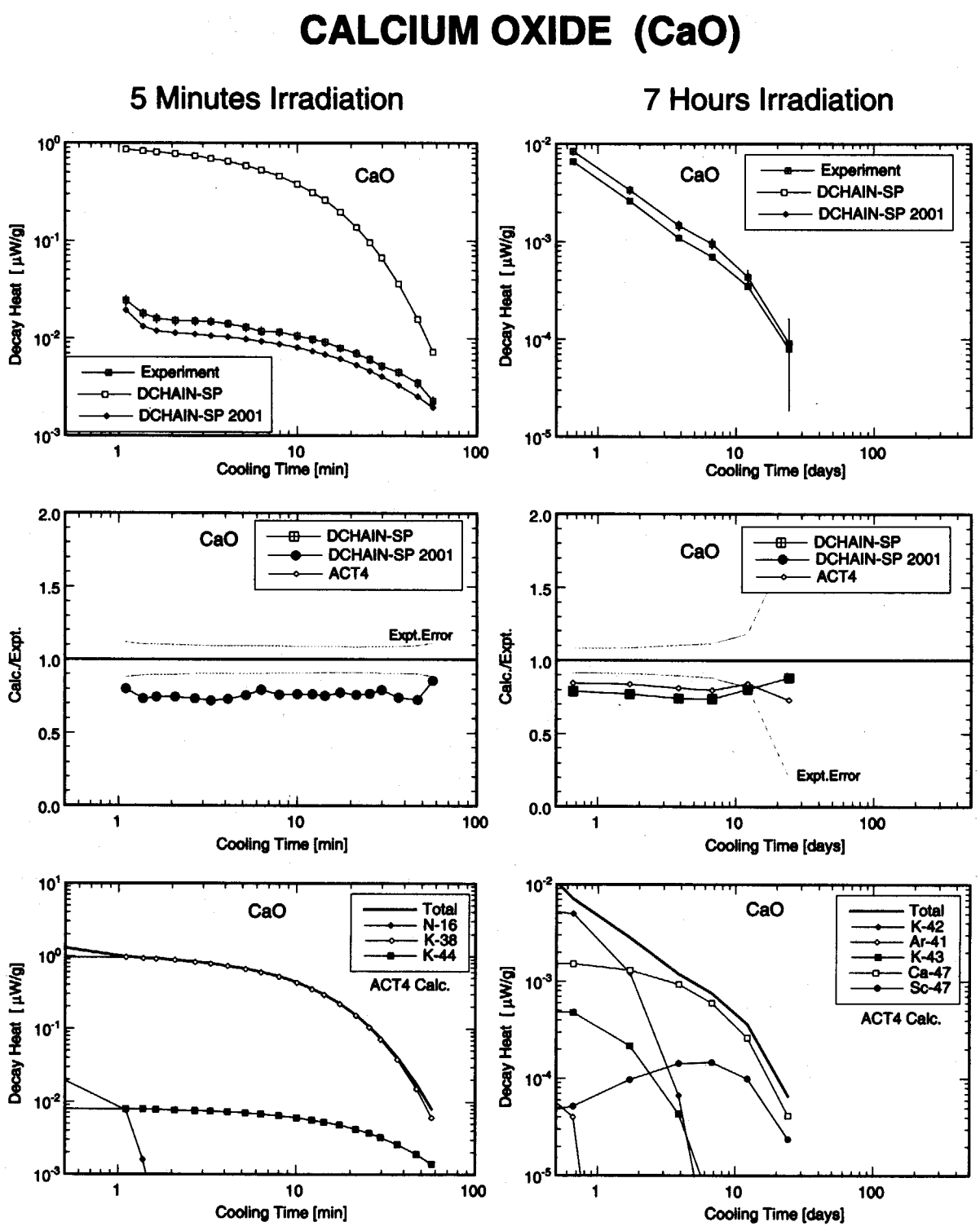

Fig. 3.6 Results for decay heat benchmark on calcium oxcide.

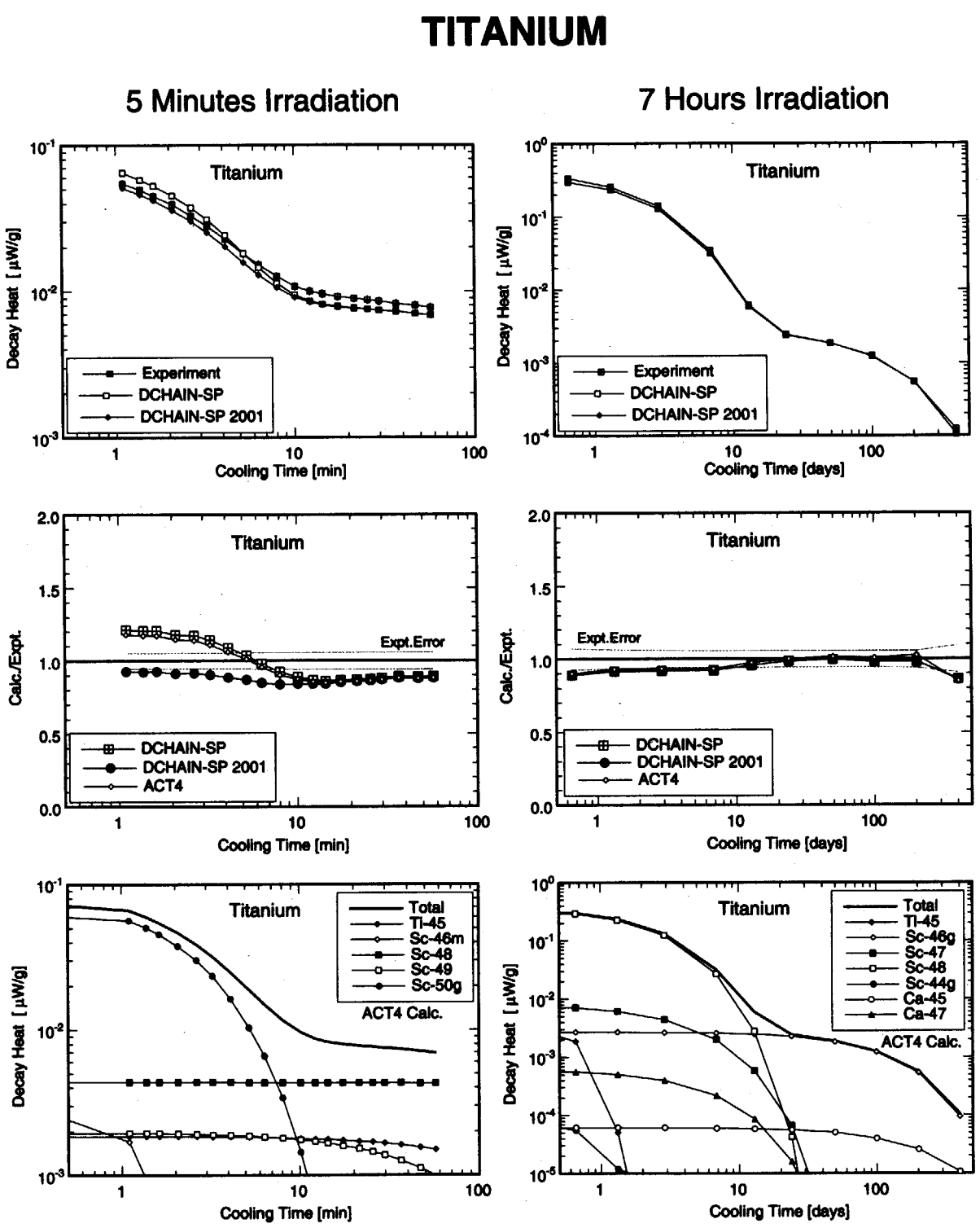

Fig. 3.7 Results for decay heat benchmark on titanium.

VANADIUM

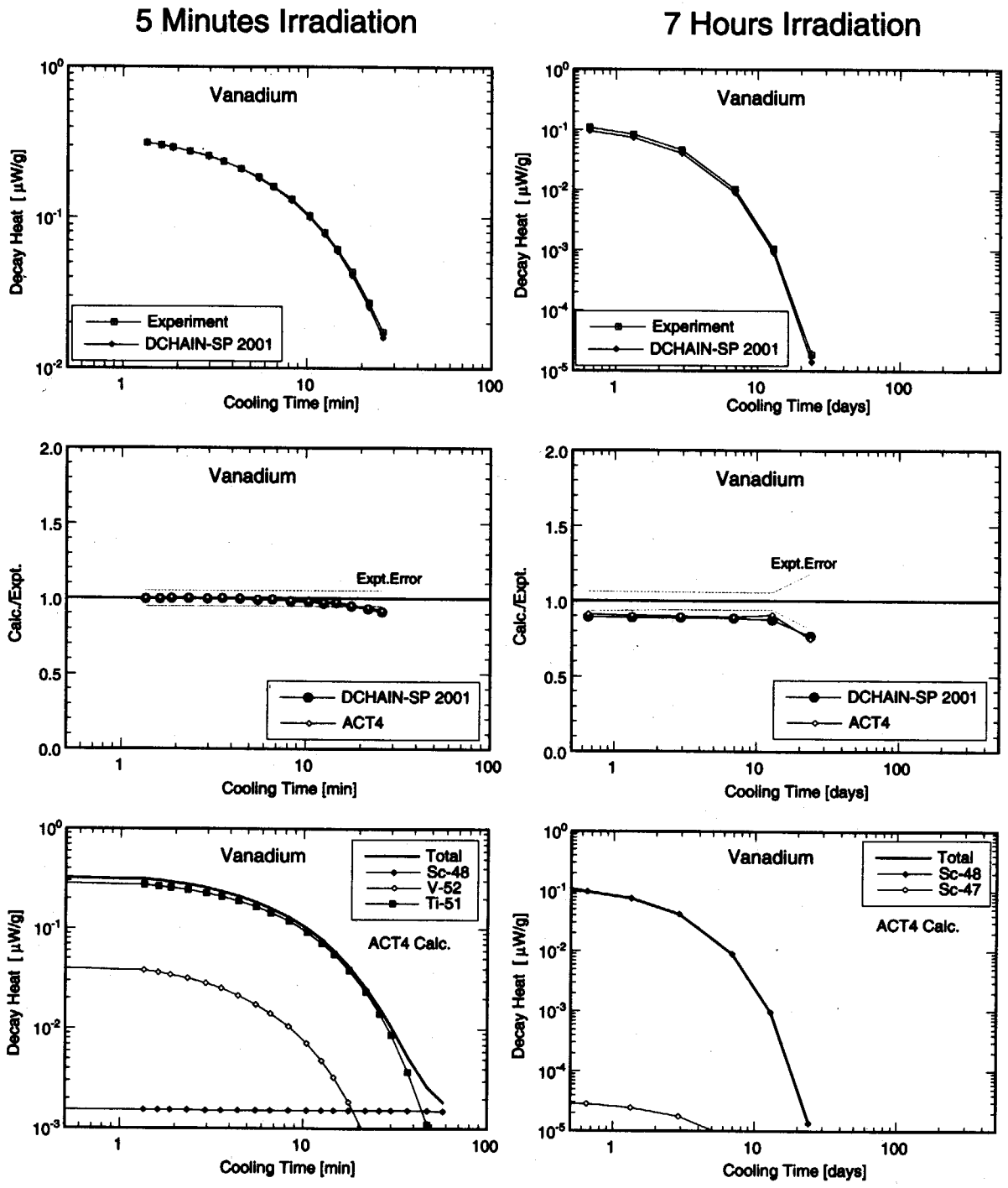

Fig. 3.8 Results for decay heat benchmark on vanadium.

CHROMIUM

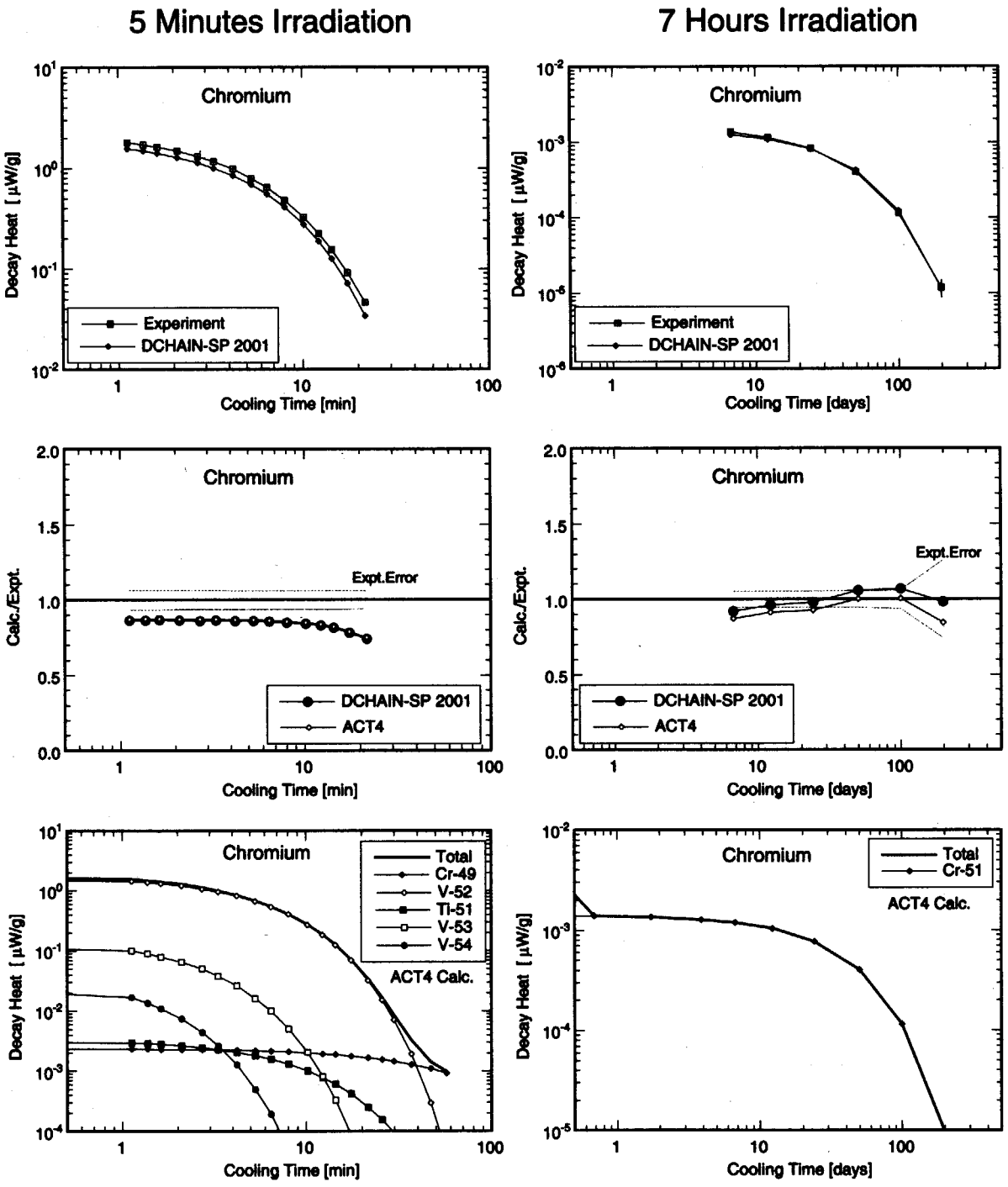

Fig. 3.9 Results for decay heat benchmark on chromium.

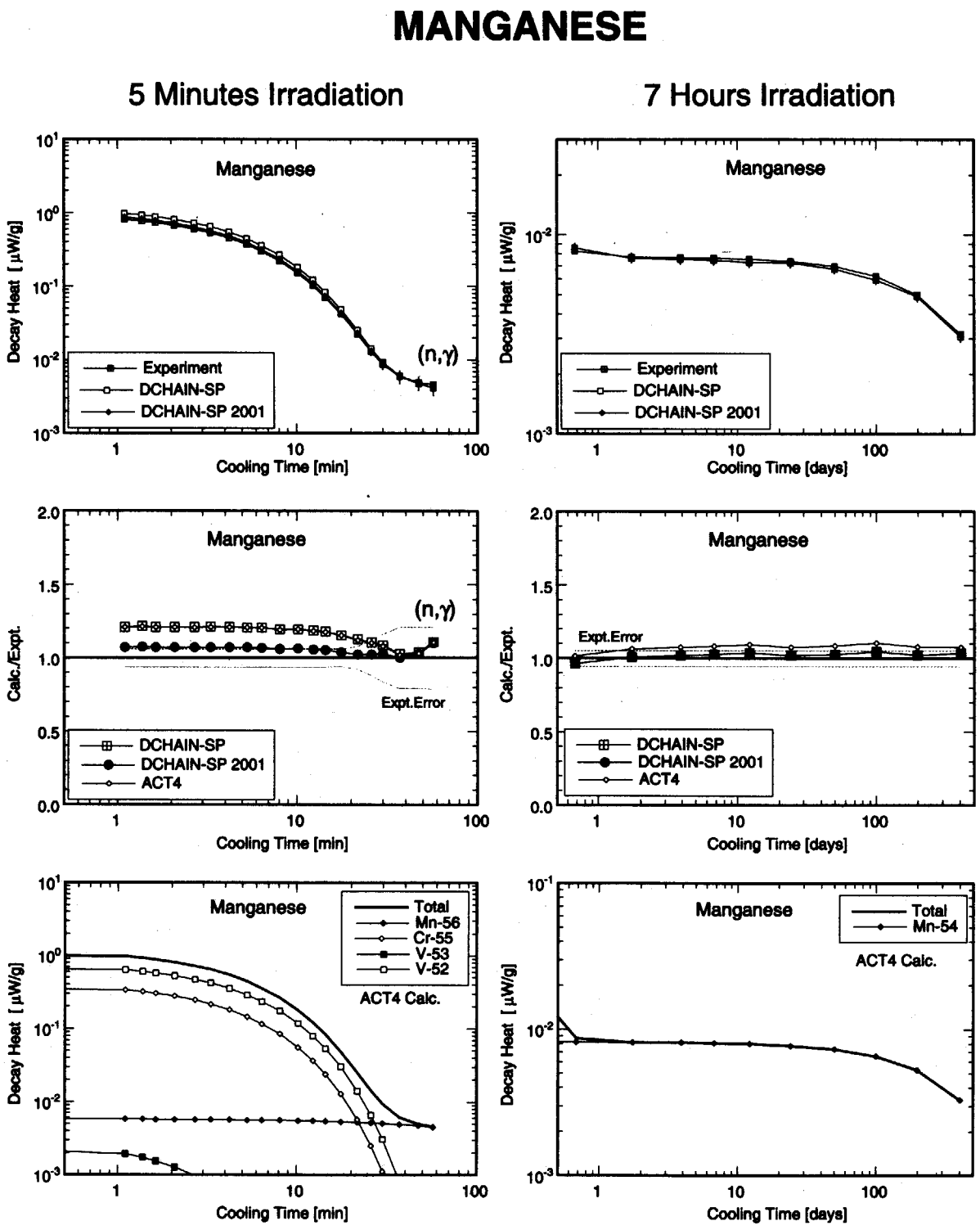

Fig. 3.10 Results for decay heat benchmark on manganese.

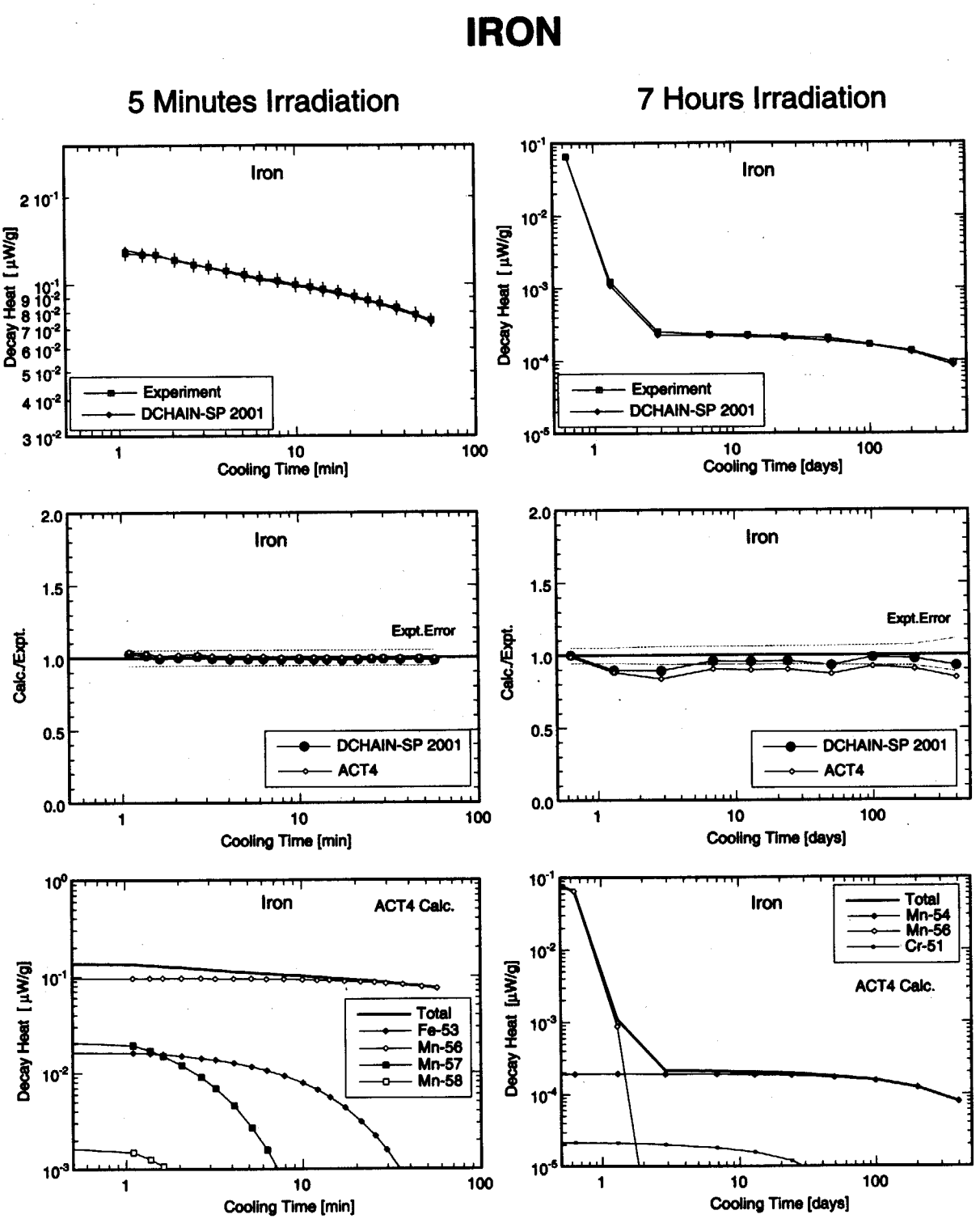

Fig. 3.11 Results for decay heat benchmark on iron.

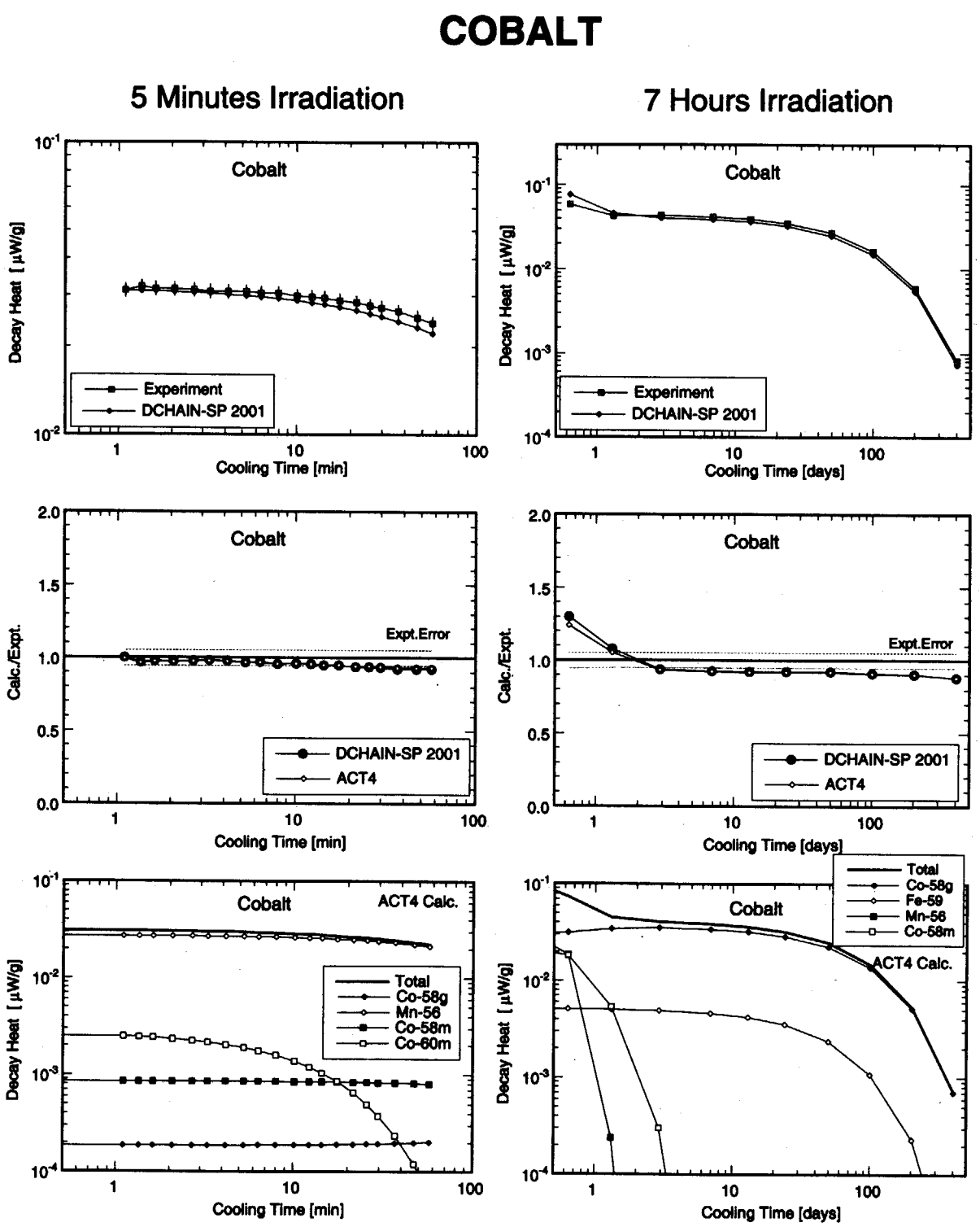

Fig. 3.12 Results for decay heat benchmark on cobalt.

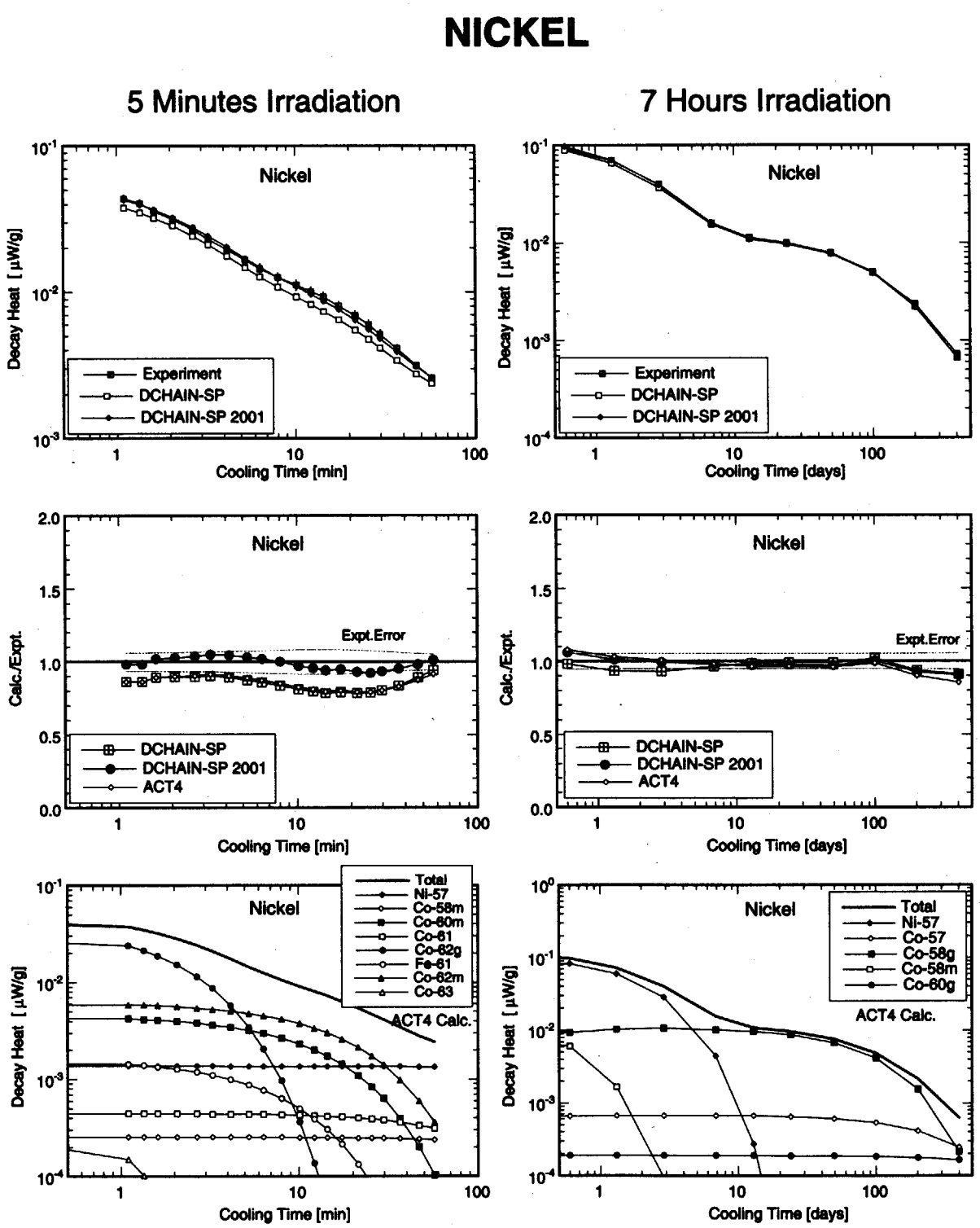

Fig. 3.13 Results for decay heat benchmark on nickel.

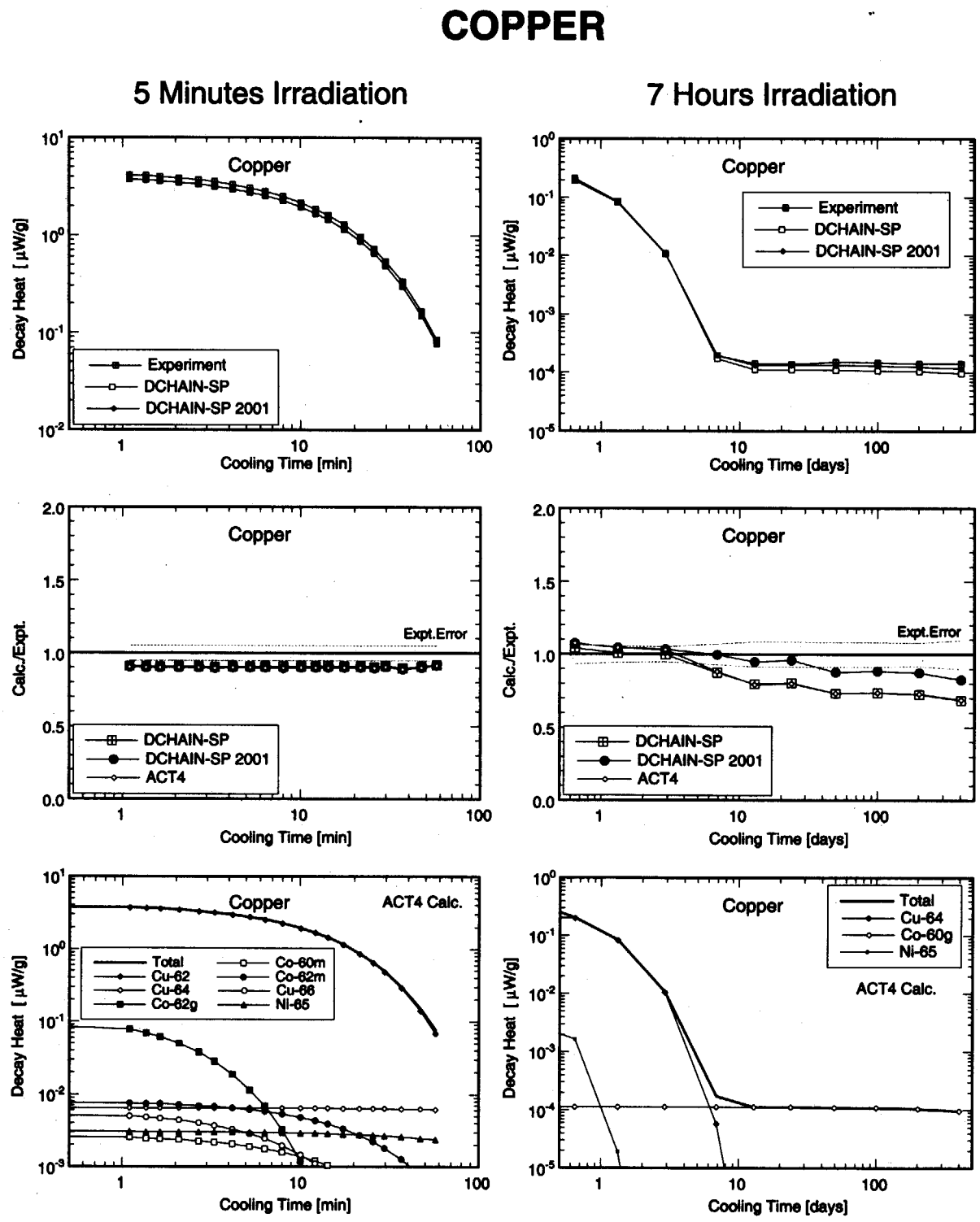

Fig. 3.14 Results for decay heat benchmark on copper.

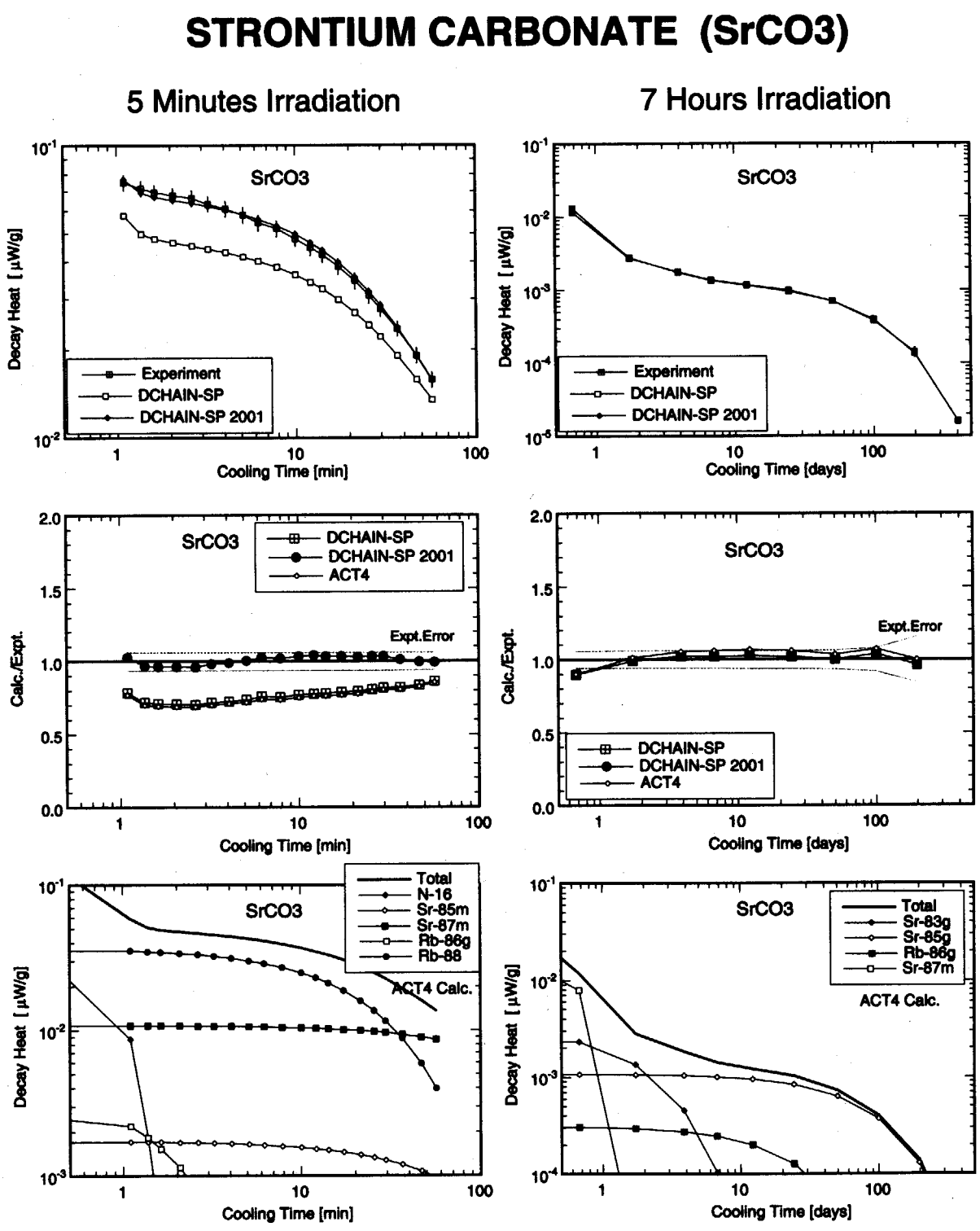

Fig. 3.15 Results for decay heat benchmark on strontium carbonate.

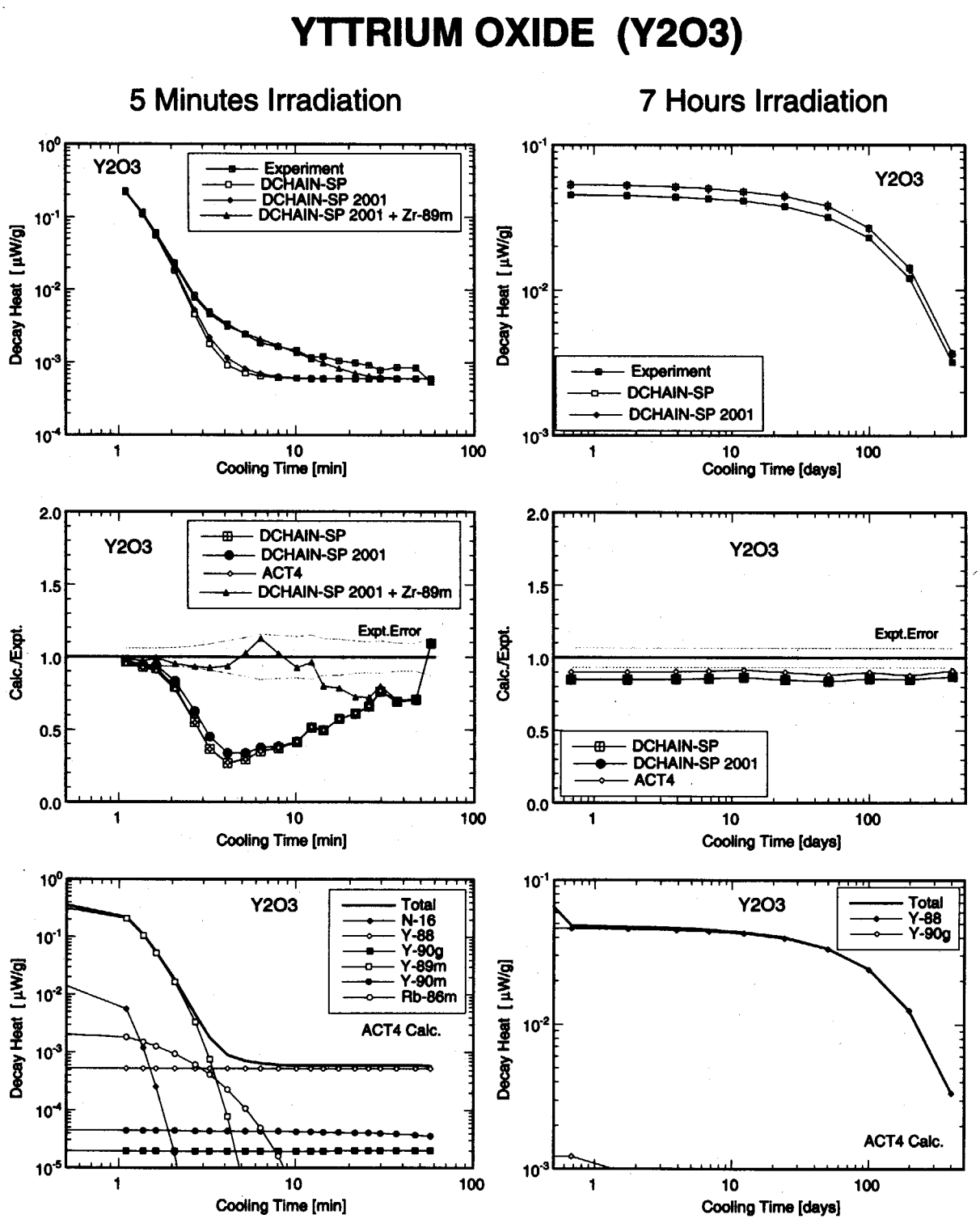

Fig. 3.16 Results for decay heat benchmark on yttrium oxide.

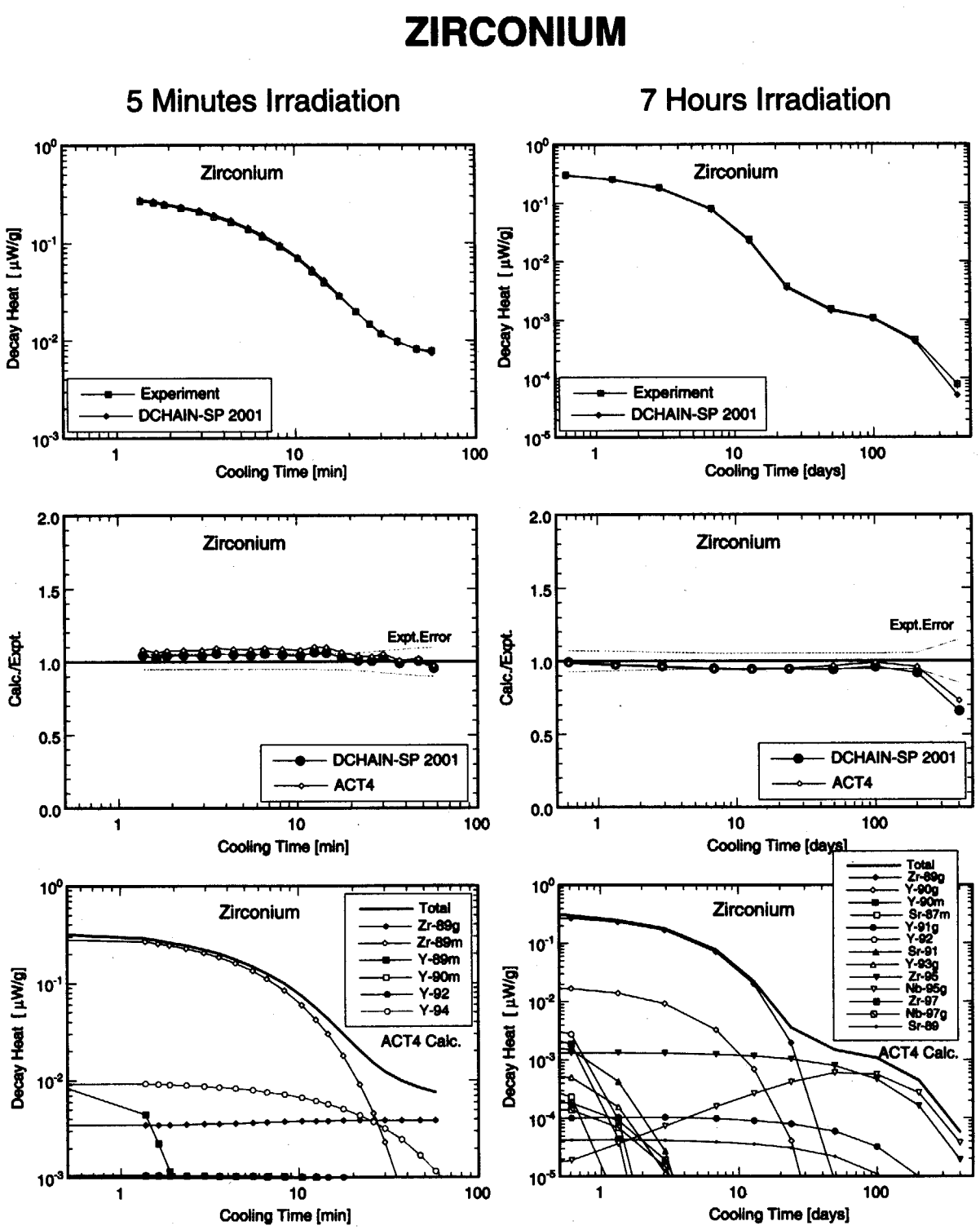

Fig. 3.17 Results for decay heat benchmark on zirconium.

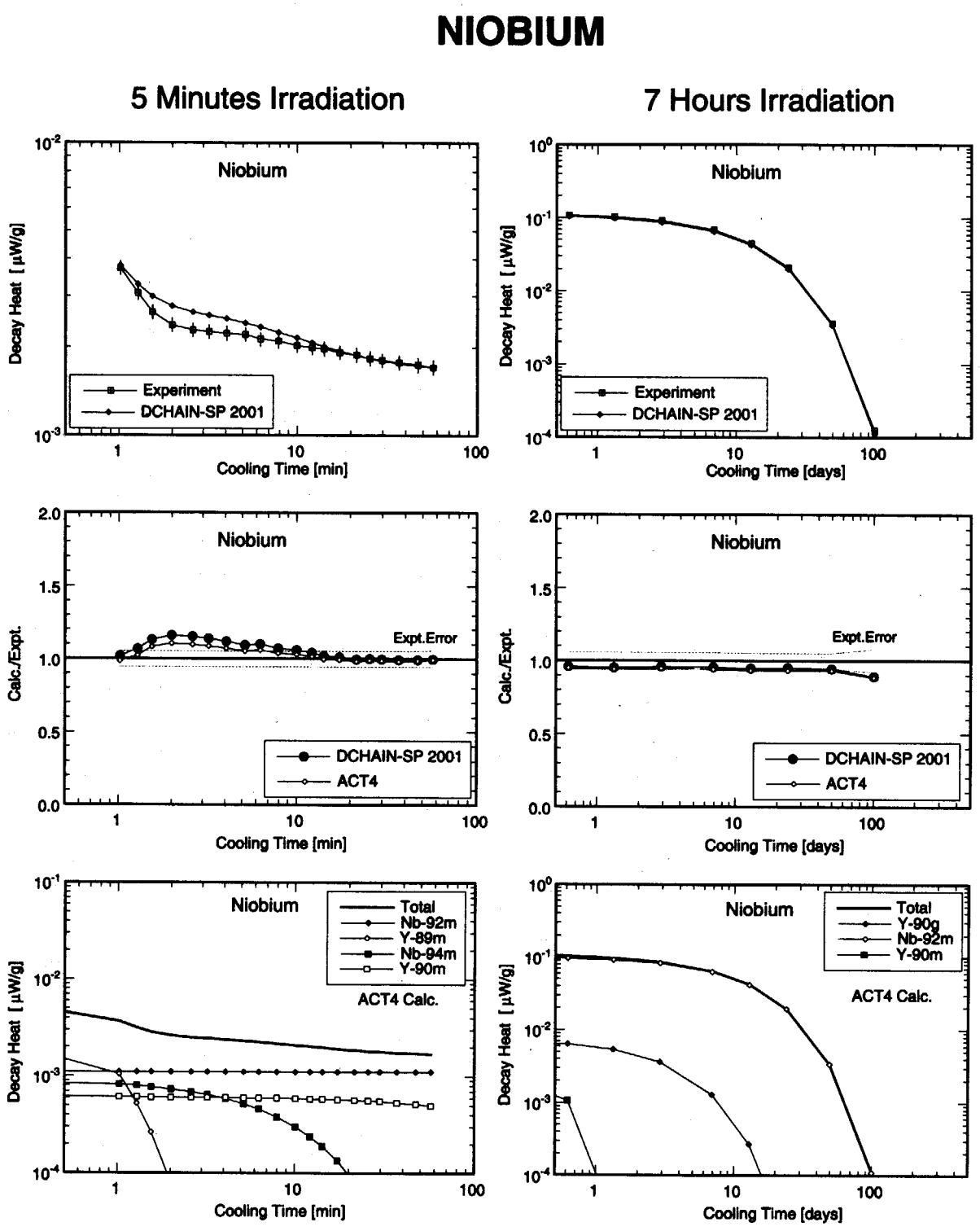

Fig. 3.18 Results for decay heat benchmark on niobium.

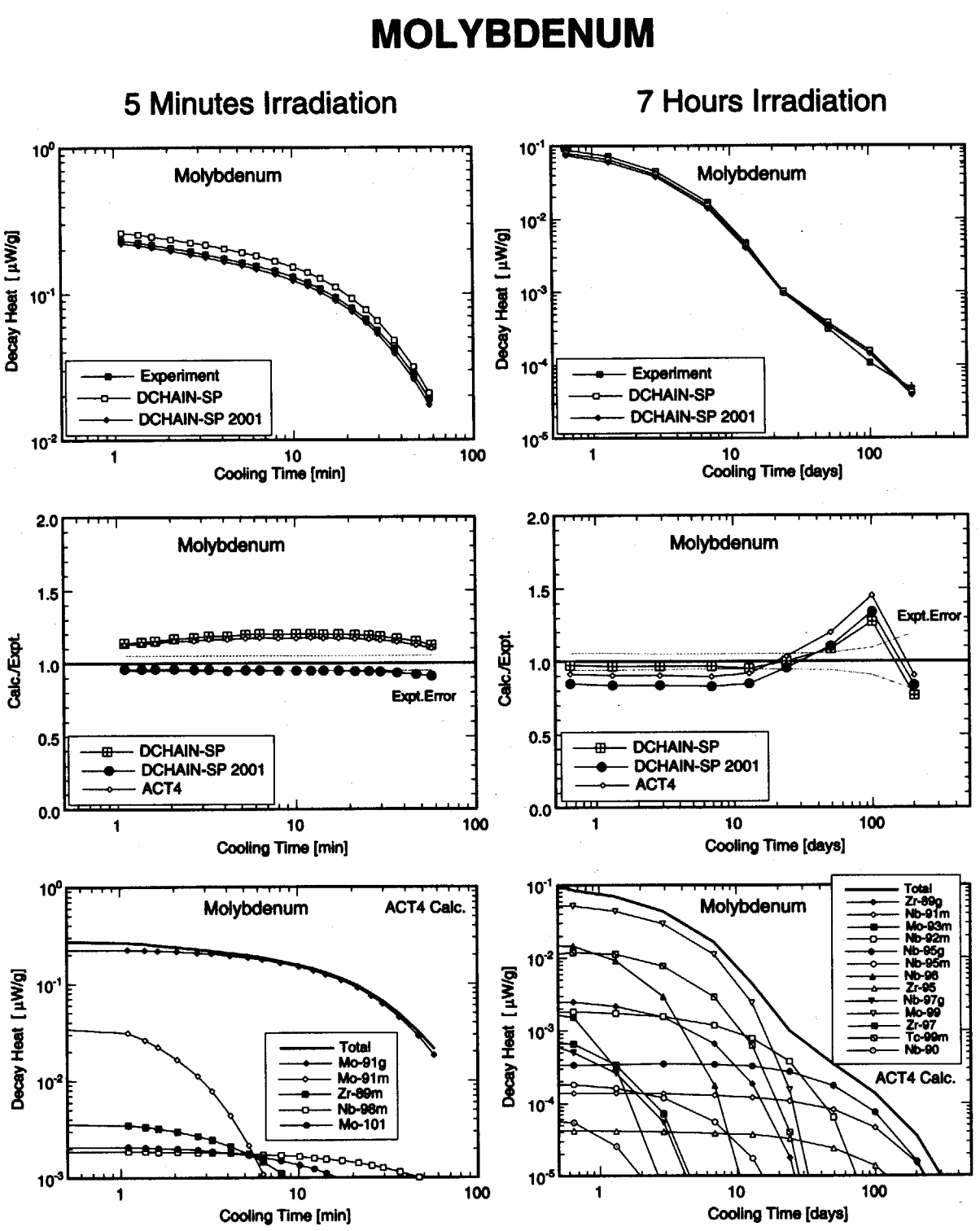

Fig. 3.19 Results for decay heat benchmark on molybdenum.

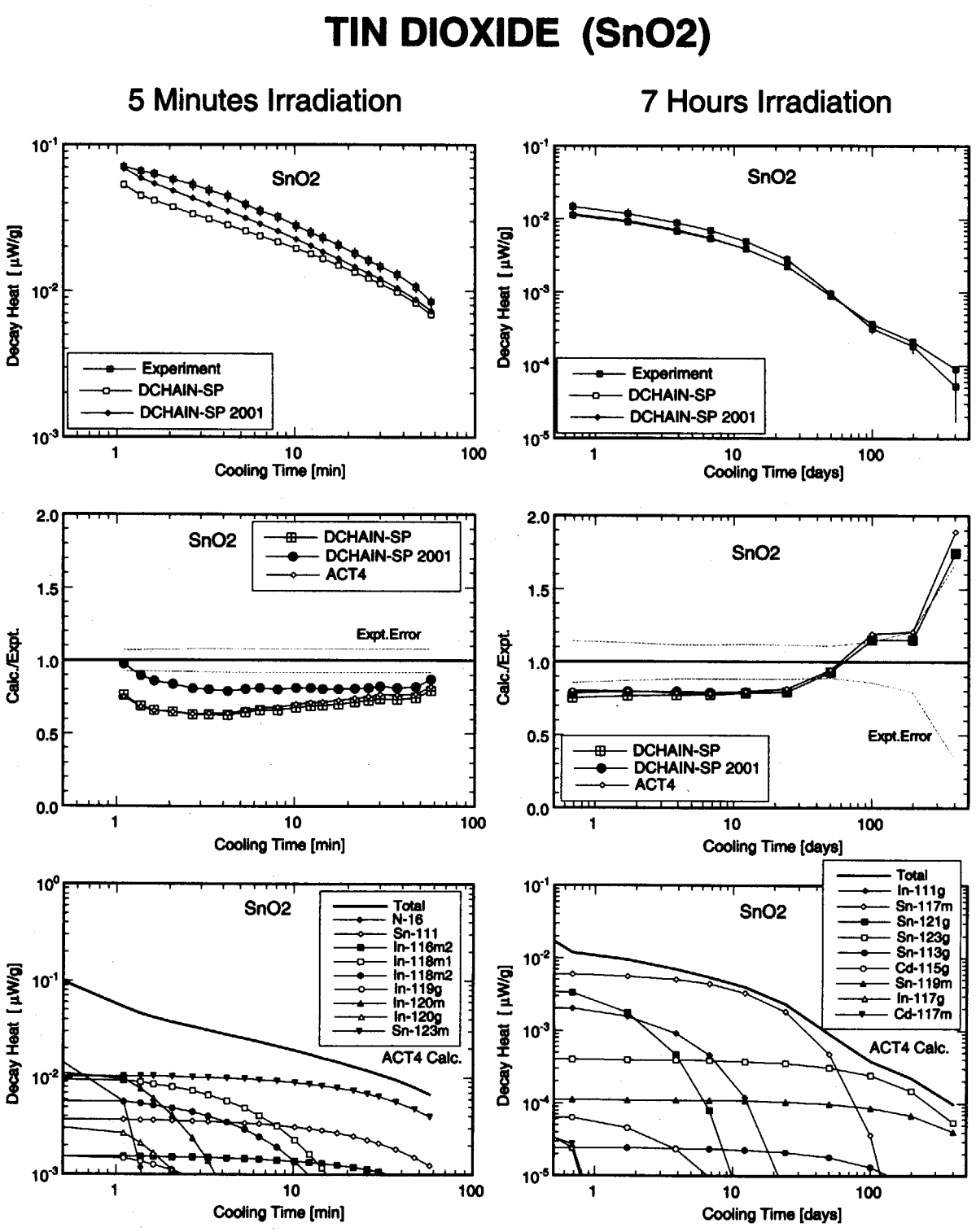

Fig. 3.20 Results for decay heat benchmark on tin dioxide.

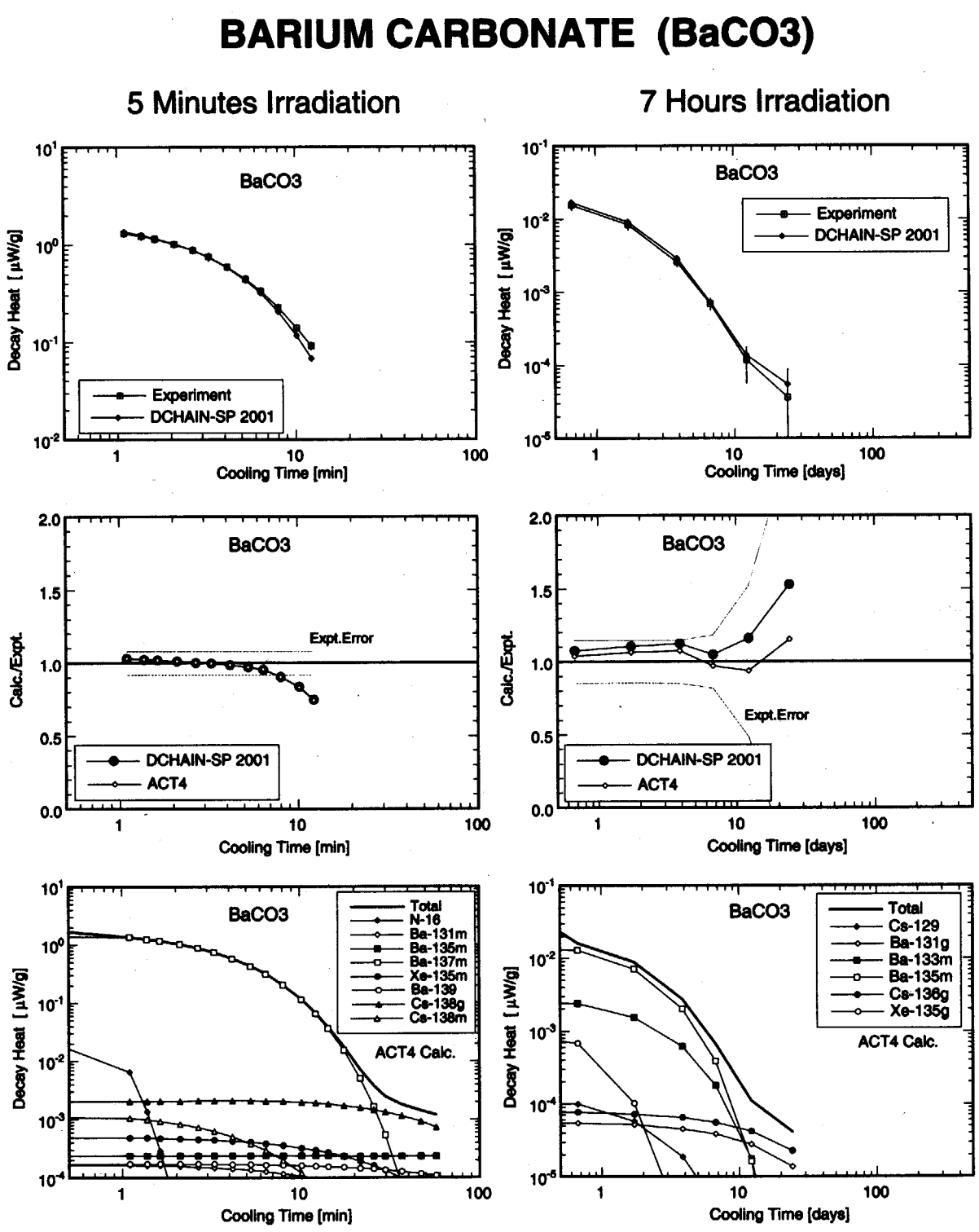

Fig. 3.21 Results for decay heat benchmark on barium carbonate.

TANTALUM

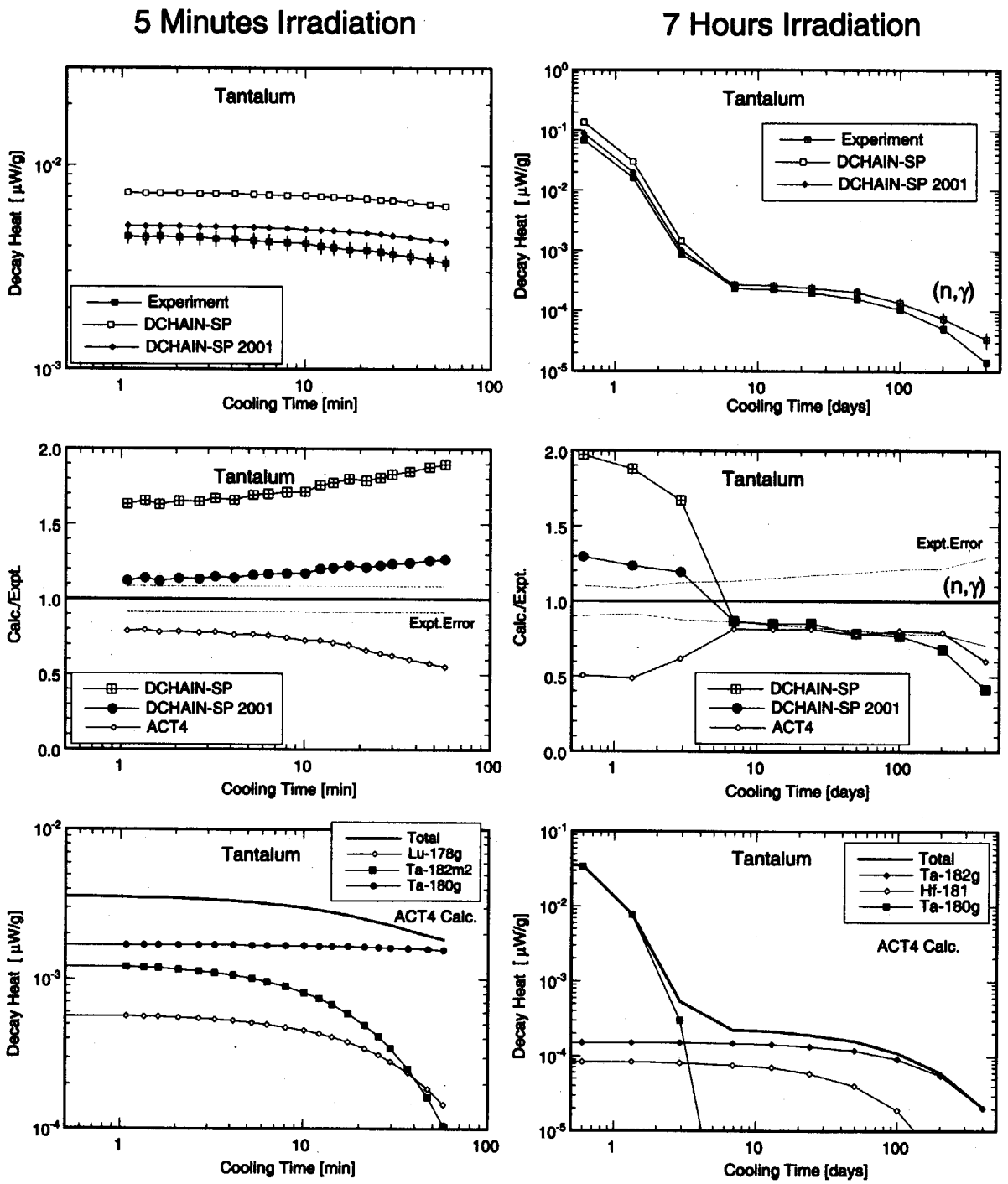

Fig. 3.22 Results for decay heat benchmark on tantalum.

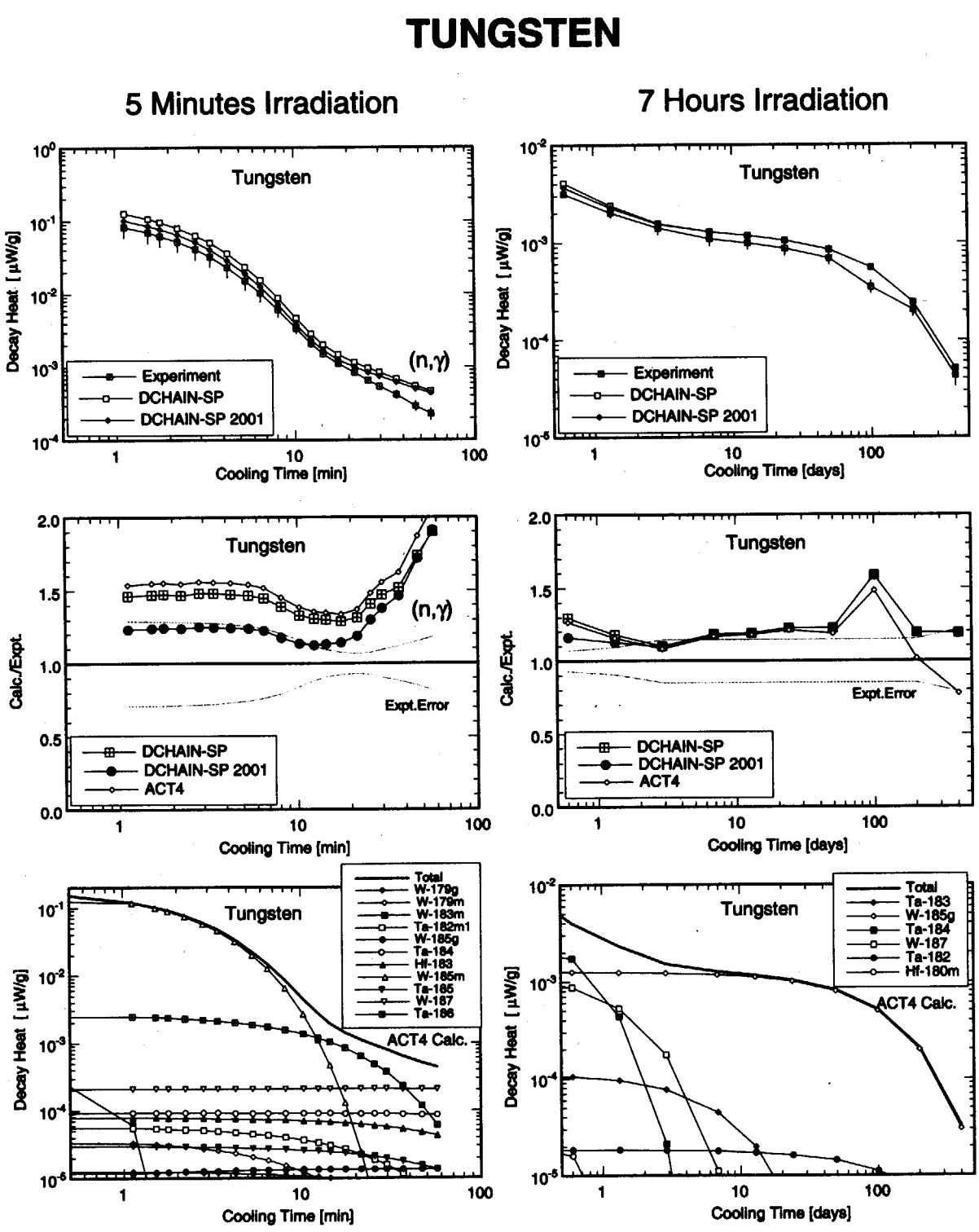

Fig. 3.23 Results for decay heat benchmark on tungsten.

RHENIUM

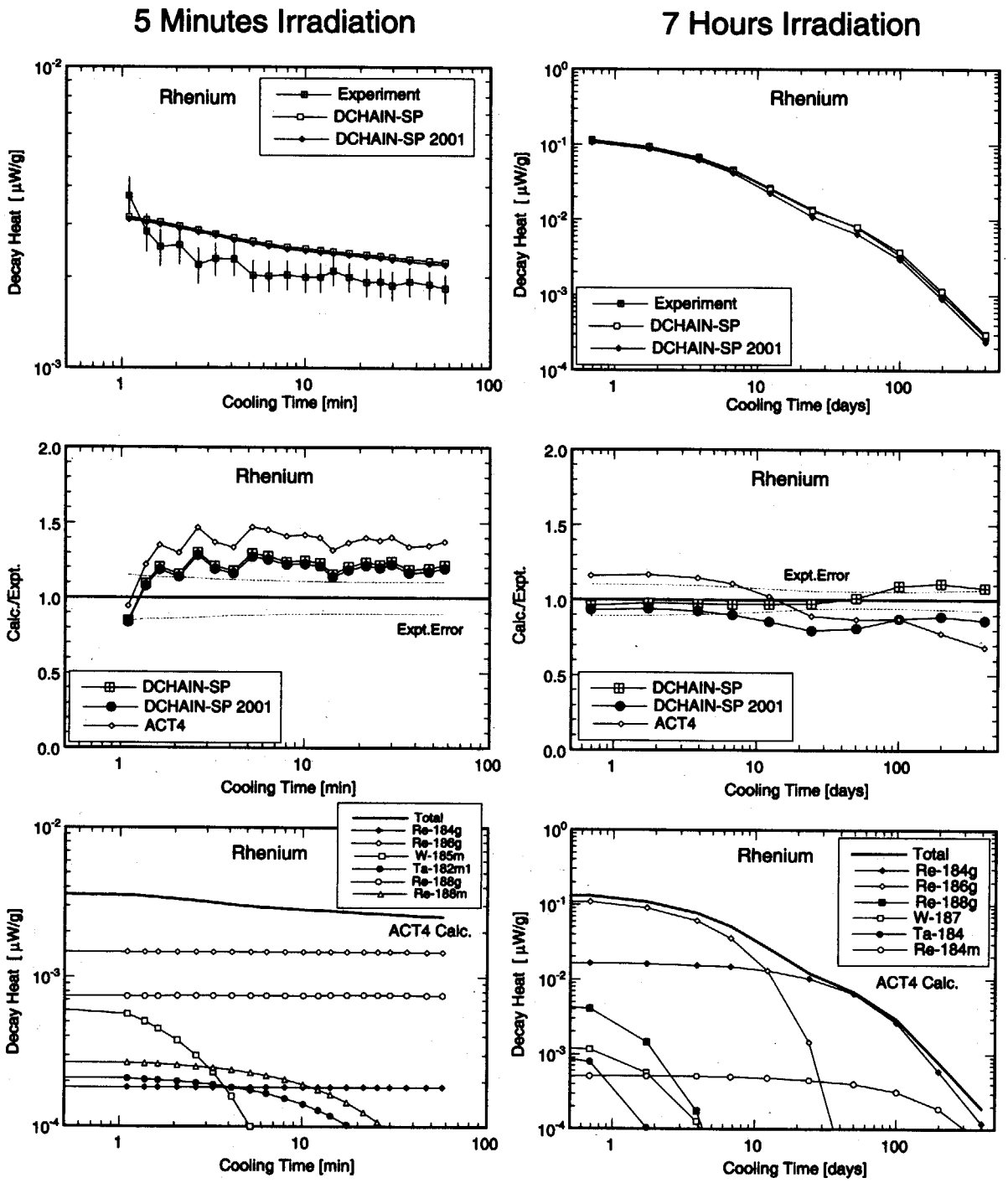

Fig. 3.24 Results for decay heat benchmark on rhenium.

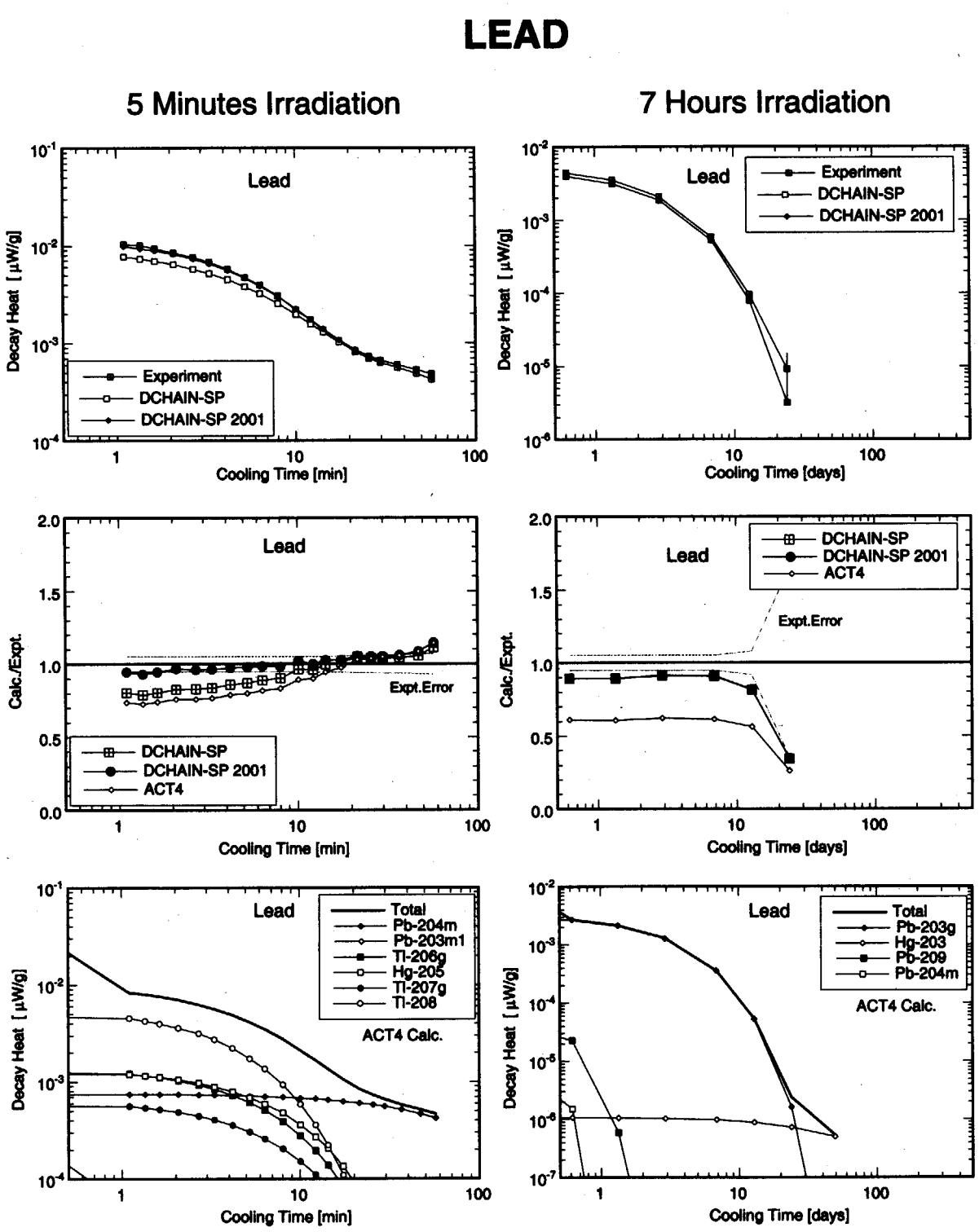

Fig. 3.25 Results for decay heat benchmark on lead.

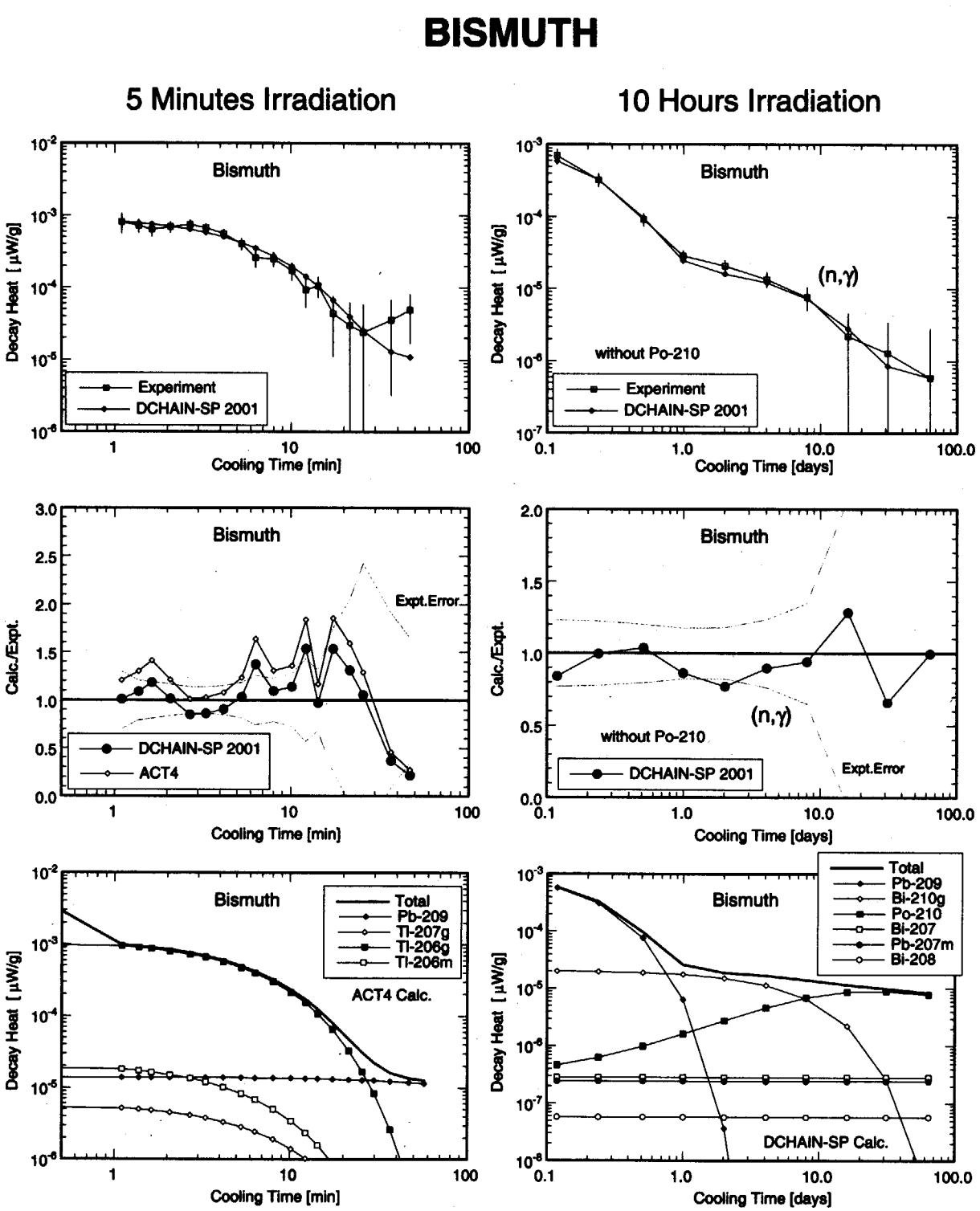

Fig. 3.26 Results for decay heat benchmark on bismuth.

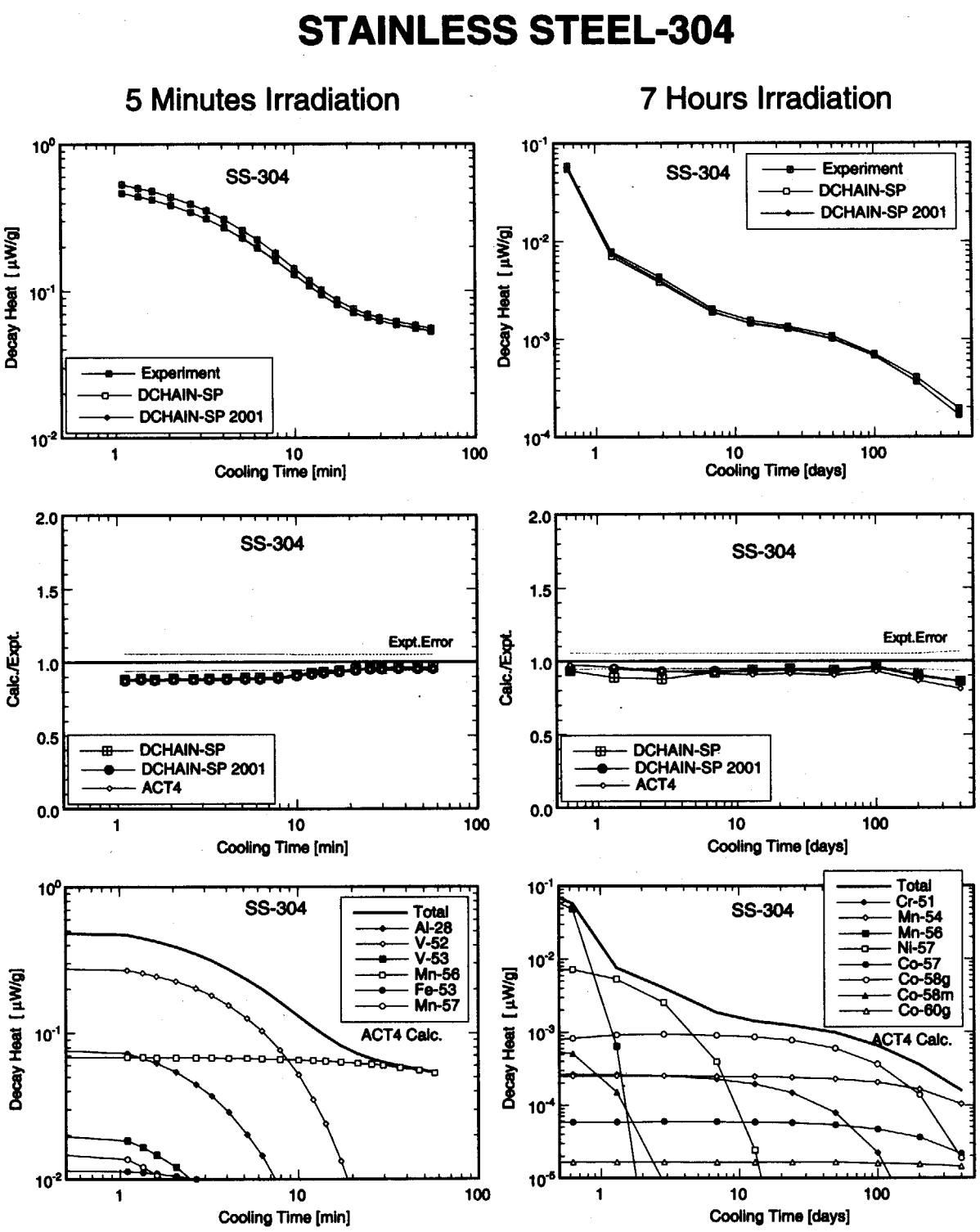

Fig. 3.27 Results for decay heat benchmark on stainless steel 304.

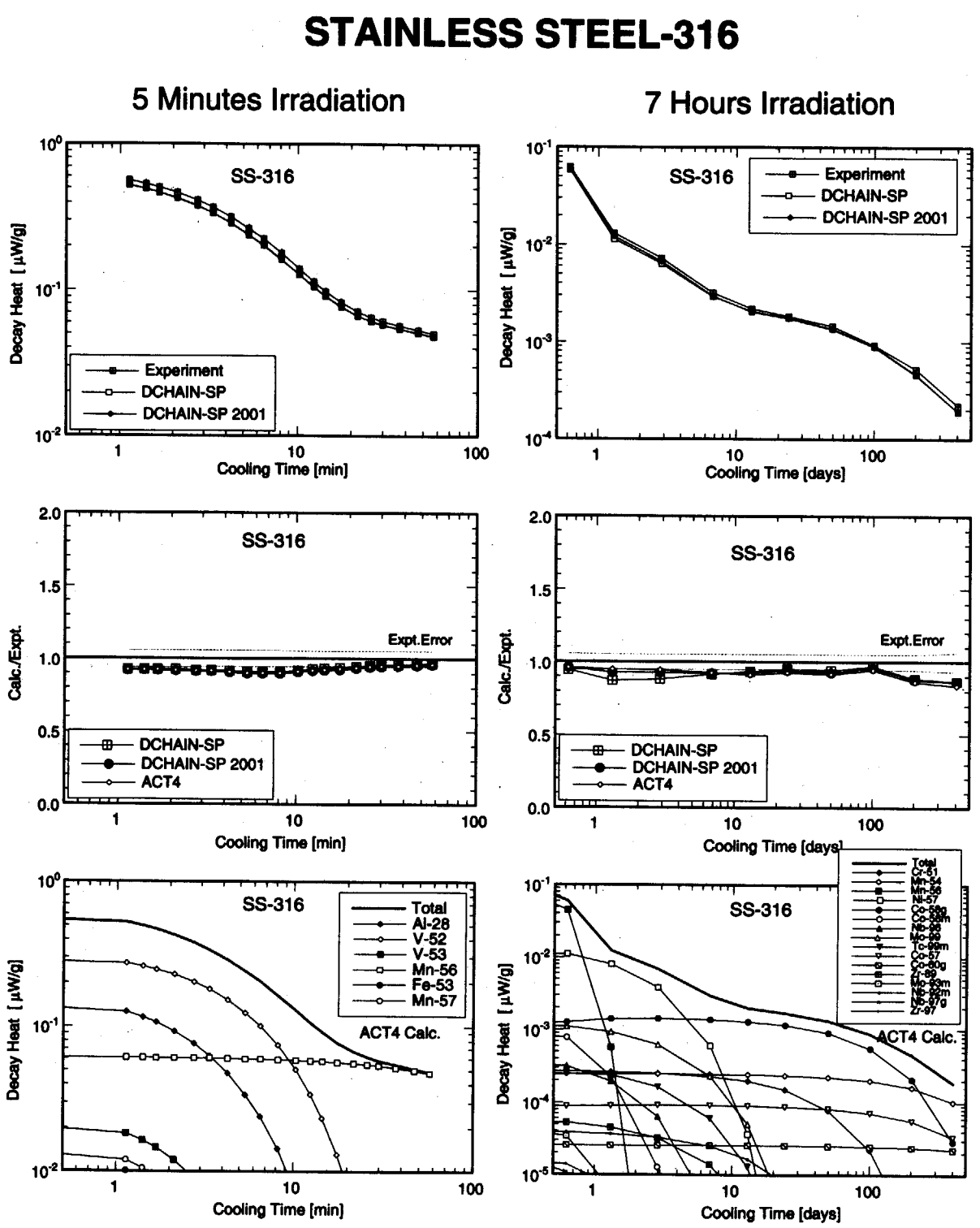

Fig. 3.28 Results for decay heat benchmark on stainless steel 316.

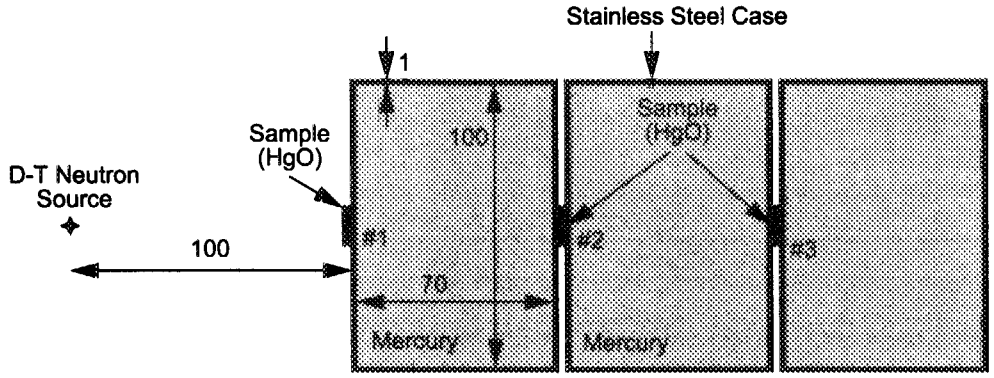

Fig. 4.1 Experimental configuration of the induced radioactivity and decay heat measurement experiments for mercury samples.

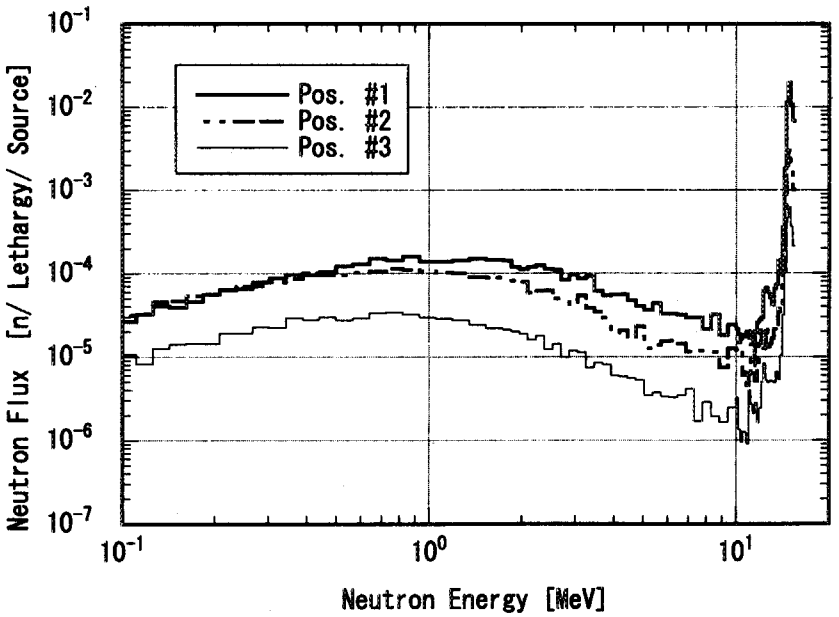

Fig. 4.2 Neutron flux spectra for the three positions in the integral experimental assembly of mercury for the induced radioactivity and decay heat measurement experiments.

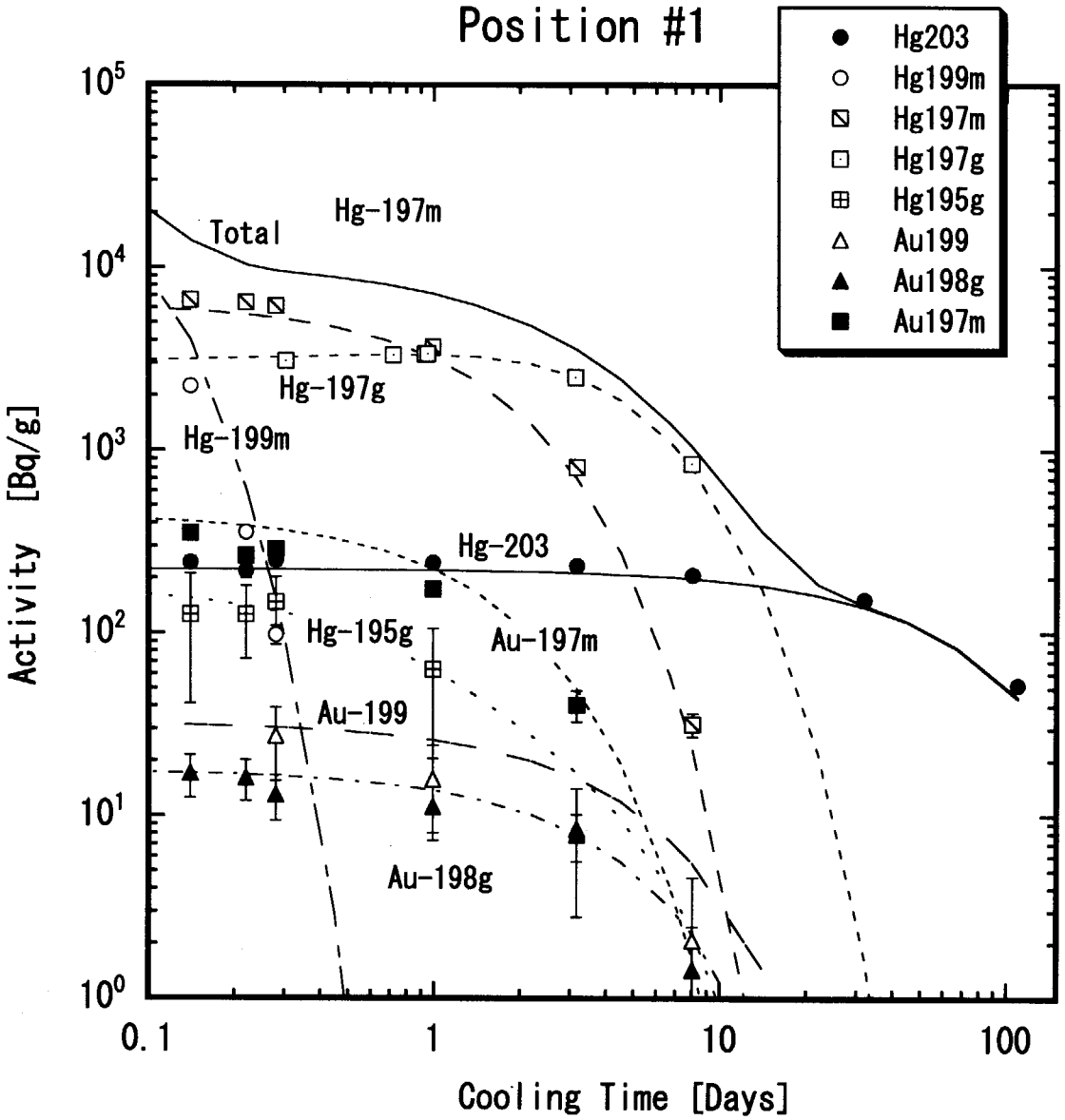

Fig. 4.3 Comparison of experimental (symbols) and calculated (lines) induced radioactivity for the mercury oxide samples irradiated at the position #1

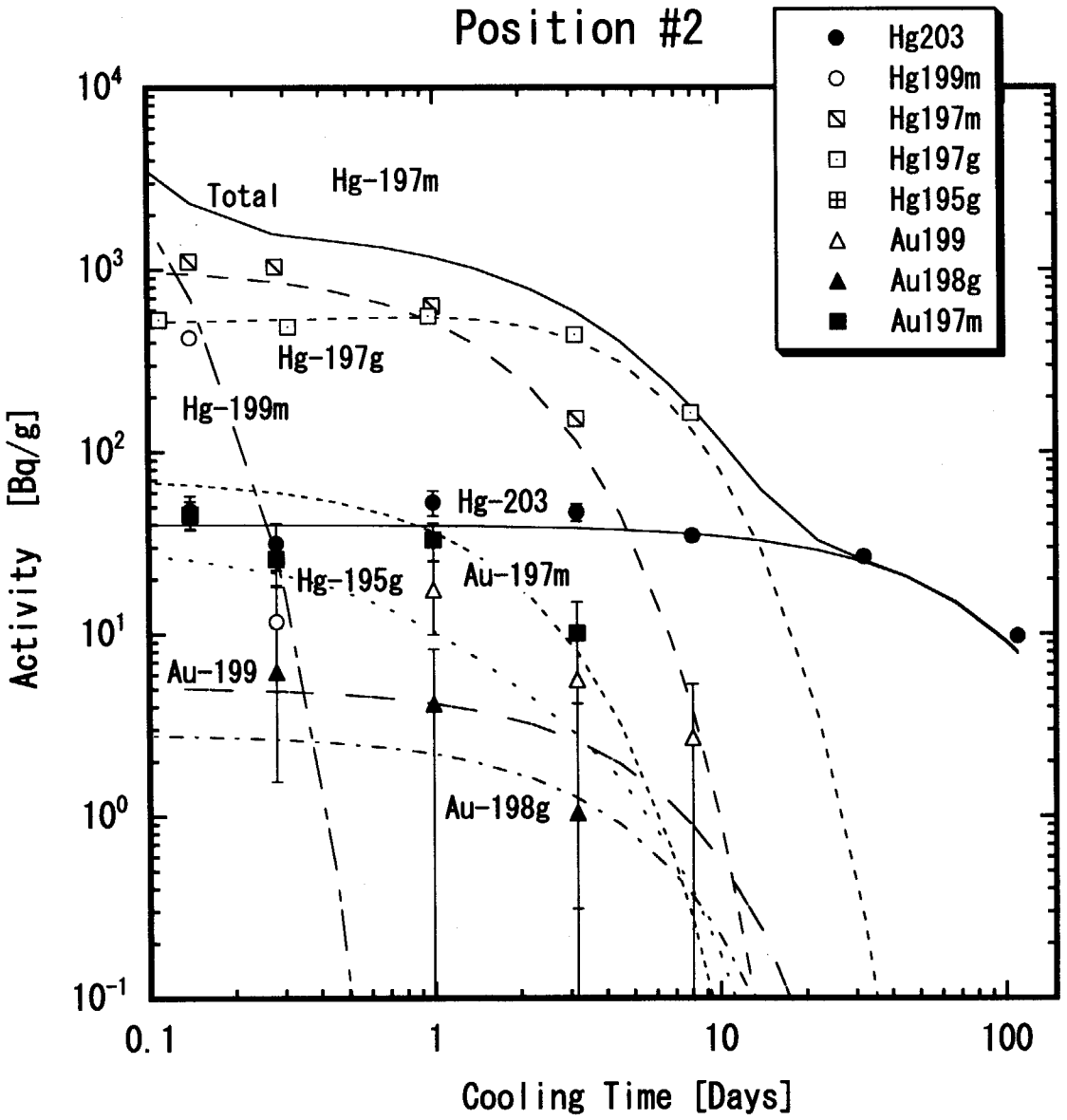

Fig. 4.4 Comparison of experimental (symbols) and calculated (lines) induced radioactivity for the mercury oxide samples irradiated at the position #2

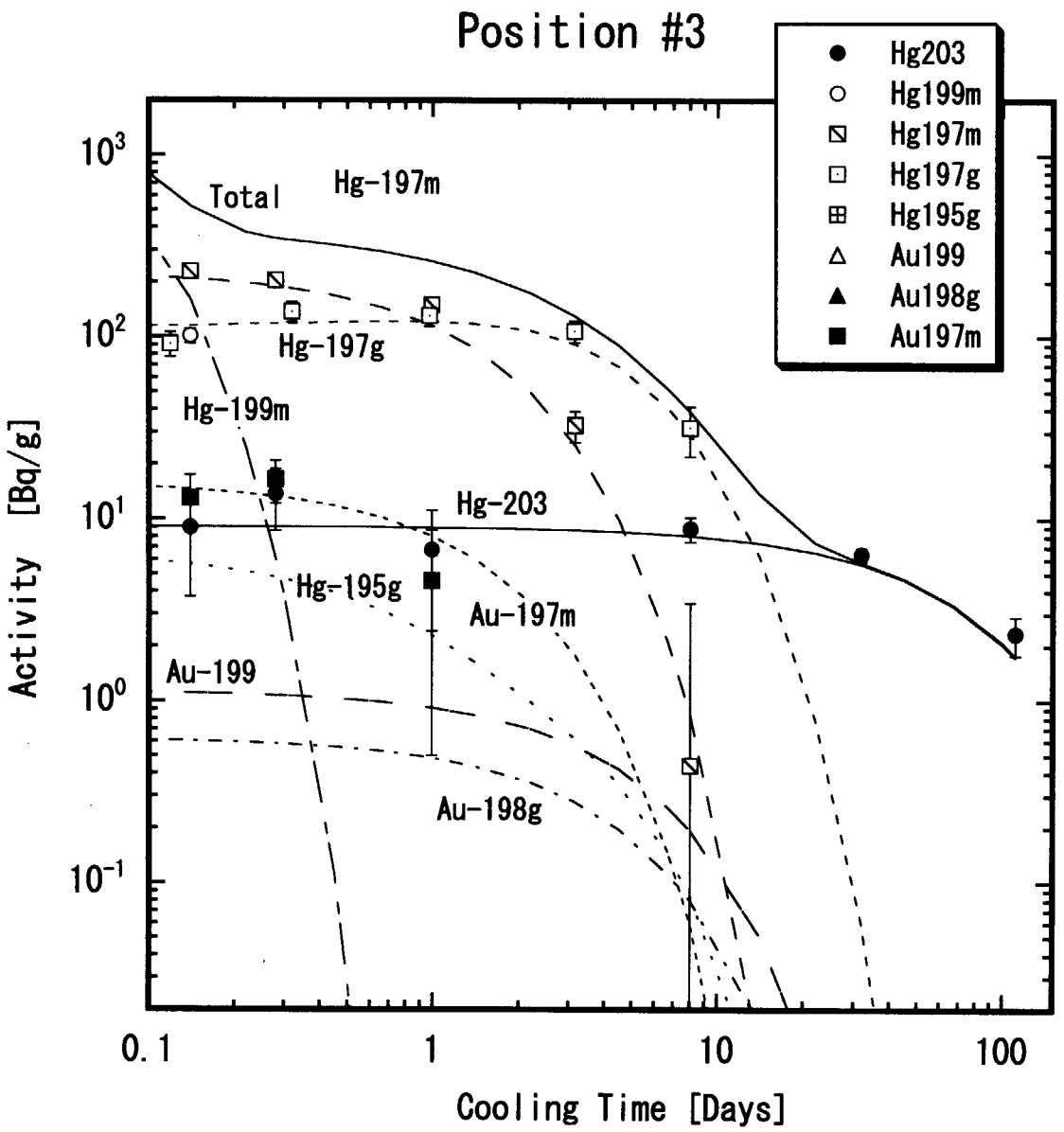

Fig. 4.5 Comparison of experimental (symbols) and calculated (lines) induced radioactivity for the mercury oxide samples irradiated at the position #3

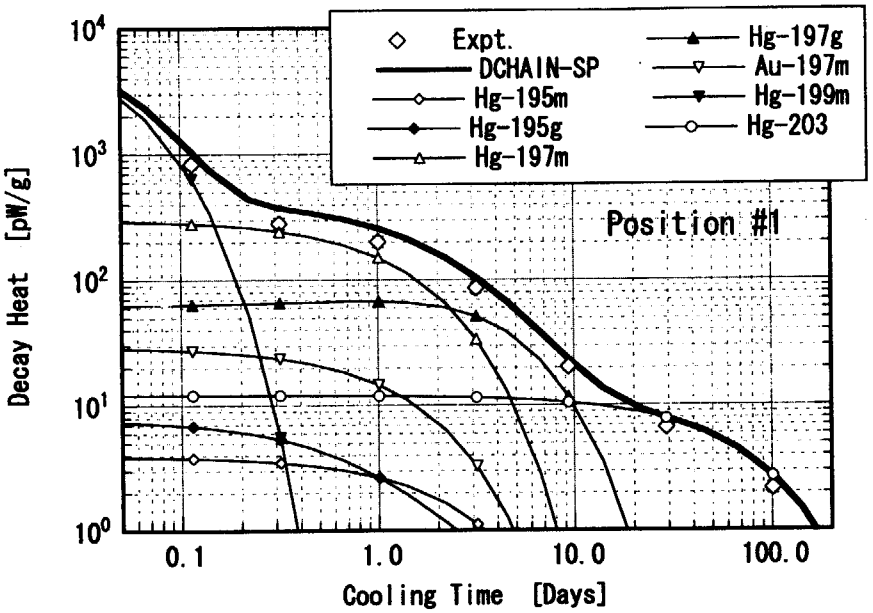

Fig. 4.6 Comparison of experimental decay heat values for the mercury oxide sample irradiated at the position #1 with those calculated by DCHAIN-SP. The upmost bold line denoted as DCHAIN-SP is to be compared with the experimental data. The contribution by each nuclide is based on the DCHAIN-SP calculation.

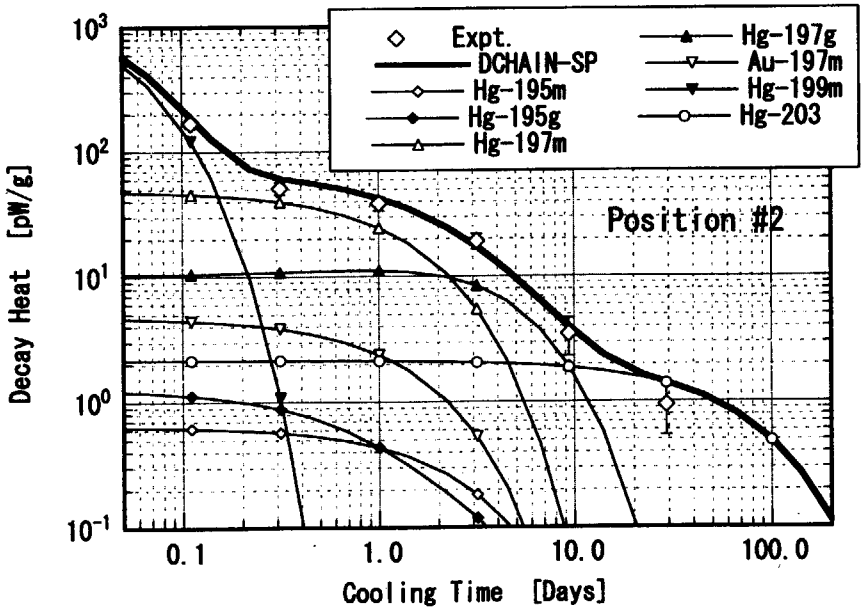

Fig. 4.7 Comparison of experimental decay heat values for the mercury oxide sample irradiated at the position #2 with those calculated by DCHAIN-SP. The upmost bold line denoted as DCHAIN-SP is to be compared with the experimental data. The contribution by each nuclide is based on the DCHAIN-SP calculation.

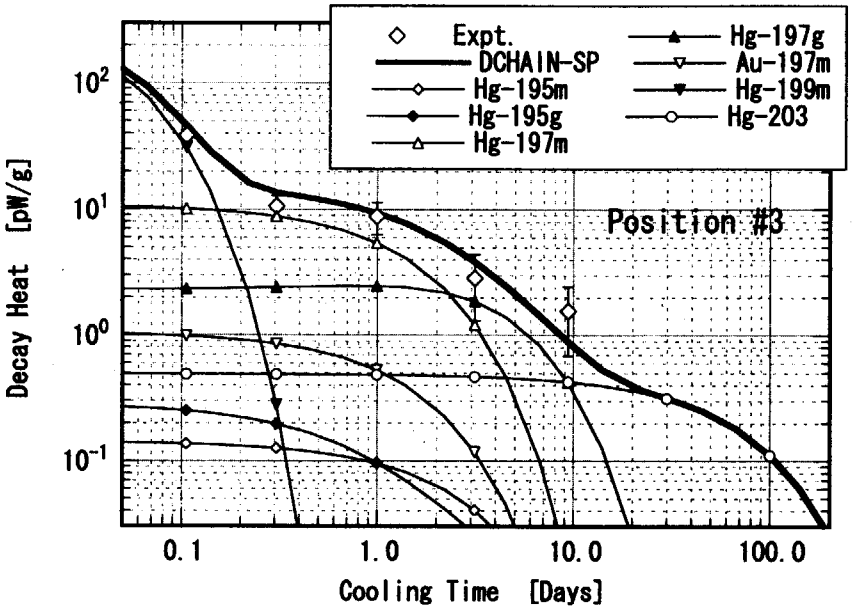

Fig. 4.8 Comparison of experimental decay heat values for the mercury oxide sample irradiated at the position #3 with those calculated by DCHAIN-SP. The upmost bold line denoted as DCHAIN-SP is to be compared with the experimental data. The contribution by each nuclide is based on the DCHAIN-SP calculation.

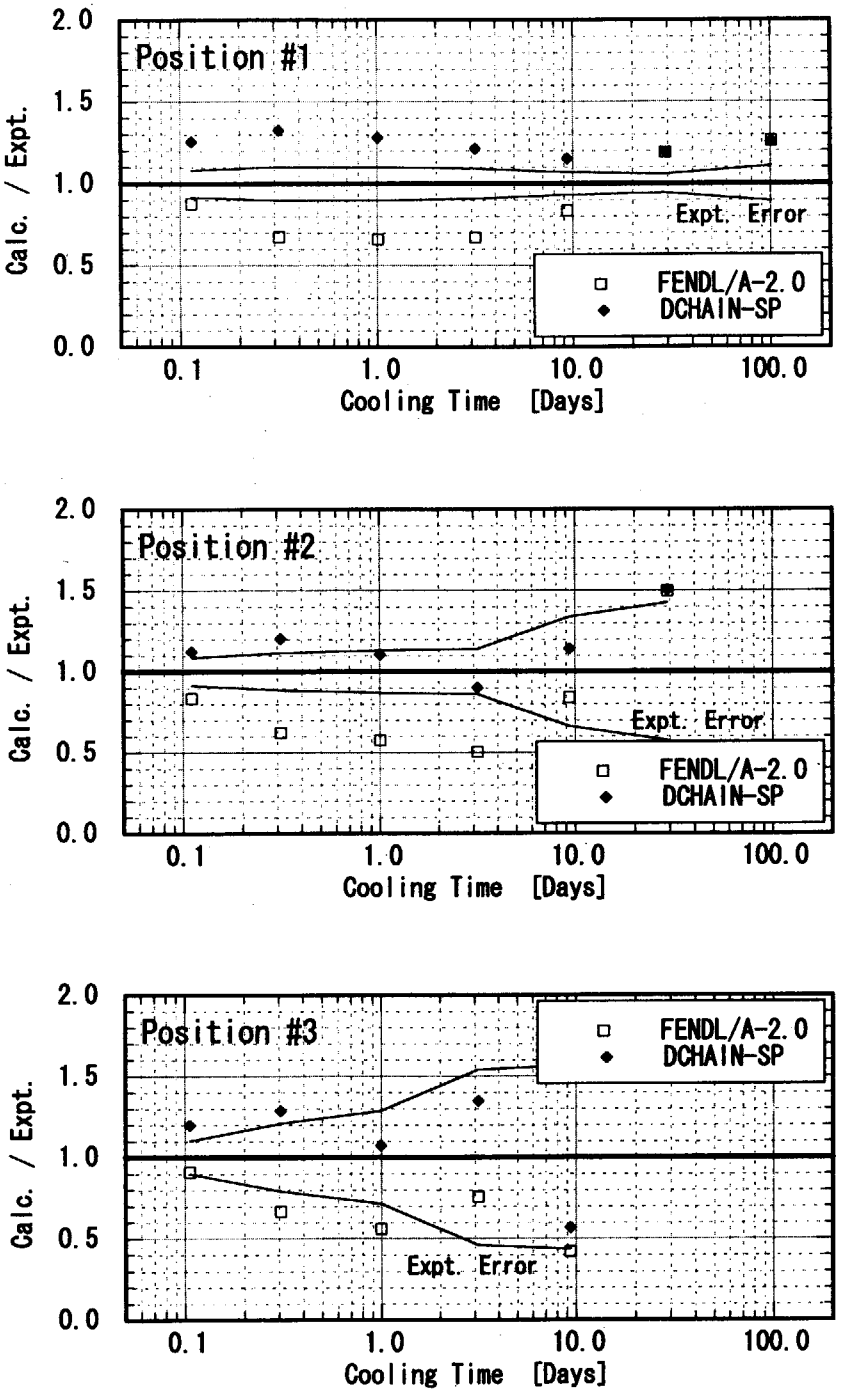

Fig. 4.9 The C/E values for the decay heat of mercury oxide samples as a function of cooling time. The values denoted as FENDL/A-2.0 and DCHAIN-SP are the DCHAIN-SP calculation with the previous and the revised activation cross section library, respectively.

This is a blank page.

国際単位系 (SI) と換算表

表 1　SI基本単位および補助単位

量	名称	記号
長さ	メートル	m
質量	キログラム	kg
時間	秒	s
電流	アンペア	A
熱力学温度	ケルビン	K
物質量	モル	mol
光度	カンデラ	cd
平面角	ラジアン	rad
立体角	ステラジアン	sr

表 2　SIと併用される単位

名称	記号
分，時，日	min，h，d
度，分，秒	°，′，″
リットル	l，L
トン	t
電子ボルト	eV
原子質量単位	u

1 eV = 1.60218 × 10^{-19} J
1 u = 1.66054 × 10^{-27} kg

表 3　固有の名称をもつSI組立単位

量	名称	記号	他のSI単位による表現
周波数	ヘルツ	Hz	s^{-1}
力	ニュートン	N	m·kg/s^2
圧力，応力	パスカル	Pa	N/m^2
エネルギー，仕事，熱量	ジュール	J	N·m
工率，放射束	ワット	W	J/s
電気量，電荷	クーロン	C	A·s
電位，電圧，起電力	ボルト	V	W/A
静電容量	ファラド	F	C/V
電気抵抗	オーム	Ω	V/A
コンダクタンス	ジーメンス	S	A/V
磁束	ウェーバ	Wb	V·s
磁束密度	テスラ	T	Wb/m^2
インダクタンス	ヘンリー	H	Wb/A
セルシウス温度	セルシウス度	℃	
光束	ルーメン	lm	cd·sr
照度	ルクス	lx	lm/m^2
放射能	ベクレル	Bq	s^{-1}
吸収線量	グレイ	Gy	J/kg
線量当量	シーベルト	Sv	J/kg

表 4　SIと共に暫定的に維持される単位

名称	記号
オングストローム	Å
バーン	b
バール	bar
ガル	Gal
キュリー	Ci
レントゲン	R
ラド	rad
レム	rem

1 Å = 0.1 nm = 10^{-10} m
1 b = 100 fm^2 = 10^{-28} m^2
1 bar = 0.1 MPa = 10^5 Pa
1 Gal = 1 cm/s^2 = 10^{-2} m/s^2
1 Ci = 3.7 × 10^{10} Bq
1 R = 2.58 × 10^{-4} C/kg
1 rad = 1 cGy = 10^{-2} Gy
1 rem = 1 cSv = 10^{-2} Sv

表 5　SI接頭語

倍数	接頭語	記号
10^{18}	エクサ	E
10^{15}	ペタ	P
10^{12}	テラ	T
10^{9}	ギガ	G
10^{6}	メガ	M
10^{3}	キロ	k
10^{2}	ヘクト	h
10^{1}	デカ	da
10^{-1}	デシ	d
10^{-2}	センチ	c
10^{-3}	ミリ	m
10^{-6}	マイクロ	μ
10^{-9}	ナノ	n
10^{-12}	ピコ	p
10^{-15}	フェムト	f
10^{-18}	アト	a

（注）

1. 表1－5は「国際単位系」第5版，国際度量衡局 1985年刊行による。ただし，1 eVおよび1 uの値はCODATAの1986年推奨値によった。
2. 表4には海里，ノット，アール，ヘクタールも含まれているが日常の単位なのでここでは省略した。
3. barは，JISでは流体の圧力を表わす場合に限り表2のカテゴリーに分類されている。
4. EC閣僚理事会指令ではbar，barnおよび「血圧の単位」mmHgを表2のカテゴリーに入れている。

換算表

力

N(=10^5 dyn)	kgf	lbf
1	0.101972	0.224809
9.80665	1	2.20462
4.44822	0.453592	1

粘度　1 Pa·s(N·s/m^2) = 10 P(ポアズ)(g/(cm·s))
動粘度　1 m^2/s = 10^4 St(ストークス)(cm^2/s)

圧力

MPa(=10 bar)	kgf/cm^2	atm	mmHg(Torr)	lbf/in^2(psi)
1	10.1972	9.86923	7.50062 × 10^3	145.038
0.0980665	1	0.967841	735.559	14.2233
0.101325	1.03323	1	760	14.6959
1.33322 × 10^{-4}	1.35951 × 10^{-3}	1.31579 × 10^{-3}	1	1.93368 × 10^{-2}
6.89476 × 10^{-3}	7.03070 × 10^{-2}	6.80460 × 10^{-2}	51.7149	1

エネルギー・仕事・熱量

J(=10^7 erg)	kgf·m	kW·h	cal(計量法)	Btu	ft·lbf	eV
1	0.101972	2.77778 × 10^{-7}	0.238889	9.47813 × 10^{-4}	0.737562	6.24150 × 10^{18}
9.80665	1	2.72407 × 10^{-6}	2.34270	9.29487 × 10^{-3}	7.23301	6.12082 × 10^{19}
3.6 × 10^6	3.67098 × 10^5	1	8.59999 × 10^5	3412.13	2.65522 × 10^6	2.24694 × 10^{25}
4.18605	0.426858	1.16279 × 10^{-6}	1	3.96759 × 10^{-3}	3.08747	2.61272 × 10^{19}
1055.06	107.586	2.93072 × 10^{-4}	252.042	1	778.172	6.58515 × 10^{21}
1.35582	0.138255	3.76616 × 10^{-7}	0.323890	1.28506 × 10^{-3}	1	8.46233 × 10^{18}
1.60218 × 10^{-19}	1.63377 × 10^{-20}	4.45050 × 10^{-26}	3.82743 × 10^{-20}	1.51857 × 10^{-22}	1.18171 × 10^{-19}	1

1 cal = 4.18605 J (計量法)
= 4.184 J (熱化学)
= 4.1855 J (15 °C)
= 4.1868 J (国際蒸気表)

仕事率　1 PS (仏馬力)
= 75 kgf·m/s
= 735.499 W

放射能

Bq	Ci
1	2.70270 × 10^{-11}
3.7 × 10^{10}	1

吸収線量

Gy	rad
1	100
0.01	1

照射線量

C/kg	R
1	3876
2.58 × 10^{-4}	1

線量当量

Sv	rem
1	100
0.01	1

（86年12月26日現在）

Reliability Assessment of High Energy Particle Induced Radioactivity Calculation Code DCHAIN-SP 2001 by Analysis of Integral Activation Experiments with 14 MeV Neutrons